UNIVERSIDADE FEDERAL DE SANTA CATARINA
CENTRO TECNOLÓGICO - CTC
PROGRAMA DE PÓS-GRADUAÇÃO EM ENGENHARIA ELÉTRICA

Felipe Augusto Tondo

Strategies for Efficient Resource Allocation in Direct-to-Satellite IoT Networks

Florianópolis
2024

Felipe Augusto Tondo

Strategies for Efficient Resource Allocation in Direct-to-Satellite IoT Networks

Tese submetida ao Programa de Pós-Graduação em Engenharia Elétrica da Universidade Federal de Santa Catarina para a obtenção do título de doutor em Engenharia Elétrica.
Orientador Prof. Richard Demo Souza, Dr.
Coorientador Prof. Samuel Montejo-Sánchez, Dr., Universidad Tecnológica Metropolitana (UTEM) Chile.

Florianópolis
2024

Felipe Augusto Tondo

Strategies for Efficient Resource Allocation in Direct-to-Satellite IoT Networks

O presente trabalho em nível de [doutorado] foi avaliado e aprovado por banca examinadora composta pelos seguintes membros:

Prof. Glauber Brante, Dr.
Universidade Tecnológica Federal do Paraná (UTFPR)

Prof. Samuel Baraldi Mafra, Dr.
Instituto Nacional de Telecomunicações (INATEL)

Prof. Evelio Martín García Fernández, Dr.
Universidade Federal do Paraná (UFPR)

Certificamos que esta é a **versão original e final** do trabalho de conclusão que foi julgado adequado para obtenção do título de doutor em Engenharia Elétrica.

———————————————————
Prof. Telles Brunelli Lazzarin, Dr.
Coordenação do Programa de
Pós-Graduação

———————————————————
Prof. Richard Demo Souza, Dr.
Orientador

Florianópolis, 2024.

Este trabalho é dedicado a toda a minha família, em especial aos meus pais, Jorge e Denise, ao meu irmão Ramon, à minha amada namorada Patricia, sua mãe Iraci e seu amado pai Lino (*in memoriam*). Ofereço este trabalho também aos meus estimados professores.

AGRADECIMENTOS

Inicialmente, agradeço a Deus por ter me dado condições e persistência nessa caminhada. Também agradeço o apoio incondicional fornecido pela minha namorada, Patrícia Cini, sem a qual não teria dado o primeiro passo e nem chego tão longe. Foram muitas etapas difíceis, mas que, com seu apoio, tornaram-se mais leves. Agradeço à sua mãe Iraci, por estar sempre ao nosso lado, apoiando e dedicando seu tempo e sua atenção. Agradeço imensamente meu pai Jorge, minha mãe Denise e meu irmão Ramon por sempre estarem ao meu lado. Amo todos vocês.

Ninguém faz nada sozinho e tive sempre ao meu lado os melhores professores. Agradeço aos meus estimados professores, Richard Demo Souza Dr., e Samuel Montejo-Sánchez Dr. que, mesmo sabendo do desafio que seria me orientar, sempre estiveram comigo ao longo dessa jornada. Além de todo conhecimento adquirido, aprendi o que é trabalhar em equipe e com profissionais que, acima de tudo, são exemplos de dedicação, sabedoria e humildade. Minha gratidão eterna.

Gostaria de agradecer a todos que estiveram comigo ao longo dessa trajetória. Meus estimados amigos da cidade de Oulu, que me deram suporte e acolhimento no período de intercâmbio. Ao meu querido professor de Oulu, Onel Luis Alcaraz López Dr., que me acolheu como se fossemos amigos de longa data. Meus queridos amigos, Guilhermo, Thaíse e Leonardo, além de seus pais Jaqueline e Cláudio. Meu querido amigo Jorge, sua esposa Taise e a pequena Sofia. Com o apoio de vocês, tudo ficou mais fácil e tranquilo. Agradeço a Deus por ter pessoas assim ao meu lado.

*"Tenha coragem de seguir seu coração e sua intuição.
Eles de alguma forma já sabem o que você realmente
quer se tornar. Todo o resto é secundário."*
(Steve Jobs, 2005)

RESUMO

As futuras redes de sexta geração (6G) deverão fornecer serviços inovadores onipresentes, mas os atuais sistemas de comunicação terrestre ainda são consideravelmente limitados por restrições de infraestrutura e cobertura. Para fornecer cobertura global, prevê-se que os sistemas de comunicação via satélite sejam incorporados nas redes 6G. Em particular, os satélites de órbita baixa (LEO, do inglês *Low Earth Orbit*) possuem custo reduzido e baixa latência em comparação com os sistemas de satélite tradicionais, sendo uma alternativa economicamente e tecnicamente promissora para comunicações móveis e aplicações de Internet das Coisas (IoT, do inglês *Internet of Things*). As estratégias para alocação eficiente de recursos em redes de satélites LEO para aplicações 6G e IoT apresentadas nesta tese exploram: (i) a alocação da carga de tráfego oferecida para maximizar a métrica de desempenho desejada; (ii) o número de canais disponíveis, a localização geográfica dos dispositivos IoT e a trajetória dos satélites LEO para aumentar a eficiência temporal das janelas de visibilidade; e (iii) as técnicas de Acesso Múltiplo Não Ortogonal (NOMA, do inglês *Non-Orthogonal Multiple Access*) para melhorar o *goodput* e a eficiência energética. Primeiro, consideramos um sistema de comunicação direto para o satélite (DtS) onde um *cluster* de dispositivos IoT está sob a cobertura da constelação de satélites LEO, enquanto slotted Aloha é usado como técnica de controle de acesso ao meio no uplink. Como cada posição relativa da constelação em relação ao conjunto de dispositivos IoT leva a uma taxa de transferência diferente para uma determinada carga de tráfego, propomos uma nova estratégia de distribuição de carga de tráfego baseada em aproximação convexa sucessiva para maximizar a taxa de transferência do sistema. O método proposto aloca adequadamente a carga de tráfego entre as diferentes posições da constelação em relação ao *cluster* IoT, supera outras estratégias recentemente propostas baseadas em heurísticas para alocação de carga de tráfego e ainda atinge uma taxa de transferência estável e não nula, mesmo para grandes cargas de tráfego. Segundo, esta tese propõe novas estratégias de agendamento para redes de Internet das Coisas Direta ao Satélite (DtS-IoT, do inglês *Direct-to-Satellite Internet of Things*) inspiradas em aplicações comerciais tais como LacunaSat. Considerando o gateway a bordo do satélite LEO e múltiplos canais, esses mecanismos aproveitam a disponibilidade de vários canais e a capacidade de alterar a ordem de agendamento de transmissão de alguns dispositivos dentro de uma janela de tempo de visibilidade para melhorar a eficiência do uplink. Os resultados mostram que o número médio de uplinks por volta e por dispositivo visível aumenta com o número de canais disponíveis, proporcionando uma melhoria de quase 80% em termos de eficiência no uplink do sistema. Além disso, exploramos que a combinação das estratégias de agendamento pode aumentar ainda mais o desempenho do sistema, garantindo uma eficiência de uplink superior a 50%, como elucidado nos algoritmos de implementação com quatro, seis e oito canais. Finalmente, este documento

introduz dois novos esquemas DtS-IoT usando NOMA por domínio de potência com potência de transmissão fixa ou controlada no uplink. O modelo de sistema proposto considera que os dispositivos IoT usam a tecnologia de longo alcance para transmitir pacotes de dados para o satélite equipado com um gateway habilitado para decodificar através do Cancelamento de Interferência Sucessiva (SIC, do inglês *Successive Interference Cancellation*). Assume-se também que os dispositivos IoT possuem um preditor da órbita do satélite. Usando dados reais de localização geográfica e trajetória, avaliamos o desempenho do número médio de transmissões decodificadas com sucesso, *goodput* e eficiência energética em função do número de dispositivos na rede. Os resultados mostram o comparativo entre as métricas de desempenho para ambos os esquemas propostos. Comparando os esquemas de transmissão fixa e controlada com Aloha para 100 (600) dispositivos, encontramos melhorias de *goodput* de 65% (29%) e 52% (101%), respectivamente. Notavelmente, a abordagem controlada aproveita as oportunidades de transmissão à medida que o tamanho da rede aumenta, superando as outras estratégias.

Palavras-chave: IoT. Satélites LEO. Aproximacão convexa sucessiva. Tecnologia de longo alcance. NOMA por domínio de potência.

RESUMO EXPANDIDO

Introdução

A sociedade moderna exige mais dados e conexões mais rápidas rumo aos futuros sistemas de comunicação 6G. Em 2023, 88% dos brasileiros com mais de dez anos acessaram a Internet, totalizando quase 164,5 milhões de usuários(INSTITUTO BRASILEIRO DE GEOGRAFIA E ESTATÍSTICA, 2024). Apesar da ampla conectividade nas áreas urbanas, a infraestrutura limitada continua sendo um obstáculo significativo em vários setores, como o agronegócio brasileiro, por exemplo(EMPRESA BRASILEIRA DE PESQUISA AGROPECUÁRIA, 2020). Para melhorar ainda mais a produtividade e a competitividade, as redes não terrestres (NTN, do inglês *Non Terrestrial Networks*) surgem como uma solução viável, pois não exigem instalação de grande infraestrutura e podem fornecer conectividade global(CENTENARO *et al.*, 2021). Além disso, o grupo 3GPP (do inglês, *3rd Generation Partnership Project*) já começou a trabalhar em especificações para oferecer cobertura global de IoT ao incorporar NTN na versão 17(NOKIA, 2023). Nesse contexto, os satélites do tipo LEO desempenham um papel fundamental nas NTNs e surgem com grande interesse, tanto da academia quanto da indústria.

Os satélites LEO operam em altitudes entre 160 e 2000 km acima da Terra, resultando em uma cobertura sobre a área alvo por apenas alguns minutos. Sistemas de comunicação direta ao satélite apresentam desafios tais como longas distâncias, baixo consumo de energia e o efeito Doppler (WU *et al.*, 2019). A integração de tecnologias de longo alcance, como NB-IoT (do inglês *Narrowband Internet of Things*), Sigfox e LoRaWAN, tem ganhado atenção recentemente na indústria espacial, intensificando a quantidade de lançamentos e missões espaciais. Devido a aspectos essenciais como alta sensibilidade do receptor, baixas taxas de dados e tolerância ao efeito Doppler, a tecnologia LoRaWAN pode viabilizar uma conectividade eficiente entre dispositivos IoT e satélites. Em 1º de abril de 2019, a Lacuna Space lançou seu primeiro CubeSat, demonstrando as capacidades de um satélite LEO equipado com um *gateway* espacial para recepção de sinais LoRaWAN(SEMTECH CORPORATION, 2019). Outras empresas, como Sateliot e Swarm, estão ativamente desenvolvendo suas constelações de satélites com tecnologias semelhantes, enquanto a Starlink expande seu potencial com quase 7000 satélites já em órbita(SPACE.COM, 2025).

À medida que a cobertura de redes IoT se torne global com o uso de satélites LEO, os sistemas DtS-IoT se expandem para suportar um grande número de dispositivos conectados, levando à congestão da rede e problemas de qualidade de serviço (QoS, do inglês *Quality of Service*). Devido às limitações de conectividade dos dispositivos, os protocolos de controle de acesso ao meio (MAC, do inglês *Medium Access Control*) tornam-se essenciais, e seu desenvolvimento deve priorizar confiabilidade e simplici-

dade. Embora os protocolos de acesso aleatório (RA, do inglês *Random Access*) sejam valorizados por sua simplicidade, o aumento no número de dispositivos conectados leva a congestionamento significativo da rede e colisões de mensagens, comprometendo a confiabilidade e exigindo soluções alternativas. Compreender os desafios e limitações das comunicações DtS-IoT é crucial para desenvolver estratégias de alocação eficiente de recursos nesse tipo de comunicação.

Pelo fato de que o sinal transmitido percorre longas distâncias, um dos principais desafios é o atraso na comunicação para aplicações críticas que exigem tempo real, tais como saúde e segurança pública. Além disso, a largura de banda é um fator limitante, pois sua restrição compromete a transmissão de grandes volumes de dados, podendo gerar congestionamento na rede (LEDESMA *et al.*, 2024). A cobertura também representa uma limitação. Embora a constelação de satélites possa fornecer cobertura para grandes regiões, o movimento orbital e a descontinuidade podem prejudicar o desempenho da rede. O problema da escalabilidade surge à medida que o número de dispositivos IoT cresce, exigindo protocolos eficientes para o gerenciamento da conectividade e dos dados transmitidos. Por fim, um fator crítico é o efeito Doppler, que afeta diretamente as comunicações IoT via satélite. Esse fenômeno, causado pelo deslocamento relativo entre o satélite e os dispositivos terrestres, pode gerar variações na frequência do sinal, tornando necessário o desenvolvimento de técnicas de compensação e sincronização para minimizar seus impactos (NOKIA, 2023).

Objetivos

O objetivo desta tese é propor estratégias para a alocação eficiente de recursos em redes IoT de comunicação direta com satélites. O foco principal do trabalho está concentrado nas melhorias de indicadores de desempenho, como rendimento, eficiência energética e confiabilidade.

Metodologia

Inspirado no modelo de sistema proposto por (MUNARI *et al.*, 2021), desenvolveu-se uma nova estratégia para otimizar a alocação de carga de tráfego em redes do tipo DtS-IoT. Desta forma, um grupo de dispositivos IoT transmite suas informações para múltiplos satélites usando o protocolo slotted Aloha. O link de comunicação entre os dispositivos em terra e o satélite é modelado por um canal com apagamento. Ao contrário de (MUNARI *et al.*, 2021), a avaliação foi conduzida considerando diferentes probabilidades de apagamento em função da quantidade de satélites e também das diferentes posições ocupadas ao longo da passada de cobertura. As métricas analisadas incluem a relação entre throughput e carga do canal, bem como o impacto das

interseções entre os throughputs individuais de cada satélite. A remoção dessas multi-plicidades é destacada como um fator essencial para a correta avaliação da eficiência da rede. Os resultados obtidos são comparados com mecanismos tradicionais, tais como a distribuição uniforme e não-uniforme da carga do canal.

Para de aumentar a eficiência na quantidade de uplinks realizados em redes de comunicação DtS-IoT, este trabalho propõe novos algoritmos de agendamento de transmissões, considerando novamente um cenário em que os dispositivos estão sob a cobertura de um satélite LEO, mas que agora utilizam modulação LoRa para transmitir seus pacotes de informação. Os esquemas propostos foram comparados com estratégias tradicionais, como o algoritmo de agendamento SALSA (AFHAMISIS; PALATTELLA, 2022). Além disso, os resultados apresentados incluem bibliotecas poderosas e de acesso livre na linguagem Python, utilizando dados reais da localização de cada dispositivo e dos tempos de visibilidade do satélite.

Por fim, a tese também apresenta o estudo de técnicas avançadas de acesso múltiplo no domínio da potência para redes DtS-IoT. Diferente da primeira estratégia de alocação de carga de tráfego que adota um modelo de canal simplificado e, também da segunda abordagem que visa apenas aumentar a quantidade de transmissões agendadas, o sinal recebido no satélite agora considera efeitos de larga e pequena escala, específicos para comunicação satelital de baixa órbita. Considerando que o satélite LEO é equipado com um decodificador LoRaWAN, dois níveis de potência de sinal recebido foram propostos para as especificações da tecnologia. O primeiro nível é definido de modo que o sinal recebido seja livre de interferência para um dado ângulo mínimo de visibilidade. Já para o segundo nível de recepção, considerou-se o efeito de figura do decodificador com o qual é possível distinguir o sinal recebido mesmo na presença da interferência (SEMTECH, 2015). Diante desse contexto, duas estratégias de transmissão de mensagens são propostas com objetivo de aplicar NOMA e SIC para aumentar a quantidade de informações exitosamente recebidas no satélite.

Resultados e Discussão

A partir das propostas apresentadas, espera-se que a estratégia de alocação ótima da carga de tráfego forneça uma avaliação abrangente do desempenho do sistema em função da quantidade de posições da constelação e do número de satélites. Ao assumir que o canal de comunicação entre os dispositivos e o satélite é modelado como um canal On-Off, onde, a probabilidade de apagamento varia de acordo com o ângulo de elevação (quanto mais próximo da linha do horizonte, maior a probabilidade de apagamento), será possível analisar a quantidade de carga que uma determinada posição consegue suportar. Além disso, importantes diagnósticos podem ser realizados, como por exemplo saber se uma determinada posição é ineficiente durante a

passagem, ou mesmo saber se outras posições estão assumindo a maior parcela da carga do canal.

Com relação ao cenário onde assume-se agendar as transmissões considerando a instalação de um gateway LoRaWAN a bordo do satélite LEO, espera-se que o número de uplink realizados seja maior do que estratégias tradicionais de agendamento, como por exemplo, agendar os dispositivos por ordem de chegada. Pelo simples fato de que cada dispositivo experimenta diferentes períodos de visibilidade durante a passagem do satélite, os algoritmos propostos buscam ocupar a janela de visibilidade total de uma forma mais eficiente, mantendo critérios como simplicidade e complexidade na sua implementação.

Finalmente, a tese apresenta os resultados considerando o uso do domínio da potência no uplink e o processo de SIC. O estudo será conduzido utilizando um modelo de canal realista, consolidado e aplicável a satélites de baixa órbita. Além disso, busca-se comparar as estratégias propostas com métodos tradicionais de transmissão, como Aloha, avaliando seu impacto no tratamento de colisões e na eficiência energética. A utilização de NOMA em cenários DtS-IoT é uma ferramenta poderosa, alinhada com as futuras implementações 6G, as quais preveem altas taxas de transmissão e uma conectividade massiva para dispositivos na rede.

Considerações Finais

A demanda por cobertura global anunciada pelos futuros sistemas 6G, aliada ao grande número de lançamentos e investimentos da indústria em satélites de baixa órbita, é um verdadeiro motivador para investimentos em pesquisa no cenário de comunicações satelitais, especialmente em DtS-IoT. Portanto, entende-se que o presente documento de tese de doutorado fornece ferramentas relevantes para comprovação da importância da implementação de redes IoT via satélite, mostrando sua aplicabilidade em cenários realistas de monitoramento da fauna e flora, agricultura, cidades inteligentes, logística e desastres ambientais.

Palavras-chave: NTN. LEO. Alocação de carga de tráfego. NOMA. SIC.

ABSTRACT

The future Sixth Generation (6G) networks are expected to provide ubiquitous innovative services, but current terrestrial communication systems are still considerably limited by infrastructure and coverage constraints. To provide global coverage, it has been envisioned that satellite communication systems will be incorporated into 6G networks. In particular, Low Earth Orbit (LEO) satellites have reduced cost and low latency compared to traditional satellite systems, being an economically and technologically promising alternative for mobile communications and Internet of Things (IoT) applications. The strategies for efficient resource allocation in LEO satellite networks for 6G and IoT applications presented in this thesis explore: (i) the allocation of the offered traffic load to maximize the desired performance metric; (ii) the number of available channels, the geographic location of IoT devices, and the trajectory of LEO satellites to enhance the temporal efficiency of visibility windows; and (iii) Non-Orthogonal Multiple Access (NOMA) techniques to improve goodput and energy efficiency. First, we consider a Direct-to-Satellite (DtS) communication system where a cluster of IoT devices is under the coverage of the LEO satellite constellation, while slotted Aloha is used as a medium access control technique in the uplink. Since each relative position of the constellation to the cluster of IoT devices leads to a different throughput for a given traffic load, we propose a novel traffic load distribution strategy based on Successive Convex Approximation to maximize the system throughput. This proposed method adequately allocates the traffic load among the different constellation positions concerning the IoT cluster, outperforms other recently proposed strategies based on heuristics for traffic load allocation and still achieves a stable non-zero throughput even for large traffic loads. Secondly, this thesis proposes new multiple-access scheduling strategies for Direct-to-Satellite IoT (DtS-IoT) networks inspired by commercial applications such as LacunaSat. Considering the gateway on board the LEO satellite and multiple channel frequencies, these mechanisms take advantage of the availability of multiple frequency channels and the ability to change the transmission scheduling order of some devices within a visibility time window to improve uplink efficiency. The numerical results show that the average number of uplinks per lap and per visible device increases with the number of available channels, providing an improvement of almost 80% in terms of system uplink efficiency. Additionally, we explore that the fusion of scheduling strategies can further boost the system performance while guaranteeing an uplink efficiency greater than 50%, as elucidated across the implementation algorithms with four, six, and eight multiple channels. Finally, this document introduces two novel DtS-IoT schemes using power domain NOMA in the uplink with either fixed or controlled transmit power. The proposed system model considers that the IoT devices use Long Range technology to transmit data packets to the satellite in orbit, equipped with a Successive Interference Cancellation-enabled gateway. We also assume the IoT devices are empowered with

a satellite orbit predictor. Using real geographic location and trajectory data, we evaluate the performance of the average number of successfully decoded transmissions, goodput, and energy efficiency as a function of the number of network devices. Numerical results show the trade-off between perform metrics for both proposed schemes. Comparing fixed and controlled schemes with regular Aloha for 100 (600) devices, we find goodput improvements of 65% (29%) and 52% (101%), respectively. Notably, the controlled approach effectively leverages transmission opportunities as the network size increases, outperforming the other strategies.

LIST OF FIGURES

LIST OF TABLES

LIST OF ABBREVIATIONS AND ACRONYMS

1G	First Generation
3GPP	3rd Generation Partnership Project
5G	Fifth Generation
6G	Sixth Generation
AWGN	Additive White Gaussian Noise
CDMA	Code Division Multiple Access
CRDSA	Contention Resolution Diversity Slotted Aloha
CSMA	Carrier Sense Multiple Access
CTP	Controlled Transmission Power
DtS	Direct-to-Satellite
DtS-IoT	Direct-to-Satellite IoT
EoT	Economy of Things
FCFS	First-Come-First-Serve
FLFS	First-Leave-First-Serve
FTP	Fixed Transmission Power
GEO	Geosynchronous Earth Orbit
IoT	Internet of Things
IRSA	Irregular Repetition Slotted Aloha
ITLD	Intelligent traffic load distribution
L2L-A	LoRa-to-LEO with Alternating Channels
L2L-P	LoRa-to-LEO with Permutation of scheduled times
LEO	Low Earth Orbit
LoRa	Long Range
LoRaWAN	Long Range Wide Area Network
MAC	Medium Access Control
MEO	Medium Earth Orbit
MIMO	Multiple-Input Multiple-Output
mMTC	massive Machine Type Communication
MTC	Machine Type Communications
NB-IoT	Narrowband Internet of Things
NOMA	Non-Orthogonal Multiple Access
NS	Network Server
NTN	Non-Terrestrial Network
PSO	Particle Swarm Optimization
RA	Random Access
SALSA	Scheduling Algorithm for LoRa to LEO Satellites
SCA	Successive Convex Approximation

SF	Spreading Factor
SIC	Successive Interference Cancellation
SIR	Signal to Interference Ratio
SNR	Signal-to-Noise Ratio
TDMA	Time Division Multiple Access
TLE	Two-Line Element

CONTENTS

1 INTRODUCTION

This chapter introduces some background on satellite-based IoT networks. Additionally, we introduce the research works reported in this thesis and the contributions of this work.

1.1 BACKGROUND

Contemporary life dynamics impose an extraordinary challenge to upcoming wireless communication systems. From the inception of the First Generation (1G) to the current era of the Fifth Generation (5G) wireless systems, researchers and industry have played important roles in providing global interconnection and raising their levels of performance and Quality of Service (QoS). However, a groundbreaking milestone was recently reached as the number of connected devices surpassed that of connected humans (RAQUEL KATIGBAK, IBM DISTINGUISHED INDUSTRY LEADER, 2023). This notable advancement opens up a new opportunity for the so-called Economy of Things (EoT), providing a diversity of applications with nearly 30 billion connected Internet of Things (IoT) devices (CISCO VISUAL, 2020).

The future 6G systems aim to overcome the limitations of 5G systems, such as device lifetime, implementation costs, communication reliability, and hardware complexity (MAHMOOD, M. R. et al., 2022). Nevertheless, such massive traffic volume in 6G could create other issues related to medium access, mobility management, traffic offloading, and interference in high-density areas (SOUTO et al., 2023). Moreover, guaranteeing global connectivity for Machine Type Communications (MTC) applications requires non-terrestrial solutions (KUA et al., 2021), which are typically expensive.

The continuous evolution of wireless technologies is leading to an exponential increase in the number of connected IoT devices and the need for extreme worldwide coverage (NASSAR; YILMAZ, 2019). Unfortunately, the current deployment of 5G networks is not able to meet the requirements of global massive connectivity (VISWANATHAN; MOGENSEN, 2020) and there is no guarantee that this will be possible with the full 5G deployment. This calls for new architectures and emerging technologies for future wireless communications systems (DOGRA et al., 2021; AKYILDIZ et al., 2020), in which the Internet of Space Things enabled by CubeSats is one of the anticipated breakthroughs to achieve the broad connectivity goals of the 6G era (AKYILDIZ et al., 2020). In fact, the main candidate technology to help truly achieve universal connectivity is satellite communications (KAWAMOTO et al., 2013; SAEED et al., 2020; FANG; AL., 2021; CHEN et al., 2020; CIONI et al., 2018; MORÓN-LÓPEZ et al., 2020), which can leverage several applications to their full potential, such as environmental monitoring, disaster prevention, smart agriculture, and industrial digitalization.

One of the reasons why satellite networks have attracted great attention from

the industry and academia is the remarkable advance in, manufacturing of satellites and rocket launching technology (CHEN et al., 2020). Nowadays, satellite networks can be composed of three types of satellites: Low Earth Orbit (LEO), Medium Earth Orbit (MEO), and Geosynchronous Earth Orbit (GEO). Among them, the most attractive in the context of IoT are the LEO satellites, which present lower costs compared to MEO and GEO satellites, modular implementation, and lower latency in the communication between the satellite and the IoT devices (QU et al., 2017). Moreover, LEO satellites also present smaller propagation loss in the communication links and potential global coverage through satellite constellations. These satellite networks bring unprecedented high-speed mobility, broadband capacity, and even ultra-density coverage, becoming a relevant component of 5G and beyond (JIANG et al., 2022). More than a thousand different CubeSat missions have been launched over the past 20 years, consequently increasing the number of satellite constellations in orbit (SAEED et al., 2020). For global coverage, LEO satellite constellations like Telesat (188-LEOs)(TELESAT, 2022), OneWeb (648-LEOs)(LORA ALLIANCE, 2023a), and Starlink (3000-LEOs)(STARLINK, 2023), might be key to providing systems with terabits-per-second capacity (AL-HRAISHAWI et al., 2023). On the other hand, small constellations are also relevant, as sparse constellations like Swarm (SWARM SPACE, 2023) and Lacuna Space (LACUNA SPACE, 2023), which can provide low cost IoT services with few LEO satellites for specific regions, considering three or two-hour gaps (CAPEZ et al., 2022).

The massive Machine Type Communication (mMTC) is critical for the connectivity demands of smart cities, factories, and logistics, facilitating global connectivity (CHOI et al., 2022). Still, remote applications, like climate and maritime logistics, struggle with limited communication infrastructure, a gap filled by adopting Non-Terrestrial Network (NTN) solutions and long-range IoT technologies (ASAD ULLAH et al., 2024; KODHELI et al., 2021). The 3rd Generation Partnership Project (3GPP) aims at the upcoming 6G system in Release 20, focusing on the seamless integration of terrestrial and NTN solutions using advanced technologies to enable new applications like teleoperation, digital twins, and autonomous vehicles (HAROUNABADI; HEYN, 2023). Moreover, DtS-IoT leads in NTN innovations using gateways on satellites, reducing infrastructure costs but facing challenges like high channel instability and multi-path losses over the orbital trajectory (FRAIRE, J. A. et al., 2022). While GEO satellites move with the Earth's orbit and provide fixed connectivity over an area, LEO satellites move at around 7 km/s, serving different regions according to their movement. Although having more complicated dynamics, LEO satellites are much less expensive than geostationary satellites and are growing fast in number.

Although the integration of terrestrial and NTN solutions has been explored for almost a decade (KAWAMOTO et al., 2013), several problems remain, as the spectrum management and energy usage of satellite networks may be even more challenging

than those of terrestrial networks (FOURATI; ALOUINI, 2021). In this thesis, the overall purpose is to design system model architectures and software-based solutions that improve the performance of DtS-IoT networks.

1.2 PROBLEM STATEMENT

In the design of a satellite IoT network, several factors are of paramount importance, directly influencing the system performance, such as constellation design, number of satellites, number of orbital planes, elevation angle, orbital plane spacing, and orbital eccentricity (SAEED et al., 2020). Added to these factors is the wireless access technique used by IoT devices. Different methods have been proposed to establish a connection between a device and a satellite, with their advantages and disadvantages. We start with indirect communication, in which data is transmitted to the satellite via a terrestrial gateway. Therefore, the biggest advantage is the possibility of using current terrestrial LPWAN technologies at the end nodes. The IoT devices connect to the terrestrial gateway, in which protocols like Long Range Wide Area Network (LoRaWAN) and SigFox can be used to connect to end nodes (RAZA et al., 2017). A disadvantage of this architecture is the limited terrestrial coverage (FRAIRE, J. et al., 2020). Another negative factor is the difficulty of installing a gateway in remote regions or in cases where monitoring is carried out for a short period, which makes the cost of the service higher.

Arguably, the most attractive method for ease of deployment is DtS-IoT (FRAIRE, J. A. et al., 2019). Figure 1 illustrates that Dts-IoT users can communicate directly with the satellite, most probably an LEO satellite, without the need for a terrestrial gateway. However, some of the challenges of this approach are the long link distance and the short communication windows. LEO satellites are concentrated at altitudes around 340 and 650 km (AKYILDIZ; KAK, 2019) and provide time windows for communication according to their passing orbit. Some manufacturers in wireless communications (AL-LIANCE, n.d.; SIGFOX, n.d.) have been working on cutting-edge technologies that are getting closer and closer to meeting the challenge of DtS-IoT. Indeed, many private sector players are investing massively in the launching of small satellites to provide DtS-IoT service, such as Lacuna Space (LACUNA SPACE, 2023) and Swarm Space (SWARM SPACE, 2023). In (FRAIRE, J. et al., 2020), interesting advances in the interconnection of technologies are presented to provide adequate DtS-IoT communication design using a satellite constellation and LPWAN technology such as LoRaWAN.

Due to the numerous yet-to-discover applications towards 6G, NTNs must be enhanced to provide high QoS, in addition to global connectivity (AZARI et al., 2022). In this regard, Medium Access Control (MAC) is a relevant research direction in DtS-IoT systems (FERRER et al., 2019). Independent of the architecture, if direct, indirect, or a combination of both, MAC techniques implemented in commercial satellite networks

Figure 1 – Illustration of the overall perspective for a Direct-to-Satellite IoT network.
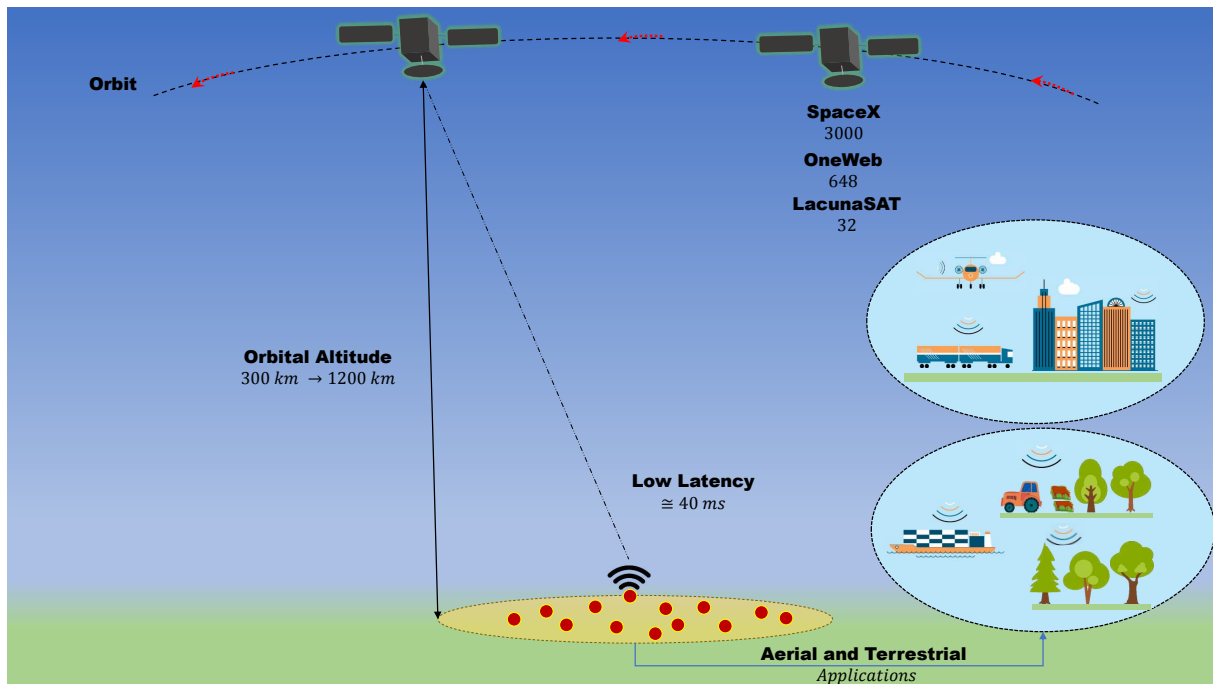
Source: The Author.

were not designed to provide scalable solutions for the growing number of devices envisioned for IoT. Traditional solutions such as Code Division Multiple Access (CDMA) and Time Division Multiple Access (TDMA), when placed in the context of LEO satellites and large device density, may lose performance due to the need for strict synchronization. Requirements such as simplicity, storage, and energy consumption should be incorporated into the designs of MAC protocols for satellite IoT networks (FERRER et al., 2019). With a focus on DtS-IoT networks, a taxonomy of MAC protocols is presented in (FERRER et al., 2019), including four groups: i) Aloha-based; ii) Reservation and adaptive protocols; iii) Interference cancellation-based; and iv) Hybrid protocols. A detailed analysis of the trade-offs involving complexity and scalability is provided. The authors finish their review with a conclusion that a better balance among different metrics should drive the design of novel MAC protocols for DtS-IoT networks. In particular, MAC protocol choice for satellite IoT networks should carefully consider the implementation complexity and energy consumption.

Therefore, Random Access (RA) protocols based on Aloha (ABRAMSON, 1970) are good candidates for the MAC layer in LEO satellite IoT networks, both in terms of simplicity of implementation and delay (FERRER et al., 2019). Indeed, they have been used for satellite communications for a long time and are even used in modern terrestrial networks, such as LoRaWAN and SigFox, and becoming also an attractive alternative for some future 6G use cases (MAHMOOD, N. H. et al., 2020). However, for a large number of transmitters, the system performance can be severely affected by collisions. One

solution for this issue is the introduction of diversity in Aloha. Modern RA schemes (BE-RIOLI et al., 2016) based on Aloha often apply Successive Interference Cancellation (SIC), allowing devices to transmit multiple copies of their messages (CLAZZER et al., 2019; STEFANOVIC; POPOVSKI, 2013; CASINI et al., 2007; LIVA, 2011; ZHAO et al., 2020). For instance, in Contention Resolution Diversity Slotted Aloha (CRDSA) devices transmit a fixed number of replicas of their messages while SIC is applied at the receiver for removing all copies once one of the messages is successfully decoded, considerably improving performance (CASINI et al., 2007). In Irregular Repetition Slotted Aloha (IRSA) devices may transmit different numbers of replicas, improving even more the network throughput (LIVA, 2011). An application of IRSA in the context of satellite communications, where the number of replications per user is optimized, is exploited in (ZHAO et al., 2020). However, methods like CRDSA and IRSA produce time diversity using replication, which may lead to a considerable increase in complexity and power consumption at the transmitters, while also demanding substantially in terms of memory and computational complexity at the receiver for the SIC operations.

Against the above background, this thesis focuses on specific problems related to traffic load allocation and multiple access strategies for DtS-IoT networks.

1.2.1 Direct-to-Satellite IoT with Multiple Satellites Coverage

Considering the context of LEO satellites with limited computational resources, RA protocols like CRDSA and IRSA may still be prohibitive. Another alternative is the spatial diversity at the receiver (ZORZI, 1997; LAMAIRE; ZORZI, 1996). Nowadays, even the use of massive Multiple-Input Multiple-Output (MIMO) antenna systems at the receiver has been considered in the context of machine-type communications using Aloha (FENGLER et al., 2019; LI, P. et al., 2020). Although promising, a small LEO satellite with several receive antennas may still not be a practical option. Spatial diversity can also be exploited with Aloha by having multiple single antenna receivers (MUNARI et al., 2015; JAKOVETIĆ et al., 2015). This idea fits well in a scenario where several satellites cover a given region, which should be more and more common with the predicted launch of hundreds of satellites in the next few years (KOZIOL, 2021). For instance, the link between devices and the multiple relays (*e.g.* LEO satellites) in coverage has been modeled considering On-Off fading (*i.e.* erasure probabilities at the satellites) in (KASSAB et al., 2020; MUNARI et al., 2021), where different analysis and optimizations were carried out. For instance, in (KASSAB et al., 2020) critical and non-critical devices coexist in a slotted Aloha-based communication system with multiple satellites.

Moreover, in (MUNARI et al., 2021), a two-phase communication system is proposed and analyzed. In the first phase, a group of clustered devices transmits their packets to multiple relays (satellites), using a simple slotted Aloha protocol. Then, in the second phase, the relays forward the decoded information to a common sink.

The channel is modeled considering On-Off fading, while expressions are provided for calculating the first phase throughput, in addition to the packet loss rate for many relays, considering equal erasure probabilities at all relays. Such setup is representative of some modern IoT LEO satellite networks with LoRaWAN technology, such as those of Lacuna Space (LACUNA SPACE, 2023) and Swarm Space (SWARM SPACE, 2023). However, in the case of a LEO satellite constellation, it is very likely that the erasure probabilities are not all the same, since some of the satellites may be at different elevation angles from the point of view of the devices.

Following (MUNARI et al., 2021), the average number of packets transmitted per slot is defined as G, and the number of users accessing the channel at the same time-slot is modeled as a Poisson random variable U. A packet is only successfully received at the k-th satellite if it has not been erased by the channel fading realization and if there is no collision of other non-erased packets transmitted by other users at the same time-slot. Thus, the throughput is defined as the number of data packets successfully received per time slot, at the k-th satellite. Additionally, the system throughput ($\mathcal{T}$) is the number of packets successfully received by at least one of the satellites per time slot. Therefore, multiplicities must be discarded, so that the system throughput is not only the sum of the throughput experienced by each satellite. For that sake, the inclusion-exclusion principle (ROSEN, 2002) can be utilized to determine the cardinality of the union of the sets of packets successfully received by each satellite, thereby discounting the intersections.

Now, let us consider an initial case where a cluster of IoT devices is covered by LEO satellites. Figure 2 shows the throughput versus the channel load, for the cases of a single satellite with different erasure probabilities $\varepsilon = 0.01$ or $\varepsilon = 0.9$, and the cases of $K = 2$ satellites with erasure probabilities $\varepsilon_1 = 0.01$ and $\varepsilon_2 = 0.9$. Moreover, in the Figure 2 we also show the sums of the individual throughputs seen by each of the $K = 2$ satellites, as well as the intersections of their throughputs. Recall that the actual throughputs are the differences between the sums of the individual throughputs and their intersections. Now, key aspects are listed below on the impact of erasure probabilities on throughput:

- First, considering the case of a single satellite, we can see from Figure 2 that a low erasure probability leads to a larger throughput at low channel loads, and a higher erasure probability is favorable at high channel loads. That is because a high erasure probability limits the collisions, which is desirable at high loads.

- However, a high erasure probability also leads to an inefficient utilization of the resources of the IoT devices. Interestingly, for $K = 2$ satellites, one with a low and another with a high erasure probability, imply large benefits, especially at low to moderate channel loads.

- The curves representing the sums and the intersections of the individual through-

Figure 2 – Throughput $\mathcal{T}$ versus channel load G, for $K = 1$ with erasure probabilities $\varepsilon \in \{0.01, 0.9\}$ and $K = 2$ with erasure probabilities $\varepsilon_1 = 0.01$ and $\varepsilon_1 = 0.9$ (analytical and simulation results). The curves in midnight blue and yellow represents the sum and intersection of the individual throughput seen at each satellite.
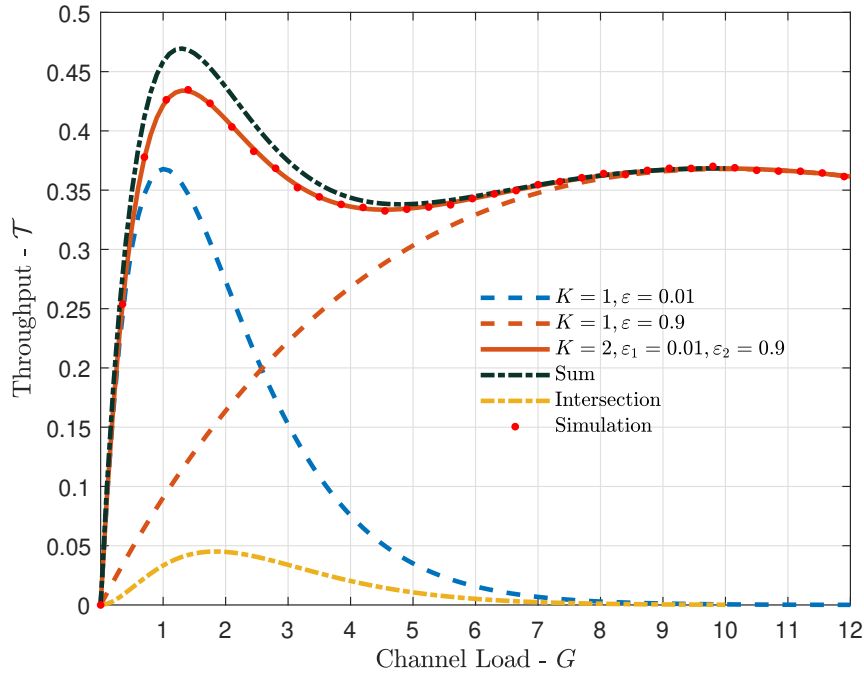
Source: The Author.

puts of the two satellites highlight the importance of removing multiplicities, as the intersection is non-negligible.

In this sense, considering the trade-offs between erasure probabilities and traffic behavior highlighted in Figure 2, if the traffic load is adequately allocated according to the erasure probability of that satellite lap, it would achieve higher throughput performance for a constellation topology. Following the above idea, the work presented in Chapter 2 introduces a novel strategy for traffic load allocation in DtS-IoT networks.

1.2.2 Efficient Uplink Transmission Scheduling Schemes in DtS-IoT Networks

To improve the efficiency of NTNs, MAC protocols should consider the implementation complexity and the satellite trajectory. Among the topics related to MAC and orbital dynamics, is the transmission scheduling of the devices. In (AFHAMISIS; PALATTELLA, 2022), the IoT devices transmit their data packets using Long Range (LoRa) technology (SEMTECH, 2022) in allocated time slots to a gateway installed onboard the satellite. The transmission time slots are assigned to each IoT device using the Scheduling Algorithm for LoRa to LEO Satellites (SALSA). When the First-Come-First-Serve (FCFS) policy is used in scenarios with a low density of ground nodes, the transmission

Figure 3 – The perceived elevation angle, with respect to the satellite, for 40 devices randomly deployed over the territory of France for an actual satellite lap (LacunaSat-3).
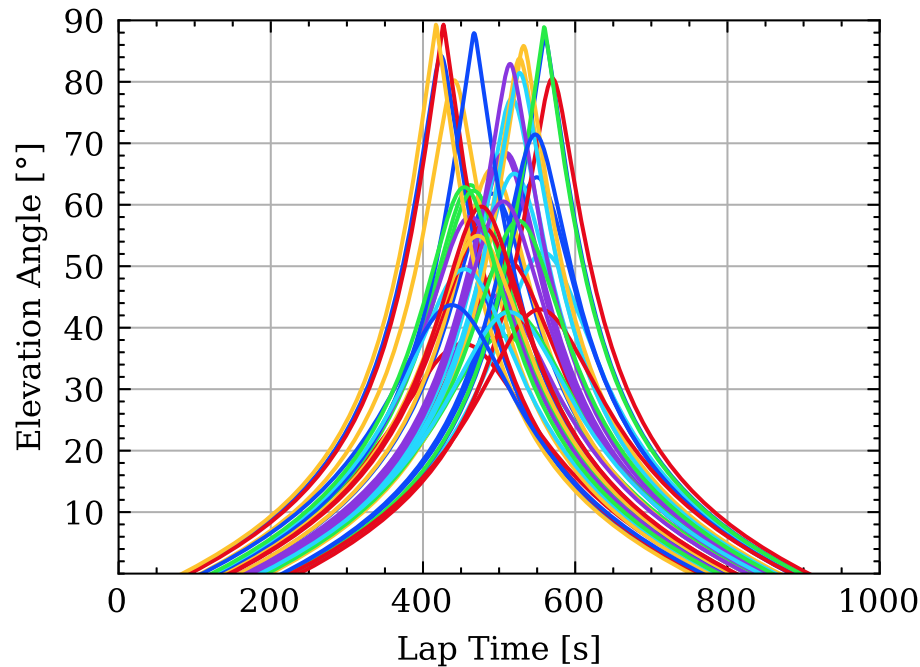
Source: The Author.

of each device mostly coincides with the first instant in which the satellite is visible to that device. However, as the number of devices increases, the scheduled transmissions decrease significantly due to multiple devices appearing within the satellite footprint almost simultaneously.

This is illustrated in Figure 3, for a real study case of the LacunaSat-3 (NANOSATS DATABASE, 2020) satellite orbiting over the region of France, with a total visibility window of around 800 seconds. The curves show the elevation angle versus time for each device. Even for 40 devices, it is notable that a good part of them have similar rise/set times leading to possible collided messages at the satellite. Despite the good performance delivered of SALSA (AFHAMISIS; PALATTELLA, 2022), the scheduling strategy that serves only the first visible IoT devices can lead to excessive network congestion or, even more importantly, to limited use of satellite coverage. To address these concerns, the work presented in Chapter 3 investigates and proposes new scheduling strategies that take advantage of multiple frequency channels and the ability to change the transmission scheduling order of some devices within a visibility time window to improve the network performance.

1.2.3 Advanced Power Domain Multiple-Access Techniques for DtS-IoT Networks

Although device scheduling is very effective in avoiding collisions, upcoming ground-to-space systems need to be highly adaptive, requiring great flexibility in resource allocation (WANG, A. et al., 2022). The amount of information and signaling demanded by scheduling techniques may be prohibitive in some DtS-IoT applications, so RA protocols become an alternative. However, despite their simplicity, RA protocols, like those employed by LoRaWAN, tend to suffer from low scalability and high collisions in dense deployments (GEORGIOU; RAZA, 2017). In NTN, the scenario worsens due to dynamic factors and temporal visibility constraints imposed throughout the satellite coverage lap.

NOMA approaches are candidate solutions to alleviate the number of unresolved collisions at the receiver and boost system efficiency (YAN et al., 2019). Furthermore, many research efforts investigate the application of power domain NOMA in DtS-IoT scenarios, but they predominantly focus on the downlink (GAO et al., 2020; M. EL-HALAWANY et al., 2022). Other studies improve the uplink performance using machine learning (TUBIANA et al., 2022) or cooperative non-orthogonal multiple access (C-NOMA) (GE et al., 2022) techniques. Regardless of the progress, the above approaches may be impractical due to the need for excessive gateway capabilities or extra information associated with device synchronization. Given the strong trend of serving a massive number of IoT devices, there is an opportunity to propose new solutions that enhance network performance in NTNs, particularly in reliability and energy efficiency.

Following recent research (ORTIGUEIRA et al., 2024), it can be assumed that IoT devices are empowered with a satellite orbit predictor. Then, one RA option is to let devices transmit in some positions spread within their visibility windows, so that due to their different geographical location it would be unlikely to have a collision. For instance, referring to Figure 3, note that if the devices, transmissions are adequately positioned at some predefined points within their visibility window, the collision probability is reduced. Moreover, knowing its relative position within the visibility windows, the device can use an appropriate power, such that NOMA and SIC become feasible at the satellite. Such options are explored in the work described in Chapter 4.

1.3 SCOPE AND ORGANIZATION OF THIS THESIS

This thesis focuses on efficient resource allocation strategies for LEO-based satellite IoT networks. Each chapter is derived from recently published or submitted works from this author that consider relevant improvements for performance indicators such as throughput, energy efficiency, and reliability. Moreover, in order to keep con-

sistency with the terminology used in the studies, an independent list of symbols is presented at the beginning of each chapter.

First, inspired by the authors of (MUNARI et al., 2021), in Chapter 2 we propose a DtS-IoT slotted Aloha system architecture that considers multiple satellite coverage and unequal erasure probabilities. This thesis investigates and proposes novel strategies for traffic load allocation to maximize the overall system throughput.

Then, in Chapter 3 we investigate further the SALSA scheduling algorithm for LoRa to LEO satellites introduced in (AFHAMISIS; PALATTELLA, 2022) and propose novel scheduling strategies for direct-to-satellite communication systems, considering new factors such as multiple channels, satellite visibility, and fairness.

In Chapter 4, considering the heterogeneity of device locations, we use the power domain NOMA to propose a new uplink RA method that considers dynamic non-geostationary parameters, such as the elevation angle and channel conditions.

Finally, Chapter 5 concludes the thesis and outlines future opportunities for advancing this work.

1.4 CONTRIBUTIONS

The main contributions of this thesis are summarized as follows:

1. A new strategy for traffic load allocation to maximize the throughput in DtS-IoT networks, including a traffic Load Allocation algorithm based on the Successive Convex Approximation (SCA) technique , as presented in Chapter 2;

2. Two new scheduling algorithms for LoRa-to-LEO networks with multiple channels, based on the SALSA algorithm, employing the permutation of scheduled times and channel alternation to improve uplink efficiency, as presented in Chapter 3;

3. Two novel DtS-IoT schemes using power domain NOMA in the uplink with either fixed or controlled transmit power to improve performance compared with regular Aloha, as presented in Chapter 4

1.4.1 Publications

The following works were published during the development of this thesis.

1. Tondo, F.A.; Montejo-Sánchez, S.; Pellenz, M.E.; Céspedes, S.; Souza, R.D. "Direct-to-Satellite IoT Slotted Aloha Systems with Multiple Satellites and Unequal Erasure Probabilities". Sensors 2021, 21, 7099. https://doi.org/10.3390/s21217099.

2. F. A. Tondo, V. D. P. Souto, O. L. Alcaraz López, S. Montejo-Sánchez, S. Céspedes and R. D. Souza, "Optimal Traffic Load Allocation for Aloha-Based IoT

LEO Constellations," in IEEE Sensors Journal, vol. 23, no. 3, pp. 3270-3282, 1 Feb.1, 2023, doi: 10.1109/JSEN.2022.3230796.

3. F. A. Tondo, M. Afhamisis, S. Montejo-Sánchez, O. L. A. López, M. R. Palattella and R. D. Souza, "Multiple Channel LoRa-to-LEO Scheduling for Direct-to-Satellite IoT," in IEEE Access, vol. 12, pp. 30627-30637, 2024, doi: 10.1109/AC-CESS.2024.3368872.

Moreover, the following work is currently under review:

1. Tondo, F.A.;J. M. de Souza Sant'Ana; Montejo-Sánchez, S.; O. L. Alcaraz López; Céspedes, S.; Souza, R.D. "Non-Orthogonal Multiple-Access Strategies for Direct-to-Satellite IoT Networks". Available from: https://arxiv.org/abs/2409.02748.

Finally, although not included in this thesis, the work in Chapter 2 was used as a basis for the development of information offloading techniques for DtS-IoT satellites, yielding the following publication:

1. Adanvo, V.F.; Mafra, S.; Montejo-Sánchez, S.;Tondo, F.A; Souza, R.D., "Improving Efficiency and Reliability in Information Offloading for LEO Satellite Networks by Inter-Satellite Communication Techniques", in IEEE Transactions on Aerospace and Electronic Systems, vol. 12, pp. 30627-30637, 2024, doi: 10.1109/TAES.2024.-3455312.

2 OPTIMAL TRAFFIC LOAD ALLOCATION FOR ALOHA-BASED IOT LEO CON-STELLATIONS

Since a single LEO satellite is insufficient for ubiquitous IoT services, and considering the trend towards employing satellite constellations in future networks (KASSAB et al., 2022), this chapter presents a novel strategy for optimizing traffic load allocation in DtS-IoT networks. Different from (MUNARI et al., 2021) and its extension in (TONDO et al., 2021), this chapter considers traffic allocation for enhanced throughput.

This chapter is organized as follows. Section 2.1 presents the related work. Section 2.2 describes the system model. Section 2.3 formulates the system throughput and presents the optimization problem in its original non-convex form. Section 2.4 adapts the SCA-based method to allocate the traffic load and transform the optimization problem into standard convex form. Section 2.5 discusses the numerical results, while Section 2.6 concludes the chapter. Moreover, Table 1 lists the symbols used in this chapter. Finally, the content of this chapter was published in (TONDO et al., 2023).

2.1 RELATED WORK

LEO satellite networks are known to have complicated spatial resource management, primarily due to the user association (JIANG et al., 2022), power constraints of the on-board battery (IVANOV et al., 2020) and traffic control (ZHANG, Z. et al., 2018). In (JIANG et al., 2022), a specific multi-objective user association problem was formulated for the overall service efficiency. In (IVANOV et al., 2020), the authors propose a spatial resource allocation intended to minimize handovers and to simplify the calculation of the time a user spends in each satellite beam spot. Moreover, in (ZHANG, Z. et al., 2018) the authors employ a technique called time-varying graphs to express temporal concepts and definitions of space satellite networks. Then, a temporal centrality-balanced traffic management scheme is further developed to enhance the network performance.

Note that IoT communication solutions based on satellite constellations must deal with situations where some satellites are under heavy traffic, while others are underutilized. These drawbacks are related to the constellation topology, the deployment of IoT devices on the ground, but fundamentally to the traffic load distribution. Therefore, it is necessary to consider different traffic load balancing strategies to reduce packet losses and to increase the system throughput. Indeed, several works introduced load balancing strategies in the last few years, as for instance (NANBA et al., 2004; LIU et al., 2021; LI, Z. et al., 2021; AL-HRAISHAWI et al., 2021; DI et al., 2019; LENG et al., 2021; KODHELI et al., 2021).

In (NANBA et al., 2004), a traffic distribution method based on linear programming that maximizes the accommodated traffic in a multiple satellite system under

Table 1 – List of Symbols - Chapter 2.

Variable	Description
G_m	Channel load at the mth position in packets per unit of time
m	Constellation position
$\emptyset$	Empty set
$\varepsilon_{m,k}$	Erasure probability at the mth position and k^{th} satellite
Q_m	Load factor offered by the IoT devices in the mth position
M	Number of constellation positions in each lap
K	Number of satellites in the constellation
u	Number of users transmitting in the same time-slot
$\alpha_{m,k}$	Number of data packets received by each LEO satellite
k	k-th Satellite in orbit
$\delta_{m,\mathbb{J}}$	Number of data packets received by multiple satellites per m constellation position
U	Poisson random variable
$\mathbb{P}$	Probability that u users transmit in the same time-slot
ω	Real number usually smaller than four
$q_{m,k}$	Success probability at the mth position and k^{th} satellite
s	Spacing between consecutive satellites
$\mathbb{J}$	Set containing the possible combinations of satellites within the constellation per position
ξ	Solution tolerance or accuracy
A	System throughput contribution per individual satellite
$\mathcal{T}_m$	System throughput for the mth position
B	System throughput portion of the multiplicities
$\mathcal{T}_{m,k}$	Throughput at the kth satellite in the mth position
G_T	Total channel load in packets per unit of time
$\beta_{m,\mathbb{J}}$	Total number of data packets per m constellation position
$\mathcal{T}_T$	Total system throughput
ε_m	Vector of erasure probabilities at the mth position
$\mathbf{Q}$	Vector that contains the load factors of all positions

Source: The Author.

satellite power constraints is proposed. In addition, the method considers the visibility probability in order to distribute the traffic to each satellite. In (LIU et al., 2021), the authors propose a load-balanced satellite handover strategy where a joint handover frequency and workload optimization problem is proposed in order to improve the system capacity. In addition, an adaptive power allocation algorithm is designed for a multiple satellite connection model. In (LI, Z. et al., 2021), the authors study an asymmetric resource allocation method in a satellite–terrestrial network and propose a model to achieve optimal resource allocation among different satellites. In (AL-HRAISHAWI et al., 2021), a novel load balancing scheduling algorithm is proposed to distribute data packets across the aggregated carriers based on channel capacities and to utilize the spectrum efficiently.

Moreover, a dense LEO based integrated terrestrial-satellite network is considered in (DI et al., 2019), while a scheduling strategy subject to backhaul capacity constraints to jointly maximize the sum rate and the number of served users is proposed. In addition, in (LENG et al., 2021), the authors study collaborative computing and resource allocation among multiple LEO satellites considering deep reinforcement learning and a max-min fairness optimization strategy to maximize the tasks completion rate. In (KODHELI et al., 2021), a LEO satellite based Narrowband Internet of Things (NB-IoT) system is investigated and a novel scheduling strategy to select the set of transmitting users is proposed to maximize a sum profit. The authors formulate different user profits based mainly on the visibility times of the LEO satellites.

However, the above works assume MAC based on TDMA (NANBA et al., 2004; LI, Z. et al., 2021; AL-HRAISHAWI et al., 2021; LIU et al., 2021) or CDMA (DI et al., 2019; KODHELI et al., 2021; LENG et al., 2021), which require tight synchronization and/or power control, and therefore demand a considerable amount of signalling that may be not practical for some IoT satellite networks (FERRER et al., 2019). In a different direction, a two-phase communication system is proposed in (MUNARI et al., 2021). In the first phase, multiple users transmit data packets to a set of uncoordinated satellites following a simple slotted Aloha policy. Then, in the second phase, the satellites forward the decoded information to a common sink. In (FORMAGGIO et al., 2020), differently from (MUNARI et al., 2021) where receivers could benefit from orthogonal channel access when transmitting to the sink, the authors focus on a case in which relays are also sharing a slotted Aloha channel when forwarding information. While in (KASSAB et al., 2022), the authors study the grant-free access for critical and noncritical services in space diversity-based models for both satellite and terrestrial applications.

Such setups are representative of some modern IoT LEO satellite networks with LoRaWAN technology, as those of Lacuna Space (LACUNA SPACE, 2023) and Swarm Space (SWARM SPACE, 2023). Moreover, the authors in (MUNARI et al., 2021) provide exact expressions for the system throughput at the first phase considering equal erasure probabilities at all satellites. However, considering equal erasure probabilities for all satellites in a LEO constellation may be unrealistic. Consequently, the model proposed in (MUNARI et al., 2021) is extended in (TONDO et al., 2021) considering different erasure probabilities at each of the visible satellites within the constellation. Moreover, an Intelligent traffic load distribution (ITLD) strategy is proposed therein to improve the overall system throughput by allocating different amounts of traffic load at different positions of the LEO constellation with respect to the IoT cluster. ITLD has been recognized in (AL-HRAISHAWI et al., 2023) as one of the recent and relevant random access techniques in the DtS-IoT context. Among all the highlighted schemes, ITLD is the only one that achieves such benefits in throughput and packet loss rate only through an allocation strategy. On the other hand, a framework of non-orthogonal

Table 2 – Review of the state-of-art on traffic allocation for LEO satellites based networks.

Ref. (First Author, Year)	Allocation Strategy	LEO Constellation	Efficiency-Aware (Throughput)	Elevation Angle	Suitability for DtS-IoT
(NANBA,2004)	Linear programming	✓	✗	✓	✗
(LIU,2021)	FBS.	✓	✗	✓	✗
(DI,2019)	Lagrangian multipliers	✓	✗	✓	✗
(LI,2021)	Predator˘prey model	✓	✗	✗	✗
(HRAISHAWI,2021)	Carrier aggregation	✗	✓	✗	✗
(WEN,2021)	DRL	✓	✓	✓	✗
(KODHELI,2021)	Linear programming	✗	✓	✓	✓
(MUNARI,2021)	Closed-form	✓	✓	✗	✓
(TONDO,2021)	ITLD	✓	✓	✓	✓

Source: The Author.

slotted Aloha protocol is proposed and analyzed in (WANG, Q. et al., 2018). In (CAS-SARÁ et al., 2020), interference cancellation is used to propose an analysis framework of diversity framed slotted Aloha. Moreover, in (ZHEN et al., 2020) a preamble and detection scheme is designed for high-dynamic LEO scenarios. Nevertheless, although ITLD (TONDO et al., 2021) exploits the potential of the different positions of the satellite constellation, using a very low complexity algorithm, it does not guarantee the optimum traffic load allocation and, consequently, the maximum system throughput may not be achieved.

Therefore, according to data traffic forecast reports in (CISCO VISUAL, 2020), more than 29 billion IoT devices will be connected to the Internet by 2023, while the number of Machine-to-Machine (M2M) connections will be 14.7 billion. In this sense, satellites can be used to offload part of the large traffic served by terrestrial networks. In (BACCO et al., 2018), the authors consider IoT/M2M data exchanges via satellite and random access techniques in order to accommodate a large set of devices. Based on energy availability, interest, and physical ties, although the work in (TSIROPOULOU et al., 2017) did not directly investigate the traffic load allocation strategies, they proposed a clustering approach that determines each device's optimal transmit power to meet the required quality of service, while the constraints are formulated via a holistic utility function.

Aiming to identify suitable benchmark schemes, Table 2 lists the state-of-the-art works on traffic load allocation for LEO satellites based networks. We can conclude that only the solutions in (KODHELI et al., 2022; MUNARI et al., 2021; TONDO et al., 2021) are suitable for the DtS-IoT scenario. However, in (KODHELI et al., 2022) the authors do not consider LEO constellations, while in (MUNARI et al., 2021) the authors focus on a single position with the same erasure probability for all satellites, what over simplifies the problem and prevents the generalization of the solution for the case of multiple positions and different erasure probabilities per satellite. Therefore, the methods that can be directly compared to the proposed approach are those in (TONDO et al., 2021).

2.1.1   Novelty and Contributions

Different from (NANBA et al., 2004; LIU et al., 2021; DI et al., 2019; LI, Z. et al., 2021; AL-HRAISHAWI et al., 2021; LENG et al., 2021; KODHELI et al., 2021), in this chapter we consider an Aloha-based network, which is in line with some practical LEO satellite networks for IoT. Using the model in (TONDO et al., 2021), where the satellites are considered to have different erasure probabilities, in this work we focus on the design of a traffic load strategy that maximizes the throughput of a direct-to-satellite[1] IoT system; guaranteeing ultra-scalability and efficient performance, without very high complexity processing that increases energy consumption in the satellite, as in (WANG, Q. et al., 2018; CASSARÁ et al., 2020; ZHEN et al., 2020). Finally, we innovate by introducing a novel algorithm based on the SCA technique (SCUTARI et al., 2014) that is able to maximize the traffic load allocation considering the different constellation positions[2]. By properly allocating the traffic load, the proposed method maximizes the system throughput, and considerably outperforms the heuristics introduced in (TONDO et al., 2021). Summarizing, the main contributions of this chapter are:

1. We propose an SCA-based optimization strategy that allocates the traffic load at each constellation position, maximizing the system throughput per lap.

2. We determine the optimal traffic load for each constellation topology and the best topology for each traffic load.

3. We demonstrate that the proposed strategy outperforms other load allocation methods proposed in the literature. We also demonstrate that, while other strategies fall to zero throughput under high traffic-load scenarios, our strategy always achieves a non-zero throughput by offloading the excess traffic to some constellation positions.

2.2   SYSTEM MODEL

We consider the uplink of an IoT network where a large number of devices directly transmit their data packets to a constellation of K LEO satellites using an Aloha-based protocol. Following (MUNARI et al., 2021; TONDO et al., 2021), the Earth-to-satellite links between the cluster of IoT devices and the LEO satellites are modeled according to the On-Off fading channel model (PERRON et al., 2003). Therefore, the quality of the link between each LEO satellite and the clustered IoT devices is defined by a given erasure probability. This model has been extensively used in the literature in the analysis of Aloha-based schemes (MUNARI et al., 2021; FORMAGGIO et al., 2020;

---

[1]   Direct-to-satellite IoT connectivity does not require a terrestrial gateway, simplifying and accelerating wide coverage deployment (FRAIRE, J. A. et al., 2019).

[2]   The satellite spacing control requires advanced techniques, and it is outside the scope of this thesis. However, with the rapid evolution of technology, the required orbit correction mechanisms should be available soon.

KASSAB et al., 2022; TONDO et al., 2021). It describes well the behavior of channels[3] whose losses are dominated by factors related to the presence of obstacles (MUNARI et al., 2021), which is typical of satellite IoT networks. Besides being of engineering significance, the On-Off fading model is mathematically amenable.

Since we consider the satellites can be in different positions with respect to the IoT devices, it is not practical to assume that all satellites perceive the same erasure probability as in (MUNARI et al., 2021). Instead, following (TONDO et al., 2021), we consider that the erasure probability seen at each satellite depends on its orbital position (or elevation angle) with respect to the clustered IoT devices. Moreover, a position is defined as the regular angle range (relative to the Earth's center) within the satellite trajectory where the erasure probability with respect to the clustered IoT devices can be assumed constant. For instance, the positions can be regarded as the so called sectors in (LOPEZ-SALAMANCA et al., 2022), which are defined by a range of elevation angles with respect to the IoT cluster that present similar error performance. Therefore, positions related to an elevation angle (relative to the clustered IoT devices on the ground) closer to $90°$ present a smaller erasure probability than those positions that correspond to elevation angles closer to $0°$ or $180°$. Moreover, the erasure probabilities could be determined as the average outage probability in a position, or in a sector, using the terminology in (LOPEZ-SALAMANCA et al., 2022). Thus, the On-Off fading channel is a relatively simple model, but still representative of satellite communications.

We define an iteration as the time that each satellite remains in the same position, while we assume that different constellation positions last for approximately the same time. Consequently, each iteration has the duration of a transmission window with the same erasure probabilities, which for simplicity we analyze in a single time slot. Besides multiple satellites, we consider M visible satellite constellation positions, and that $\varepsilon_{m,k}$ denotes the erasure probability between the kth satellite and the cluster of IoT devices in the mth constellation position, for $k \in \{1, 2, \cdots K\}$ and $m \in \{1, 2, \cdots M\}$. Moreover, each position is characterized by a vector of erasure probabilities $\varepsilon_m = [\varepsilon_{m,1}, \varepsilon_{m,2}, \cdots, \varepsilon_{m,K}]$. We associate the highest erasure probabilities to positions close to the horizon and the smallest ones to positions close to the zenith.

In addition, every passing of the satellite constellation over the IoT cluster is termed a lap. The number of positions M in which at least one satellite is visible depends on the number of satellites in the constellation and on the spacing s, in number of positions, between consecutive satellites. If the K satellites travel together and are always considered to be in the same position, then $s = 0$; if the satellites are distributed in K consecutive positions, then $s = 1$; while $s > 1$ implies that between two consecutive

---

[3] Note that it is reasonable to assume that channel conditions do not vary significantly during a time slot. That is because the typical DtS-IoT transmission is faster than the time for the elevation angle to move a sufficiently amount of degrees that would change the channel behavior (LOPEZ-SALAMANCA et al., 2022).

Table 3 – Satellite constellations with $K = 2$ satellites and spacing $s \in \{0, 1, 2, 3, 4\}$. Erasure probabilities ε_m at each visible position $m = \{1, 2, \ldots, M\}$. Non-visible positions (*i.e.,* $\varepsilon_m = \mathbf{1}$) are marked with "-".

s	Satellite	ε_1	ε_2	ε_3	ε_4	ε_5	ε_6	ε_7	ε_8
0	$k = 1$	0.9	0.5	0.5	0.9	-	-	-	-
	$k = 2$	0.9	0.5	0.5	0.9	-	-	-	-
1	$k = 1$	0.9	0.5	0.5	0.9	1.0	-	-	-
	$k = 2$	1.0	0.9	0.5	0.5	0.9	-	-	-
2	$k = 1$	0.9	0.5	0.5	0.9	1.0	1.0	-	-
	$k = 2$	1.0	1.0	0.9	0.5	0.5	0.9	-	-
3	$k = 1$	0.9	0.5	0.5	0.9	1.0	1.0	1.0	-
	$k = 2$	1.0	1.0	1.0	0.9	0.5	0.5	0.9	-
4	$k = 1$	0.9	0.5	0.5	0.9	1.0	1.0	1.0	1.0
	$k = 2$	1.0	1.0	1.0	1.0	0.9	0.5	0.5	0.9

Source: The Author.

satellites there is always $s - 1$ empty positions. Hereinafter, we refer to constellation positions as those in which at least one satellite is visible. The first position is the one in which the leading satellite is visible for the first time in the current lap, and the last position is the one in which the last satellite is seen for last time.

Example 1 *Figure 4 presents the system model considering $K = 2$ satellites traveling in adjacent positions (i.e., $s = 1$) with erasure probabilities*[4] $\varepsilon_m = [\varepsilon_{m,1}; \varepsilon_{m,2}]$ *such that each $\varepsilon_{m,k} \in \{1, 0.9, 0.5\}$.*

When the first satellite is seen for the first time by the IoT cluster, the vector of erasure probabilities is $\varepsilon_1 = [0.9; 1]$. Note that $\varepsilon_{1,2} = 1$ means that the second satellite is not yet seen by the IoT devices. In the next position, the second satellite appears on the horizon, then $\varepsilon_2 = [0.5; 0.9]$. In a similar way, in the third and fourth positions $\varepsilon_3 = [0.5; 0.5]$ and $\varepsilon_4 = [0.9; 0.5]$, respectively. Finally, in the fifth position, the first satellite leaves the visible horizon and similar to the first position only one satellite (now the second satellite) is visible, so that $\varepsilon_5 = [1; 0.9]$. Similarly, Table 3 illustrates the erasure probabilities at each position for a different satellite spacing[5] *s. Note that, the number of visible constellation positions increases with the satellite spacing, but the number of positions with both visible satellites decreases.*

---

[4] The particular value of the erasure probability depends on distance, carrier frequency, antenna gains, data rate, noise figure, random blockages, etc. Calculating the erasure probability for a given setup is outside the scope of this work. The aim is to provide tools for traffic load allocation. Although the values of the erasure probabilities are arbitrary, we can assume that is a good approximation based on the traditional On-Off fading channel literature (KASSAB et al., 2022; BERIOLI et al., 2016; MUNARI et al., 2015, 2021; PERRON et al., 2003; TONDO et al., 2021) and also studies such as (GONGORA-TORRES et al., 2022), where the authors estimate the outage probability as a function of the elevation angle.

[5] The satellite spacing control requires advanced techniques, and it is outside the scope of this work. However, with the rapid evolution of technology, the required orbit correction mechanisms should be available soon.

Figure 4 – Snapshots of the $M = 5$ visible positions of a constellation with $K = 2$ satellites with spacing $s = 1$.
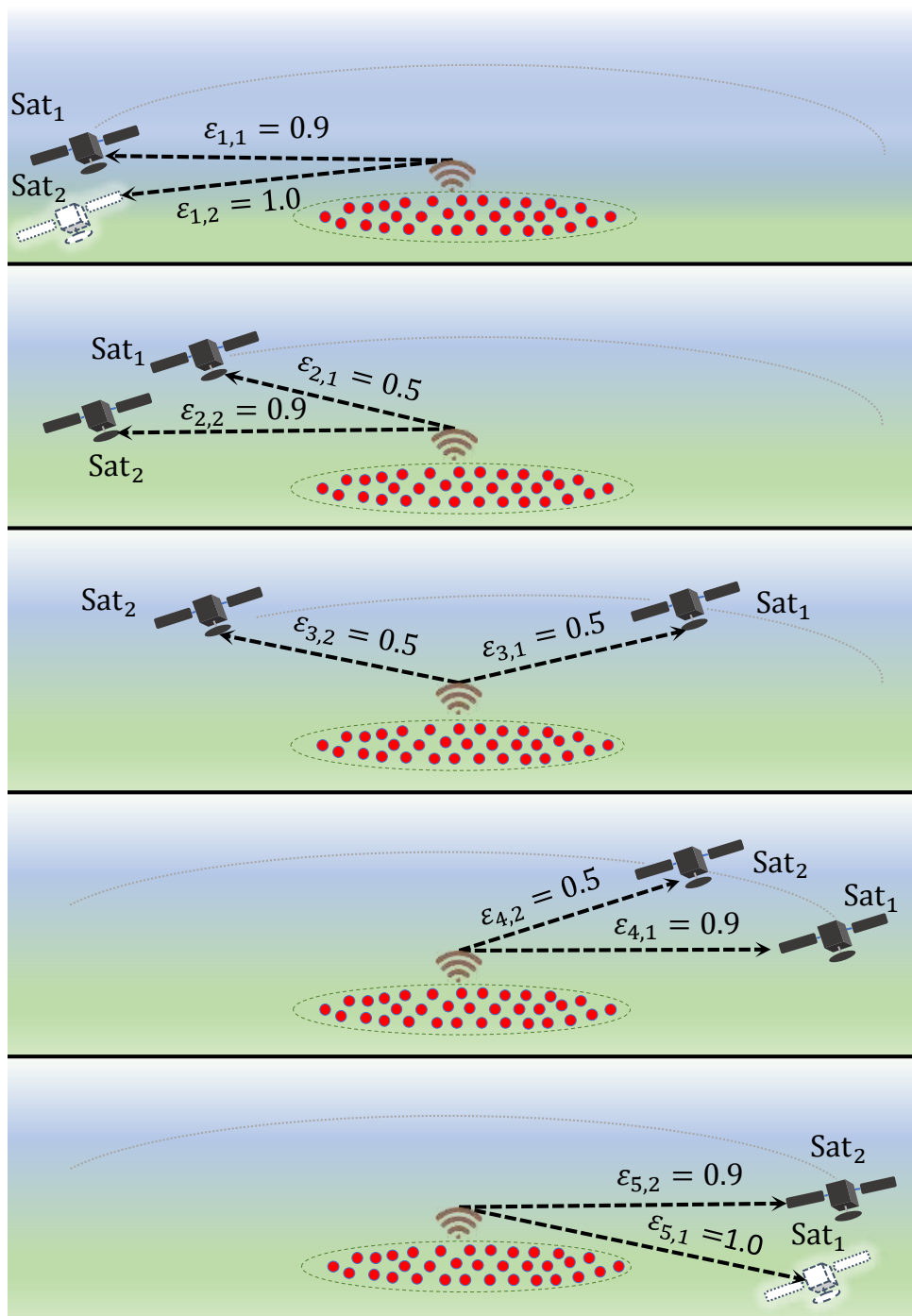
Source: The Author.

2.3   SYSTEM THROUGHPUT

We assume that a large number of clustered IoT devices share the same direct-to-satellite IoT communication, but with a very low probability of individual transmission. Therefore, the number of users accessing the channel in the same time slot per position can be modeled as a Poisson random variable U (MUNARI et al., 2021). Consequently,

the probability that u users transmit in the same time slot, considering the mth constellation position, follows the Poisson probability distribution,

$$\mathbb{P}[U = u] = \frac{(G_m)^u e^{-G_m}}{u!}, \tag{1}$$

where G_m denotes the channel load offered to the mth constellation position, such that the total channel load offered per lap (G_T) is the sum of all the loads offered at the M visible positions, *i.e.*, $G_T = \sum_{m=1}^{M} G_m$. Since u different IoT devices can transmit at the same time slot, the probability that the kth satellite successfully receives a data packet is $q_{m,k}(u) = u(1 - \varepsilon_{m,k})(\varepsilon_{m,k})^{u-1}$. Therefore, the average number of data packets successfully received at the kth satellite in a given time slot in the mth constellation position is

$$
\begin{aligned}
\mathcal{T}_{m,k} &= \sum_{u=0}^{\infty} q_{m,k}(u) \, \mathbb{P}[U = u] \\
&= \sum_{u=0}^{\infty} \left[u(1 - \varepsilon_{m,k})(\varepsilon_{m,k})^{u-1} \frac{(G_m)^u e^{-G_m}}{u!} \right] \\
&= G_m(1 - \varepsilon_{m,k}) e^{-G_m(1-\varepsilon_{m,k})} \\
&= Q_m \alpha_{m,k} e^{-Q_m \alpha_{m,k}}, \tag{2}
\end{aligned}
$$

where

$$\alpha_{m,k} = G_T(1 - \varepsilon_{m,k}), \tag{3}$$

and Q_m is the fraction of the total load that is offered by the IoT devices in the mth constellation position, such that $0 \leq Q_m \leq 1$, $\sum_{m=1}^{M} Q_m = 1$ and $G_m = Q_m G_T$, so that $G_T = \sum_{m=1}^{M} Q_m G_T$.

The system throughput for the mth position is defined as the number of different data packets received by at least one satellite at each time slot. Therefore, multiplicities must be discarded, *i.e.*, when data packets are successfully received by more than one satellite. In (TONDO et al., 2021), it is shown that the system throughput in this case becomes

$$
\begin{aligned}
\mathcal{T}_m &= \sum_{\substack{\forall \mathbb{J} \subseteq \{1,\cdots,K\} \\ \mathbb{J} \neq \emptyset}} \frac{(-1)^{|\mathbb{J}|+1} G_m \prod_{k \in \mathbb{J}}(1 - \varepsilon_{m,k})}{e^{G_m(1-\prod_{k \in \mathbb{J}} \varepsilon_{m,k})}} \\
&= \sum_{\substack{\forall \mathbb{J} \subseteq \{1,\cdots,K\} \\ \mathbb{J} \neq \emptyset}} (-1)^{|\mathbb{J}|+1} Q_m \beta_{m,\mathbb{J}} \, e^{-Q_m \delta_{m,\mathbb{J}}},
\end{aligned} \tag{4}
$$

where

$$\beta_{m,\mathbb{J}} = G_T \prod_{k \in \mathbb{J}}(1 - \varepsilon_{m,k}), \tag{5}$$

$$\delta_{m,\mathbb{J}} = G_T \left(1 - \prod_{k \in \mathbb{J}} \varepsilon_{m,k} \right), \tag{6}$$

and $\mathbb{J}$ is a set containing the possible combinations of satellites within the constellation.

In order to facilitate the understanding, in the particular case of $K = 2$ satellites we have the set $\mathbb{J} = \left\{ \{1\}, \{2\}, \{1,2\} \right\}$ and therefore its throughput can be computed as

$$\mathcal{T}_m = \underbrace{\sum_{k=1}^{2} Q_m \alpha_{m,k} e^{-Q_m \alpha_{m,k}}}_{(I)} \underbrace{- Q_m \beta_{m,\{1,2\}} e^{-Q_m \delta_{m,\{1,2\}}}}_{(II)} \tag{7}$$

where (I) is the contribution of each satellite to the throughput at that position, while (II) compensates for multiplicities[6] (when both satellites receive the same packet, which should not increase the throughput further). In general, there will be K terms in (I), while all the combinations with more than a single satellite among K satellites would appear in (II) (ROSEN, 2002). For the proof, please refer to Appendix A.

Finally, from the above it is clear that the system throughput is directly influenced by the number of LEO satellites, their positions, and erasure probabilities, as stated in (4). Another factor that greatly influences the system throughput per position (per lap) is the traffic load per position (per lap). Let us define the total system throughput as the sum of the contributions of each constellation position, i.e.

$$\mathcal{T}_T = \sum_{m=1}^{M} \mathcal{T}_m(Q_m, G_T). \tag{8}$$

Therefore, to maximize the overall system throughput it is necessary to adequately accommodate the traffic load offered per lap (G_T) by the IoT devices in the traffic load for each constellation position (G_m), according to the satellite constellation topology. Thus, the following optimization problem can be defined,

$$
\begin{aligned}
\underset{\mathbf{Q}}{\text{Maximize}} \quad & \mathcal{T}_T = \sum_{m=1}^{M} \mathcal{T}_m(Q_m, G_T) \\
\text{subject to:} \quad & \sum_{m=1}^{M} Q_m = 1, \\
& 0 \leq Q_m \leq 1 \,\forall\, m.
\end{aligned}
\tag{9}
$$

where $Q_m \in \mathbf{Q}$ and $\mathbf{Q}$ is the vector that contains the load factors of all positions (*i.e.,* $\mathbf{Q} = [Q_1, \cdots, Q_m, \cdots, Q_M]$).

Unfortunately, the above optimization problem is non-convex since $\mathcal{T}_m(Q_m, G_T)$ is a sum of non-linear concave and convex functions. For instance, note that part (I)

---

[6] Note that, $\beta_{m,\{1,2\}} = G_T(1 - \varepsilon_{m,1})(1 - \varepsilon_{m,2})$ and $\delta_{m,\{1,2\}} = G_T(1 - \varepsilon_{m,1}\varepsilon_{m,2})$, while $\beta_{m,\{k\}} = \delta_{m,\{k\}} = \alpha_{m,k}$, so $\beta_{m,\mathbb{J}}$ and $\delta_{m,\mathbb{J}}$ must be used only for $|\mathbb{J}| > 1$.

in (7) is concave, while part (II) is convex. Thus, standard convex optimization tools cannot be directly applied. In the following section, we propose a novel traffic allocation strategy based on the SCA technique. For the sake of simplicity, to properly allocate the traffic load, we consider the IoT devices' positions are perfectly known, all IoT devices in each lap share the same visibility time (which is valid for clusters of small size), and that there is an efficient mechanism to estimate the rise and set time of each satellite.

2.4 SCA-BASED OPTIMIZATION METHOD

The optimization problem in (9) can be solved by the SCA method (SCUTARI et al., 2014), which has been used for solving nonconvex optimization problems, where in each iteration the nonconvex feasible set is approximated by an inner convex approximation (BECK et al., 2010). The SCA approach has been used in several optimization problems related to wireless communications in (DU et al., 2016; DENG et al., 2020; KUMAR et al., 2021; ZHANG, X. et al., 2022; LÓPEZ et al., 2022), as well as in IoT networks assisted by satellites (DAI et al., 2020; MAO et al., 2020; MA et al., 2021; FANG et al., 2023).

First, let us rewrite (4) as a function of Q_m, as

$$
\mathcal{T}_T = \sum_{m=1}^{M} \sum_{\substack{\forall \mathbb{J} \subseteq \{1, \cdots, K\} \\ \mathbb{J} \neq \emptyset}} (-1)^{|\mathbb{J}|+1} \, Q_m \beta_{m,\mathbb{J}} \, e^{-Q_m \delta_{m,\mathbb{J}}} \, .
\tag{10}
$$

Then, (10) can be approximated around a fixed operating point $\tilde{Q}$ as $\mathcal{T}_T = A(\mathbf{Q}) + \widetilde{B}(\mathbf{Q}, \widetilde{\mathbf{Q}})$. The function $A(\mathbf{Q})$ collects the system throughput contribution of each individual satellite, at each position, to the overall throughput as

$$
A(\mathbf{Q}) = \sum_{m=1}^{M} \sum_{k=1}^{K} Q_m \alpha_{m,k} e^{-Q_m \alpha_{m,k}},
\tag{11}
$$

while $\widetilde{B}(\mathbf{Q}, \widetilde{\mathbf{Q}})$ compensates the multiplicities, and at a certain iteration it can be written as

$$
\begin{aligned}
\widetilde{B}(\mathbf{Q}, \widetilde{\mathbf{Q}}) &= B(\widetilde{\mathbf{Q}}) + \sum_{m=1}^{M} (Q_m - \widetilde{Q}_m) \frac{d}{dQ_m} B(Q_m) \Big|_{Q_m = \widetilde{Q}_m} \\
&= \sum_{m=1}^{M} Q_m C_m(\widetilde{Q}_m) + \underbrace{B(\widetilde{\mathbf{Q}}) - \sum_{m=1}^{M} \widetilde{Q}_m C_m(\widetilde{Q}_m)}_{\text{constant}}
\end{aligned}
\tag{12}
$$

by using the first-order Taylor approximation of $B(\mathbf{Q})$ around $\tilde{\mathbf{Q}}$, where

$$
C_m(\widetilde{Q}_m) = \frac{d}{dQ_m} B(Q_m) \Big|_{Q_m = \widetilde{Q}_m}
\tag{13}
$$

and

$$B(\mathbf{Q}) = \sum_{m=1}^{M} \sum_{\substack{\mathbb{J} \subseteq \{1,\dots,K\} \\ |\mathbb{J}|>1}} (-1)^{|\mathbb{J}|+1} Q_m \beta_{m,\mathbb{J}} \, e^{-Q_m \delta_{m,\mathbb{J}}}. \tag{14}$$

Then, the optimization problem in (9) can be approximated in the vicinity of $\widetilde{\mathbf{Q}}$ to

$$\underset{\mathbf{Q}}{\text{Minimize}} \quad \widetilde{\mathcal{T}}_T = -A(\mathbf{Q}) - \sum_{m=1}^{M} Q_m C_m(\widetilde{Q}_m)$$

$$\text{subject to:} \sum_{m=1}^{M} Q_m - 1 = 0, \tag{15}$$

$$-Q_m \leq 0 \, \forall \, m,$$

$$Q_m - 1 \leq 0 \, \forall \, m,$$

which is in a standard convex form (BOYD; VANDENBERGHE, 2004).

The optimization problem in (15) can be efficiently solved using standard convex optimization tools of Matlab® such as CVX (GRANT; BOYD, 2020) or fmincon (THE MATHWORKS, 2022). Moreover, interior point methods (VARGAS et al., 1993), which are known to converge in/with polynomial time/complexity, are commonly utilized for such a convex problem (YE, 2011). Notice that since there are M variables and $2M + 1$ constraints, the overall complexity of solving (15) using interior point methods is $\mathcal{O}(M^\omega \log(1/\xi))$, where ξ captures the solution tolerance or accuracy and ω is some real number usually smaller than four (YE, 2011).

Once (15) is solved, its output yields a new operating point $\widetilde{\mathbf{Q}}$ around which the linearization in (12) can be recalculated, leading to a new solution to the problem in (15). Such process can be iterated until a given convergence criteria is reached. Algorithm 1 summarizes the proposed iterative technique based on SCA for computing the optimal traffic load at each constellation position. Finally, notice that the overall complexity of Algorithm 1 is $\mathcal{O}(NM^\omega \log(1/\xi))$ assuming a fixed number N of iterations.

Algorithm 1 Traffic Load Allocation based on SCA

1: **Input**: $\{K, M, \varepsilon_m, G_T\}$: number of satellites, total visible constellation positions, the vector of erasure probabilities and the traffic load offered per lap;

2: Choose load factors $\{\widetilde{Q}_m\}$ such that problem constraints in (15) are satisfied, $\forall m \in \{1, 2, \cdots M\}$;

3: **Repeat:**

4:    Compute $\{Q_m\}$ by solving (15), $\forall m \in \{1, 2, \cdots M\}$;

5:    Update $\{\widetilde{Q}_m\} \leftarrow \{Q_m\}$;

6: **Until** convergence within a given tolerance or the maximum number of iterations is reached;

7: **Output:** $Q_m, \forall m \in \{1, 2, \cdots M\}$.

2.5   NUMERICAL RESULTS

In this section, we evaluate the performance of the proposed traffic allocation strategy. In addition, we discuss the impact of the different positions and topologies of the satellite constellation on system throughput. Without loss of generality, we assume a constellation with K = 2 satellites and erasure probabilities belonging to the set $\{1, 0.9, 0.5\}$[7]. We comparatively evaluate the performance of the proposed SCA-based technique against three other traffic load distributions (presented and discussed in (TONDO et al., 2021)): *i)* Uniform, which equally distributes the traffic load among all visible positions of the constellation. Considering both fixed total traffic load and number of satellites in the constellation, topologies with a larger number of positions allocate a lower traffic load to each position, while topologies with fewer positions must allocate a higher traffic load to each one. However, this approach does not consider the satellite location or the number of satellites visible to the cluster at each position within the constellation. In such cases, performance tends to be limited, as the allocated load may be either overly optimistic or overly pessimistic, depending on the specific erasure probabilities; *ii)* Non-uniform, which assigns to each visible position of the constellation a traffic load proportional to the performance of this position when it receives a uniform traffic load. Thus, the traffic load offered in each position of the satellite constellation is proportional to the normalized system throughput that would be achieved in the same position with uniform load distribution; and *iii)* ITLD, which conveniently selects between the Uniform and Non-uniform distribution to achieve a higher overall throughput according to the total traffic load per lap. For more information about ITLD algorithm, please refer to Appendix B.

Figure 5 shows the overall throughput achieved as a function of the traffic load per lap. The satellite constellation topology features satellites traveling in adjacent positions, *i.e. s* = 1, while five constellation positions are visible for the clustered IoT devices with the following erasure probabilities $[\varepsilon_{m,1}, \varepsilon_{m,2}] \in \{[0.9, 1], [0.5, 0.9], [0.5, 0.5], [0.9, 0.5], [1, 0.9]\}$. We evaluate the performance of the SCA-based technique compared to the use of ITLD (TONDO et al., 2021), as well as the Uniform and Non-uniform traffic load distributions analyzed in (TONDO et al., 2021). The SCA-based technique outperforms all other allocation methods.

Note that, the overall maximum throughput is reached by our proposal for G_T = 28.4, a value for which ITLD performs poorly. For that total traffic load the Uniform distribution has already saturated the tolerated traffic load for some positions, while

---

7   In (TONDO et al., 2021), $\varepsilon = \{1, 0.9, 0.8, 0.7, 0.6, 0.5, 0.4, 0.3, 0.2, 0.1, 0.01\}$, while we show that the throughput increases with the number of satellites in the constellation. However, note that a scenario with more possibilities in terms of erasure probabilities increases the number of visible positions. Moreover, increasing the number of satellites also increases the number of possible topologies. Since the goal of this chapter is to demonstrate the validity of the proposed optimization strategy, we avoid the computational cost associated with large scenarios and focus on the case of K = 2 satellites.

Figure 5 – Overall throughput as a function of the traffic load per lap considering the proposed SCA-based technique, ITLD, PSO, Uniform, and Non-uniform traffic load distributions. We assume a satellite constellation with $K = 2$ and $s = 1$.

Source: The Author.
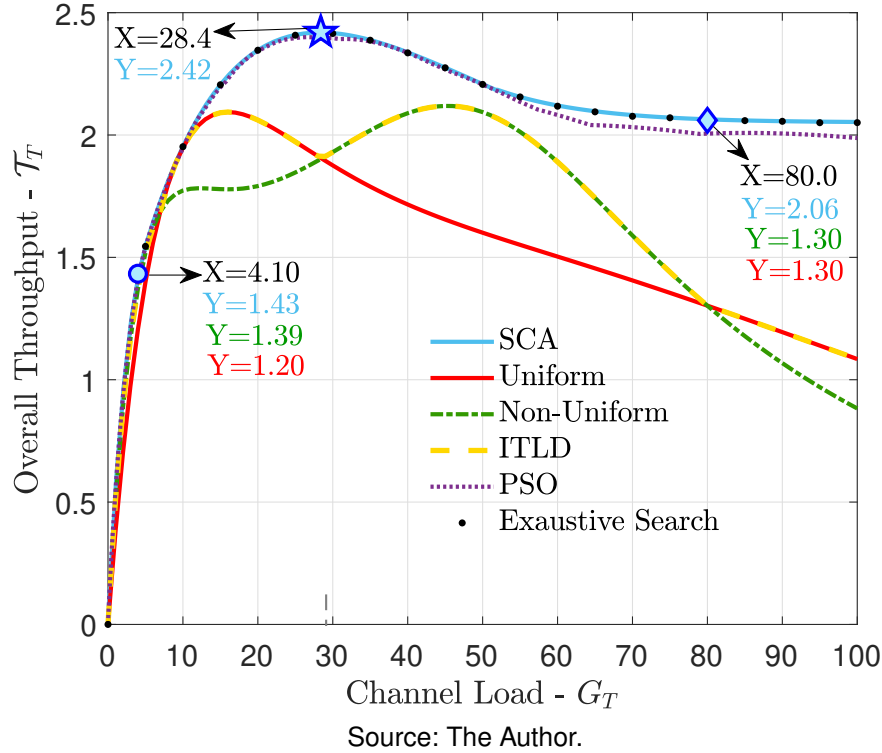
the Non-uniform distribution still does not sufficiently exploit the positions that can take high traffic loads. By its turn, the SCA-based technique allocates the traffic load to each position so that the overall throughput is the maximum achievable for the generated traffic load per lap. That is confirmed by the exhaustive search results for the maximum throughput (which are represented by black dots). The allocation strategy proposed here also guarantees that, even for very high traffic loads, the overall performance of the system remains above 2 for this topology. However, when the other allocation strategies are used, the overall throughput tends to 0 when the traffic load is extremely high. This is because our proposal assigns the excess traffic load only to the position with the least contribution in terms of system throughput, therefore not harming the overall throughput.

Moreover, three critical points are marked in blue in the throughput curve of the proposed SCA-based technique in Figure 5: *i)* a circle indicates the system throughput ($\mathcal{T}_T$ = 1.43) for low traffic load (G_T = 4.1); *ii)* a star identifies the optimum overall throughput ($\mathcal{T}_T$ = 2.42), which is reached at the optimum traffic load (G_T = 28.4) for this topology; and *iii)* a diamond indicates the system throughput ($\mathcal{T}_T$ = 2.06) when the traffic load is high (G_T = 80) and the performance tends to remain stable for our strategy. The projections of these points, the vertical dashed lines, allow identifying the

Figure 6 – Load factor Q_m in the scenario with five positions. The markers here are located in the same traffic load as in Figure 5, the circle in $G_T = 4.1$, the star in $G_T = 28.4$, and the diamond in $G_T = 80$.
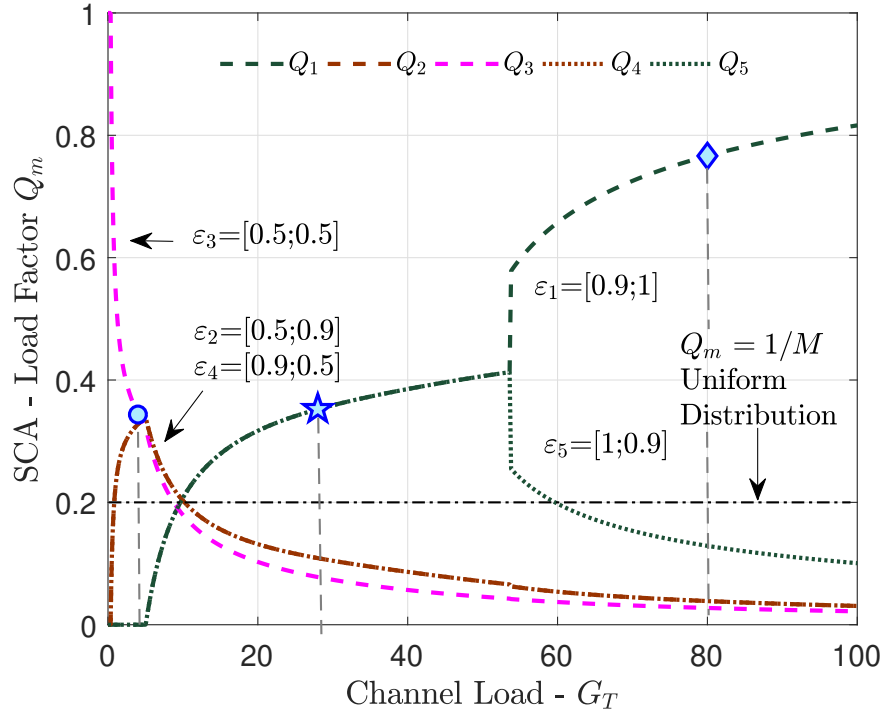
(a) Load factor Q_m selected by the proposed SCA-based optimization technique for each constellation position as a function of G_T.
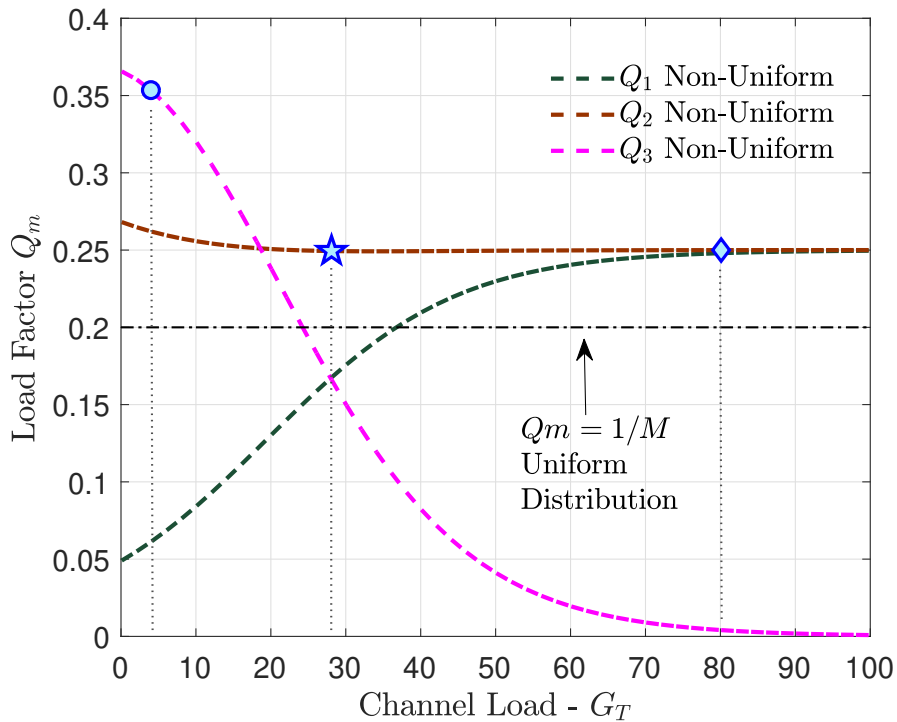
(b) Load factor Q_m selected by the Non-Uniform and Uniform distributions for each constellation position as a function of G_T. Note that in the Non-uniform distribution always $Q_1 = Q_5$ and $Q_2 = Q_4$.

Source: The Author.

throughput achieved by the other traffic allocation strategies. Note that these values are highlighted in colored text corresponding to each strategy in the legend.

Figure 6a shows the load factors for each constellation position according to the traffic load per lap when it is used the SCA-based technique, while Figure 6b shows the load factors for the Non-Uniform and Uniform distributions. Note that load factors $Q_m \in \{Q_1, Q_2, Q_3, Q_4, Q_5\}$ are related to erasure probabilities as follows $[\varepsilon_{m,1}, \varepsilon_{m,2}] \in \{[0.9, 1], [0.5, 0.9], [0.5, 0.5], [0.9, 0.5], [1, 0.9]\}$, which presupposes a symmetry between the factors $[Q_1, Q_5]$ and $[Q_2, Q_4]$, given the symmetry between the erasure probabilities in both cases, but Q_3 is associated with a unique position in the lap, with $[\varepsilon_{3,1}, \varepsilon_{3,2}] = [0.5, 0.5]$.

The analysis of the blue circle in Figure 5 and Figure 6a shows that when the traffic load is very low, it is very inefficient to allocate part of that traffic load to positions with high erasure probabilities $[\varepsilon_{m,1}, \varepsilon_{m,2}] \in \{[0.9, 1], [1, 0.9]\}$. That is why the SCA-based optimization technique assigns values close to 0 to Q_1 and Q_5. In such cases, it is better to exploit positions with lower erasure probabilities $[\varepsilon_{m,1}, \varepsilon_{m,2}] \in \{[0.5, 0.9], [0.5, 0.5], [0.9, 0.5]\}$, since the collision probabilities at the receiver are very low due to the low traffic load. Consequently, the proposed SCA-based technique selects $Q_1 = Q_5 \approx 0$, while $Q_2 = Q_4 \approx Q_3 \approx 0.33$, to exploit constellation positions suitable for low traffic load. However, Figure 6b shows that the Non-Uniform distribution approach selects $Q_1 = Q_5 \approx 0.06$, which prevents fully exploiting positions 2 and 4. Meanwhile, the Uniform distribution approach performs even worse, since it assigns $Q_m = 0.2 \; \forall m \in \{1, 2, 3, 4, 5\}$, thus perceiving unnecessary losses in the first and last positions.

Figure 7 shows the system throughput for each position and each allocation strategy. Note that there are only three curves for five positions due to the symmetry of positions 1 and 5 and positions 2 and 4. Moreover, considering $G_T = 4.1$, which corresponds to the blue circle in Figure 6, the system throughput achieved by the SCA-based technique (i.e., the sum of the throughput achieved in each position), is $\mathcal{T}_T = 2 \times 0 + 2 \times 0.429 + 0.573 = 1.43$ outperforming the Non-Uniform distribution with $\mathcal{T}_T = 2 \times 0.024 + 2 \times 0.385 + 0.579 = 1.39$ and even more the Uniform distribution with $\mathcal{T}_T = 2 \times 0.073 + 2 \times 0.316 + 0.426 = 1.20$, see Figure 5.

In addition, the comparative analysis of the curves in Figure 7 allows us to confirm that under conditions of low traffic load, the highest system throughput is associated with the positions with the lowest erasure probabilities. This is because in such conditions the probability of collisions is very low and it is more important to avoid the losses associated with the channel. Note that the highest throughput is associated with the central position where $[\varepsilon_{3,1}, \varepsilon_{3,2}] = [0.5, 0.5]$. Moreover, as one would expect, intermediate positions with $[\varepsilon_{2,1}, \varepsilon_{2,2}] = [0.5, 0.9]$ and $[\varepsilon_{4,1}, \varepsilon_{4,2}] = [0.9, 0.5]$ outperform near-horizon positions with $[\varepsilon_{1,1}, \varepsilon_{1,2}] = [0.9, 1]$ and $[\varepsilon_{5,1}, \varepsilon_{5,2}] = [1, 0.9]$.

Figure 7 – Throughput contribution for each position. The circles indicate the traffic load distribution per position G_m when $G_T = 4.1$ for: proposed SCA-based method (in blue), Uniform (in red) and Non-Uniform (in green) allocations. We take advantage of the symmetry between $\varepsilon_1 = [0.9, 1]$ and $\varepsilon_5 = [1, 0.9]$, as well as $\varepsilon_2 = [0.5, 0.9]$ and $\varepsilon_4 = [0.9, 0.5]$, to represent each position pair by a single curve.

Source: The Author.
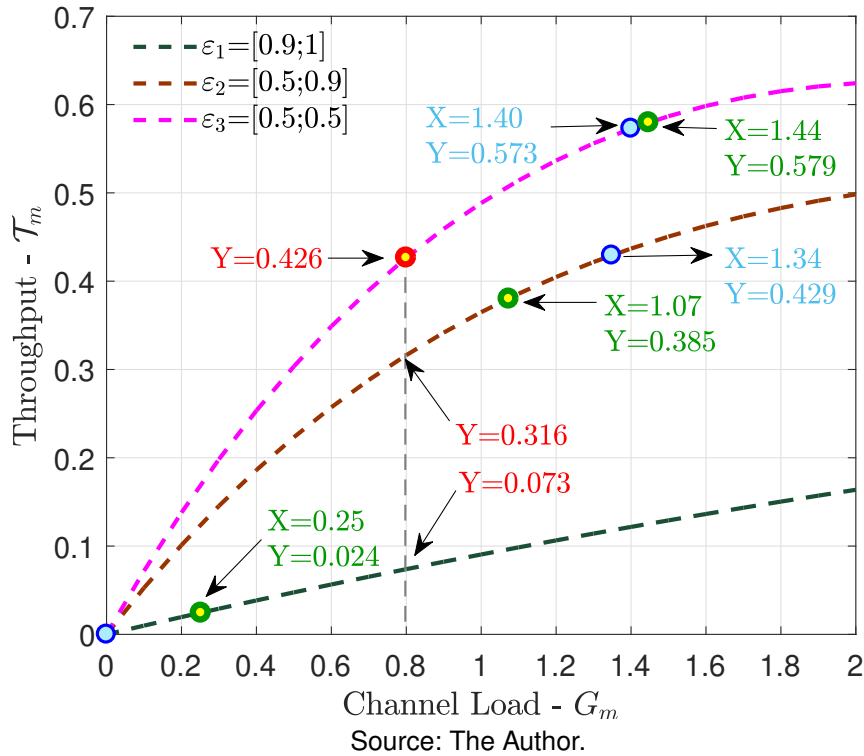
Figure 8 shows that this constellation with $K = 2$ satellites with topology $s = 1$ reaches the optimal system throughput when the traffic load per lap is $G_T = 28.4$. Now, focusing around the point marked by a blue star in Figure 5 and Figure 6a, we can see that for $G_T > 10$ the only load factors that continue to increase with the traffic load are Q_1 and Q_5, those with the highest erasure probabilities $[\varepsilon_{1,1}, \varepsilon_{1,2}] = [0.9, 1]$ and $[\varepsilon_{5,1}, \varepsilon_{5,2}] = [1, 0.9]$. This is because the maximum throughput values for the positions with the lowest erasure probabilities were already reached with relatively low traffic loads, and lowering the load factor is the way to guarantee that the throughput achieved in such positions remains the maximum when the traffic load per lap increases.

Figure 9 corroborates the above. Note that the maximum throughput $\mathcal{T}_3 = 0.626$ from the central position is associated with $G_3 = 2.2$, so that to guarantee maximum throughput in this position Q_3 must be such that $G_3 = Q_3 G_T = 2.2$. A similar analysis can be carried out for the intermediate positions, where Q_2 and Q_4 must be selected such that $G_m = Q_m G_T = 3.1$, $\forall m \in \{2, 4\}$, to guarantee $\mathcal{T}_2 = \mathcal{T}_4 = 0.528$. However, note that near-horizon positions with high erasure probabilities tolerate a much higher traffic load since a low percentage of the messages sent are received at the satellites

Figure 8 – Throughput contribution for each position. In this case we consider the optimal load traffic $G_T = 80$ (diamond) for SCA technique (blue), Uniform (red) and No-Uniform (green).

Source: The Author.
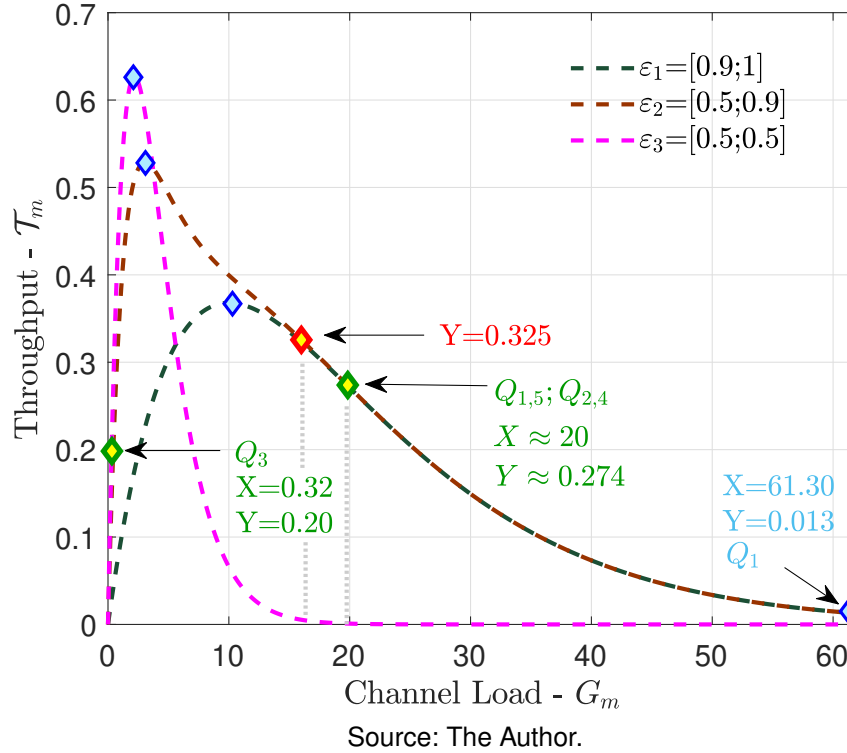
and thus significant collision probabilities occur for high traffic loads. Therefore, Q_1 and Q_5 must be selected such that $G_m = Q_m G_T = 10$, $\forall\, m \in \{1, 5\}$, to guarantee maximum throughput in these positions $\mathcal{T}_1 = \mathcal{T}_5 = 0.367$. After this analysis we can understand the contribution of each position to the overall system throughput, $\mathcal{T}_T = 2 \times \mathcal{T}_1 + 2 \times \mathcal{T}_2 + \mathcal{T}_3 = 2.42$ for $G_T = 2 \times G_1 + 2 \times G_2 + G_3 = 28.4$, see Figure 5. Moreover, the Non-Uniform distribution strategy in the face of this traffic load assigns a higher load factor to the intermediate positions ($Q_2 = Q_4 \approx 0.25$) and the same load factor to the central position and the near-horizon positions ($Q_3 = Q_1 = Q_5 \approx 0.167$), as can be seen in Figure 6b. Consequently, the system throughput with the Uniform and Non-Uniform distributions is numerically equal ($\mathcal{T}_T = 1.89$) despite the fact that the load factors are not equal, and significantly lower than the throughput achieved by the proposed SCA-based technique.

Analyzing Figure 6a after the maximum throughput point (blue star) until the traffic load per lap is approximately 50, shows that the proposed SCA-based optimization technique continues to find benefits in increasing the load factor of both extreme positions (Q_1 and Q_5). However, for $G_T > 50$ it is detrimental in terms of overall throughput to increase both load factors. From that point on, the SCA-based technique finds the maximum attainable throughput by assigning to the central position the value of Q_3 that allows it to reach the maximum throughput $\mathcal{T}_3 = 0.626$, as well as Q_2 and Q_4 to reach

Figure 9 – Throughput contribution for each constellation position. The star allows to identify the traffic load distribution per position G_m when G_T = 28.4 (traffic load value for which the maximum system throughput is reached with this constellation with K = 2 satellites with s = 1) according to: proposed SCA-based method (in blue), Uniform (in red) and Non-Uniform (in green) allocations.

Source: The Author.
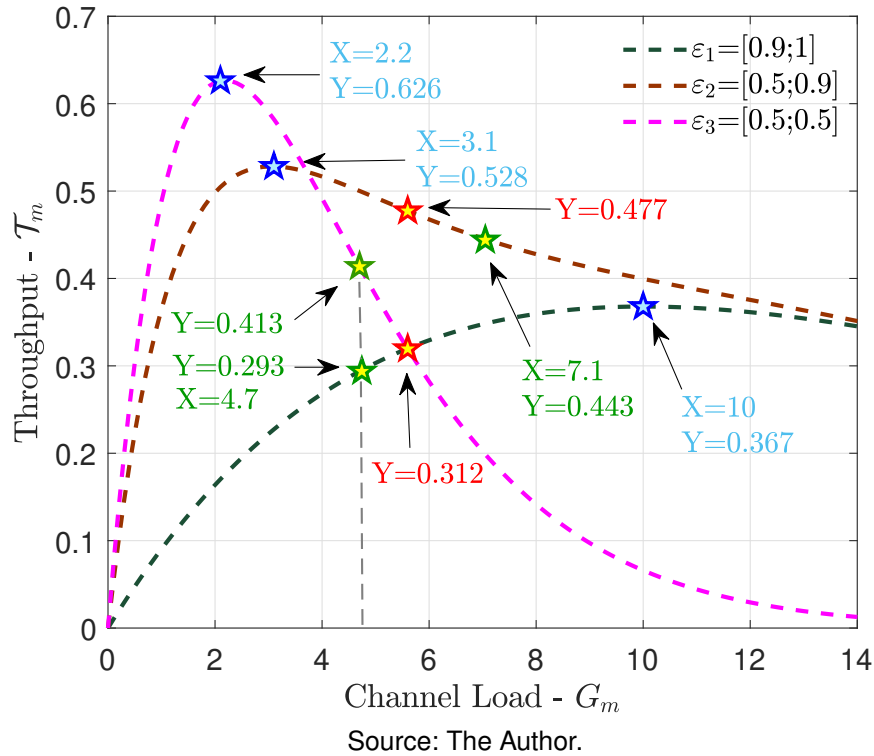
$T_2 = T_4 = 0.528$ and likewise to one of the two extreme positions, in this case to Q_5 for $\mathcal{T}_5 = 0.367$. Then, Q_1 must be such that the last position assumes the remaining traffic load, *i.e.*, $Q_1 = 1 - Q_2 - Q_3 - Q_4 - Q_5$, see Figure 5. Consequently, for extremely high traffic load values, $\mathcal{T}_1$ tends to 0 and $\mathcal{T}_T$ tends to $2 \times \mathcal{T}_2 + \mathcal{T}_3 + \mathcal{T}_5 = 2.049$. However, none of the other traffic load allocation strategies has this ability, so when ITLD, Uniform, and Non-uniform distributions are applied, for extremely high traffic load values, the overall system throughput tends to 0, as can be seen in Figure 5.

This effect can be observed by analyzing the point represented by the blue diamond in Figure 5 and Figure 6. Note that in the last four positions, the maximum throughput associated with each of those positions is achieved, as long as Q_2, Q_3, Q_4, and Q_5 guarantee that the traffic loads allocated to them is optimal for each position (*i.e.*, when SCA-based optimization technique is used), but the first position has to assume the remaining traffic load (G_1 = 61.3), so its contribution in terms of throughput is very poor, T_1 = 0.013. However, the Uniform and Non-uniform distributions achieve lower throughput ($\mathcal{T}_T$ = 1.30), when the traffic load per round is G_T = 80. Figure 6b shows than the Non-Uniform distribution perceives very low benefits in the central position,

Figure 10 – Overall throughput as a function of the traffic load per lap, using SCA-based technique with $K = 2$ satellites for different topologies $s=\{0, 1, 2, 3, 4\}$.
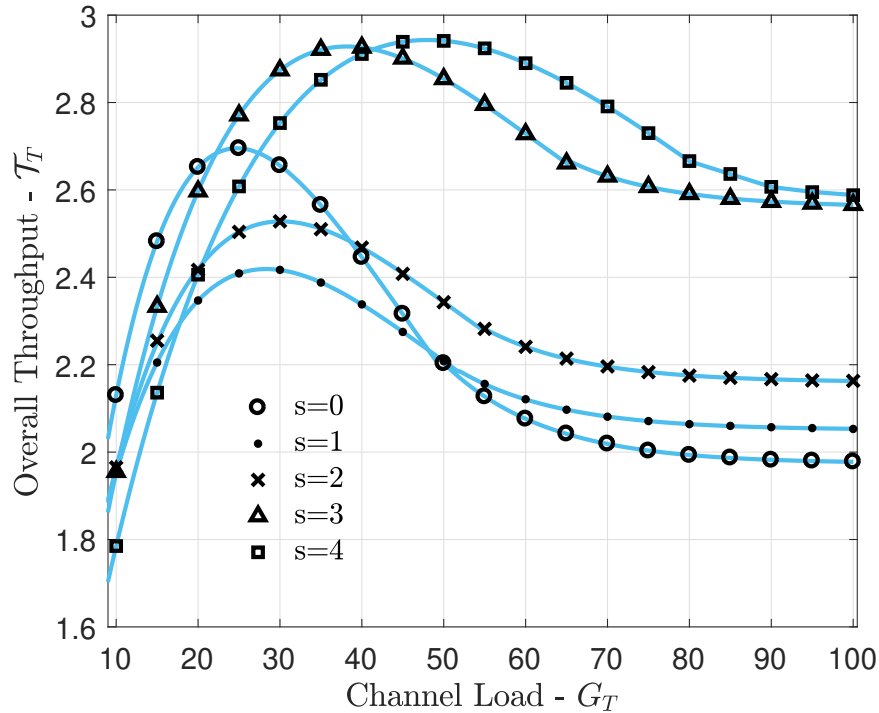
Source: The Author.

since for high traffic loads, the high collision probability at the receiver leads the system throughput to tend to 0.

Finally, Figure 10 shows the overall throughput as a function of the traffic load per lap, using SCA-based optimization technique in a constellation with $K = 2$ satellites for different topologies $s \in \{0, 1, 2, 3, 4\}$, which were represented in Table 3. By analyzing Figure 10, we can determine the most convenient topology to use if the total traffic load to be offered from the ground is known. For example, when $(G_T < 10)$ the highest throughput is achieved with the topology of $s = 0$; while for $(10 < G_T < 20)$, $s = 3$ is more convenient; and for $(G_T > 20)$, larger spacing is best, $s = 4$. This fact facilitates custom design or even dynamic adaptation of the topology if some orbital correction solution is possible. Moreover, note that as the spacing s between satellites increases, the number M of visible positions increases. Consequently, the stable value of throughput for high-traffic loads decreases with decreasing satellite spacing s, as nullifying the system throughput achieved by a position is more detrimental for topologies with fewer visible positions of the satellite constellation. Also note that the stable throughput value of a topology is approximately the maximum throughput achieved by this topology decremented by 0.367. This is because 0.367 is the maximum throughput achievable by one satellite on the horizon when the other satellite is no longer visible to the clustered IoT devices, except for the topology with $s = 0$ since both satellites are always together. Fig-

Table 4 – Optimal channel load per lap and per position, which allow to achieve the maximum system throughput by the proposed SCA-based method in a constellation with $K = 2$ satellites for different topologies with $s \in \{0, 1, 2, 3, 4\}$.

s	G_T^*	G_1^*	G_2^*	G_3^*	G_4^*	G_5^*	G_6^*	G_7^*	G_8^*
0	**24.8**	10.2	2.2	2.2	10.2	-	-	-	-
1	**28.4**	10	3.1	2.2	3.1	10	-	-	-
2	**30.2**	10	2	3.1	3.1	2	10	-	-
3	**38.2**	10	2	2	10.2	2	2	10	-
4	**48.0**	10	2	2	10	10	2	2	10

Source: The Author.

Table 5 – Maximum throughput per lap and per position achieved by the proposed SCA-based method in a constellation with $K = 2$ satellites for different topologies with $s \in \{0, 1, 2, 3, 4\}$.

s	$\mathcal{T}_T^*$	$\mathcal{T}_1^*$	$\mathcal{T}_2^*$	$\mathcal{T}_3^*$	$\mathcal{T}_4^*$	$\mathcal{T}_5^*$	$\mathcal{T}_6^*$	$\mathcal{T}_7^*$	$\mathcal{T}_8^*$
0	**2.70**	0.72	0.63	0.63	0.72	-	-	-	-
1	**2.42**	0.37	0.53	0.63	0.53	0.37	-	-	-
2	**2.53**	0.37	0.37	0.53	0.53	0.37	0.37	-	-
3	**2.93**	0.37	0.37	0.37	0.72	0.37	0.37	0.37	-
4	**2.94**	0.37	0.37	0.37	0.37	0.37	0.37	0.37	0.37

Source: The Author.

ure 10 and Table 4 show that the optimal traffic load ($G_T \in \{24.8, 28.4, 30.2, 38.2, 48\}$), which allows reaching the maximum overall throughput of each topology, increases with the increase of satellite spacing ($s \in \{0, 1, 2, 3, 4\}$). This is because a greater number of visible positions ($M \in \{4, 5, 6, 7, 8\}$) allows a greater traffic load to be assigned more efficiently.

These results and trends are expected, as well as the fact that the maximum value of overall throughput achieved by each topology increases with s, except for the topology with $s = 0$, which reaches a maximum overall throughput greater than the topologies with $s = 1$ and $s = 2$. In order to better understand the performance of the different topologies in terms of system throughput, it is necessary to analyze Table 5. Note that precisely the position that allows reaching the highest throughput per position ($\mathcal{T}_m = 0.72$) are those with $[\varepsilon_{m,1}, \varepsilon_{m,2}] = [0.9, 0.9]$, corresponding to the topology with $s = 0$, also the second highest throughput value per position ($\mathcal{T}_m = 0.63$) is reached twice by the topology with $s = 0$. Consequently, the overall throughput from the topology with $s = 0$ ($\mathcal{T}_T = 2.70$) is greater than that achieved by the topologies with $s = 1$ ($\mathcal{T}_T = 2.42$) and $s = 2$ ($\mathcal{T}_T = 2.53$).

2.6   FINAL CONSIDERATIONS

This work introduced a novel optimal traffic load allocation strategy for Aloha-based IoT LEO constellations. The link between the cluster of IoT devices and each satellite in the constellation was modelled by an erasure probability, following the On-Off fading channel model. In order to maximize the achievable system throughput, we proposed a low-complexity SCA-based technique that considerably outperforms three previously proposed heuristics. Moreover, we analyzed in detail the traffic load allocation per position, while highlighting the superiority of the proposed technique, which achieves a non-zero throughput even if the traffic load is extremely high.

3 MULTIPLE CHANNEL LORA-TO-LEO SCHEDULING FOR DIRECT-TO-SATELLITE IOT

Amid the diversity of applications in MAC protocols for satellite-based IoT communications over the past decade, several challenges remain due to the trade-off between the number of devices and the visibility window constraints. As discussed in Chapter 1, the authors of SALSA propose a First-Come-First-Served (FCFS) scheduling strategy where resource allocation is assigned to devices considering their initial visibility in the satellite footprint (AFHAMISIS; PALATTELLA, 2022). However, following the FCFS policy, in a dense scenario, many devices may not be able to successfully transmit during the satellite visibility window due to excessive congestion. To address this drawback and inspired by SALSA, this chapter presents two novel low computational cost scheduling strategies for DtS-IoT networks.

Specifically, Section 3.1 begins by discussing the related state-of-the-art literature. Section 3.2 describes the system model, while Section 3.3 formulates the proposed scheduling methods. Section 3.4 presents the simulation method and parameters, while Section 3.5 discusses the simulation results. Section 3.6 concludes the chapter. Furthermore, Table 6 provides a list of symbols used in this chapter. Finally, the content of this chapter was published in (TONDO et al., 2024a).

3.1 RELATED WORK

In recent years, great strides have been made in low-power wide area networks (LPWANs). The remarkable success of LoRa technology (SEMTECH, 2022) redefined the concepts of long-range connectivity and low energy consumption, opening a new opportunity for IoT communication systems (AFHAMISIS; PALATTELLA, 2022). However, in particular cases, such as dense deployments or long transmission distances like in DtS-IoT scenarios, the LoRaWAN protocol (LORA ALLIANCE, 2023b) has some limitations (ÁLVAREZ et al., 2022). This motivated a recently introduced variant in (LORA ALLIANCE, 2020) that can improve throughput performance in very dense scenarios, but it is still not able to avoid collisions or operate with high energy efficiency.

A recent work (FRAIRE, J. A. et al., 2022) discusses some challenges in DtS-IoT related to the channel, the orbital dynamics, and the highly constrained IoT devices. The authors state that existing IoT MAC schemes need to be critically reviewed, especially those aiming to enable effective communication of thousands of devices with the gateway in a relatively short period. In large clusters, with many devices competing for data transmission opportunities during a satellite lap with an ALOHA-based protocol such as LoRaWAN, the probability of collision will be high, leading to problems in terms of scalability and energy efficiency (ORTIGUEIRA et al., 2021). Furthermore, with the advent of 5G communications and beyond, clustering algorithms aimed at reducing

Table 6 – List of Symbols - Chapter 3.

Variable	Description
δ	Guard times
n	IoT device
τ	LoRa airtime
$R_{m,n}$	Rise-time for each device n during m satellite lap
m	Satellite lap
$S_{m,n}$	Set-time for each device n during m satellite lap
$\mathbb{V}_m$	Set of visibility time intervals of each device in the m satellite lap
$\mathbb{T}_m$	Set containing the allocated time windows for each device
$\mathbb{F}_m$	Set containing the free time in that m^{th} lap.
$\mathbb{J}_m$	Set containing the joined or scheduled devices in that m^{th} lap
$\mathbb{D}_m$	Set containing the discarded or unscheduled devices in that m^{th} lap
$\mathbb{P}_m$	Set containing the devices in $\mathbb{J}_m$ with $S_{m,n} > \max E_{m,n}$
p	The proportion of Ω and guard times plus LoRa airtime
$B_{m,n}$	The scheduled beginning time for the uplink of the nth device in the mth lap
$E_{m,n}$	The scheduled ending time for the uplink of the nth device in the mth lap
Ω	The time not used by FCFS after the transmission of the last scheduled uplink
$W_{m,n}$	Transmission window interval for the nth device during the mth lap
H	Total number of available frequency channels
M	Total number of satellite laps
N	Total number of IoT devices
$V_{m,n}$	Visible time interval for each device n during m satellite lap

Source: The Author.

the complexity of resource allocation are appealing (MUKHERJEE et al., 2021), particularly in dense DtS-IoT scenarios. A traffic allocation strategy for ALOHA networks was recently proposed in (TONDO et al., 2023), which achieves non-zero throughput even in cases with very high traffic load but is very energy inefficient in this regime. In this sense, the authors (GAMAGE et al., 2023) introduced LMAC, an efficient Carrier Sense Multiple Access (CSMA) protocol designed for LoRa networks. This protocol aims to achieve a significant advancement in LoRa communications, promising a 2.2× improvement in performance and a substantial 2.4× reduction in energy consumption compared to the ALOHA mechanism. Across three advancing versions of LMAC, this study attracts considerable interest in Direct-to-Satellite (DtS) scenarios, thanks to its implementation of channel load balancing based on the global locations of the IoT nodes and gateways.

In DtS-IoT, the choice of MAC protocol considerably affects the system performance in terms of throughput and energy efficiency (PARRA et al., 2023). Notice that the devices are spread over the footprint of the LEO satellite, with different visibility times, the MAC protocol can exploit this characteristic and optimize the uplink resources

using appropriate device scheduling. Indeed, SALSA algorithm is based on the knowledge of the visibility times (AFHAMISIS; PALATTELLA, 2022). Specifically, time slots are assigned to each device based on those visibility times to avoid collisions and replication. Moreover, uplink policies and a mixed integer linear programming model to provide an upper bound in performance for scheduled LoRa-based DtS-IoT were proposed in (ÁLVAREZ et al., 2022). In addition, the authors concluded that trajectory-based policies can duplicate the amount of served IoT nodes.

Departing from LoRa-based networks, a resource allocation scheme based on genetic algorithms for load balancing was provided in (LIN et al., 2022). Therein, problems such as low efficiency in extremely non-uniform user distribution conditions and density variations were detected. In a similar line, but considering narrowband IoT, the authors in (KODHELI et al., 2022) proposed a scheduling pattern that maximizes a profit depending on data packet sizes, channel conditions, and satellite visibility time.

This chapter considers the problem of scheduling the transmissions of IoT devices in a DtS-IoT system using LoRa technology. Adopting the same set-up of (AFHAMISIS; PALATTELLA, 2022), but herein are included multiple frequency channels to simultaneously assume several transmissions corresponding to IoT nodes with similar visibility windows. In addition, the subsequent sections provide an efficient method to swap the time slots assigned to some devices based on their set times, thus creating new transmission opportunities for IoT devices that would not otherwise transmit. Furthermore, unlike the policies proposed in (ÁLVAREZ et al., 2022), the proposed method generates a collision-free channel access strategy that can be implemented with low computational complexity, so it can even be run on-board the satellite if necessary. Finally, concerning (KODHELI et al., 2022; LIN et al., 2022), the proposed approach is tailored for LoRa-based DtS-IoT networks, with low computational complexity and high effectiveness despite the dynamics of these scenarios.

Despite the acknowledged relevance of carrier sensing protocols like CSMA for LoRa technology (GAMAGE et al., 2023), their current implementation is not entirely suitable for integration with DtS-IoT scenarios. Aspects such as the high probability of hidden nodes during satellite lap require further depth investigations (HERRERÍA-ALONSO et al., 2023; FERRER et al., 2019). Ensuring comparative fairness between the proposed methods is quite a challenge, so the present approaches do not focus on CSMA or even simple ALOHA policies. We specifically aim to improve the system uplink efficiency in the SALSA scenario.

3.2   SYSTEM MODEL

We consider an IoT network that operates within the coverage of an LEO satellite, where IoT devices are uniformly distributed in fixed locations within the target area and directly transmit data packets to the satellite in allocated time slots. We also assume that

Figure 11 – The DtS-IoT system, which comprises: a gateway in the LEO satellite, IoT devices spread over the target area, the network server, and the satellite ground station.
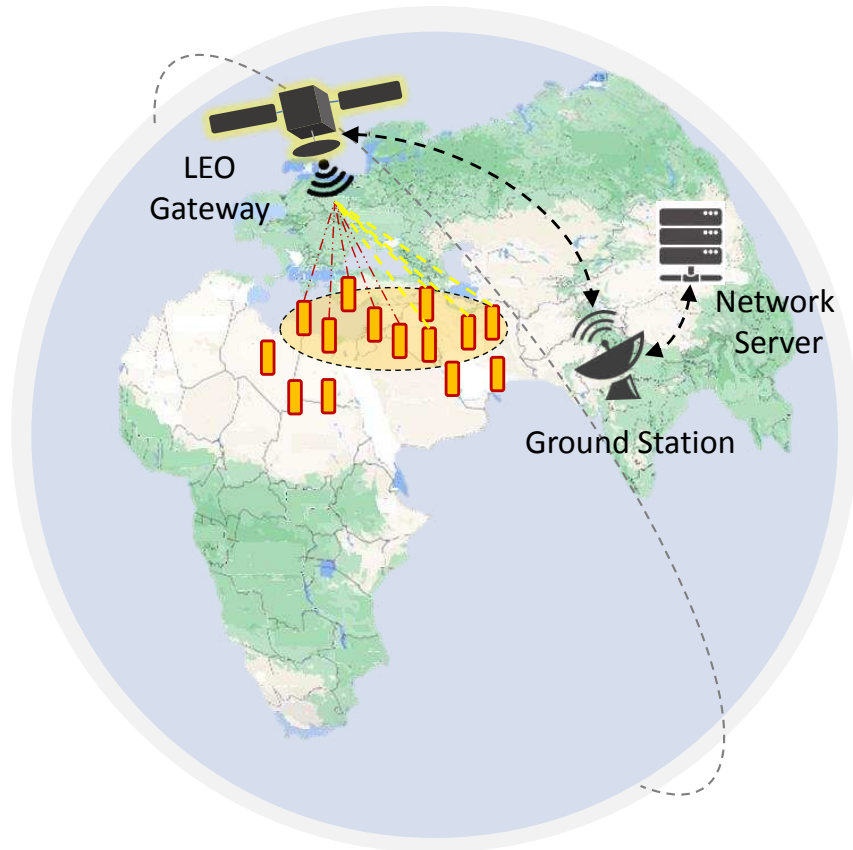
Source: The Author.

the devices utilize the LoRa communication technology (SEMTECH, 2022). Figure 11 illustrates the scenario, with a cluster of IoT nodes on the ground communicating with a gateway on board the LEO satellite. The LEO satellite connects with a ground station that forwards the received packets to a Network Server (NS). Furthermore, the system dynamics are affected by orbit parameters, satellite footprint, and the target area, with each device having different visibility times during one satellite lap.

We denote the total number of satellite laps as M and the total number of IoT devices within the target area as N. Due to the system dynamics, each device appears and disappears from the satellite footprint at different times in each satellite lap. Such times are termed as rise-time $R_{m,n}$ and set-time $S_{m,n}$, for $m \in \{1, 2, ..., M\}$ and $n \in \{1, 2, ..., N\}$. Thus, each device n is visible for the satellite lap m during a time window defined by the interval $V_{m,n} = \left[R_{m,n}, S_{m,n} \right]$. Moreover, we assume that the IoT devices generate traffic with the same priority and always have information to transmit (full-buffer assumption), but can only transmit when they are within the satellite's footprint. The NS is responsible for scheduling collision-free uplink transmissions, at most one per

Table 7 – LoRa airtime τ according to Spreading Factor SF = 12, Europe Region EU868, BW = 125 kHz (THE THINGS NETWORK, 2023a).

Pay	$51 - 48$	$47 - 43$	$42 - 38$	$37 - 33$	$32 - 28$	$27 - 23$	$22 - 18$
τ (ms)	2793.50	2629.60	2465.80	2302.00	2138.10	1974.30	1810.40

Source: The Author.

device per lap, taking into account the visibility time of each IoT device. We assume a configuration for extended coverage with a Spreading Factor (SF) equal to 12 and 125 kHz bandwidth. Note that the required SF or bandwidth will depend on the orbit height and target area (THE THINGS NETWORK, n.d.). We consider the availability of multiple channels in our system model, which favors the allocation of transmission resources in practical scenarios with numerous devices deployed in the target area. This approach is consistent with LoRa and allows more efficient utilization of visible time windows, which improves overall system performance. We denote as *H* the total number of available frequency channels.

The NS must consider the visibility times of each device and the time-on-air per packet (τ) to correctly schedule the uplinks. In Table 7, we list the value of τ for different payload sizes according to the regional parameters for Europe (EU868), based on (THE THINGS NETWORK, 2023a). Moreover, as in (AFHAMISIS; PALATTELLA, 2022), we include two guard times δ = 10 ms, before and after each transmission, to avoid collisions due to synchronization imperfections among devices and the satellite. Thus, the NS reserves the channel for each uplink transmission considering the total time, which comprises two guard times δ and the packet τ.

Following SALSA (AFHAMISIS; PALATTELLA, 2022), the scheduled beginning time for the uplink of the nth device in the mth lap, denoted as $B_{m,n}$, is defined by the NS and depends on: *i*) the orbit dynamics; *ii*) the number of devices within the satellite footprint. A transmission from another device on the same channel is only scheduled after the end transmission time ($E_{m,n}$) of the device previously scheduled. In other words, a transmission window corresponding to the interval $T_{m,n} = \left[B_{m,n}, E_{m,n}\right]$ is allocated only for the nth device during the mth lap.

3.3   THE PROPOSED SCHEDULING METHODS

Next, we describe the proposed scheduling approaches for DtS-IoT. The methods are based on the SALSA-FCFS policy (AFHAMISIS; PALATTELLA, 2022), which works in a first-come-first-serve fashion. In SALSA-FCFS, the first device to appear in the satellite footprint is the first to transmit, and so on (*i.e.*, the scheduling queue is based on the respective rise-times). Initially, as in (AFHAMISIS; PALATTELLA, 2022), let us consider the availability of a single-frequency channel. The operation of SALSA-FCFS is illustrated next.

Figure 12 – Uplink schedules in the mth lap, including rise-time $R_{m,n}$, set-time $S_{m,n}$, beginning-time $B_{m,n}$, end-time $E_{m,n}$, and guard times (in blue). (a) SALSA-FCFS, where the 4$^{\text{th}}$ device could not be scheduled (left). (b) L2L-P, where the uplink of the 2$^{\text{nd}}$ device is rescheduled so that the 4$^{\text{th}}$ device can transmit (right).

(a) SALSA FCFS.   (b) L2L-P
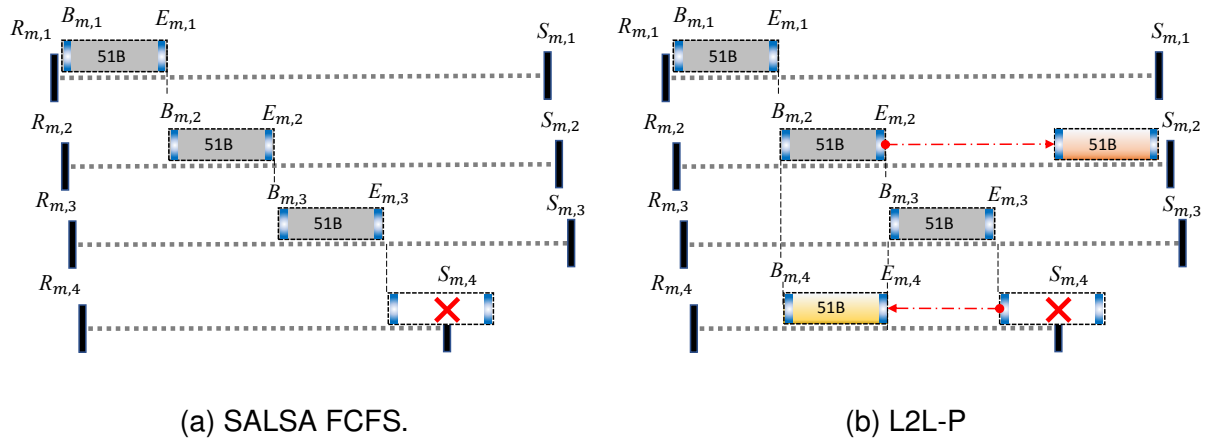
Source: The Author.

Example 1 *Let us assume N = 4 devices want to transmit payloads of* 51 *bytes (the maximum with SF12). Their rise-times $R_{m,n}$ and set-times $S_{m,n}$ are illustrated in Figure 12a. Following the SALSA-FCFS policy, the scheduled transmissions are represented by boxes whose boundaries correspond to the beginning-times $B_{m,n}$ and end-times $E_{m,n}$ for each allocated device uplink. Moreover, the guard times are highlighted in blue. Note that the 4th device is denied transmission as its remaining visibility time after the transmission of the three devices that came first (these are the ones that entered the satellite footprint first and have the lowest rise times) is not sufficient to accommodate the total time for that payload size.*

Note that assigning uplinks based solely on rise times does not guarantee to scheduling as many transmissions as possible, due to the differences in the duration of the visibility window of the devices given their locations and the satellite footprint. On the other hand, scheduling uplink transmissions by the longest set time of each device, or First-Leave-First-Serve (FLFS) allocation, would be unfair and inefficient because it would not take advantage of the timely arrival of many IoT devices. Next, we introduce a strategy that seeks to create additional transmit opportunities after the application of the FCFS policy.

3.3.1   Permutation of Scheduled Times: L2L-P

In SALSA-FCFS, a device with a short visibility time may have very few opportunities to transmit unless it is one of the first to appear in the footprint. The situation gets

worse with the network density, as many devices may have intersecting visibility times. Add to that the fact that the duration of the visibility times may be considerably different among devices. To deal with these problems, we consider the permutation of the scheduled times from the initial SALSA-FCFS scheduling (AFHAMISIS; PALATTELLA, 2022), looking for the reallocations that allow scheduling uplinks discarded by the FCFS policy.

Algorithm 2 describes in detail the implementation of the proposed LoRa-to-LEO with Permutation of scheduled times (L2L-P) approach in the mth lap. Algorithm inputs include the rise and set times based on the relative locations of the devices concerning the satellite orbit, as well as transmission beginning and end times scheduled by the SALSA-FCFS schedule. We define $\mathbb{V}_m = \{V_{m,1}, \cdots, V_{m,N}\}$ as the set whose elements are the visibility time intervals of each device in that lap. The algorithm checks which devices are allocated a transmit window considering the SALSA-FCFS policy, and constructs the set $\mathbb{T}_m = \{T_{m,1}, \cdots, T_{m,N}\}$ containing the intervals corresponding to the allocated time windows for each device. At this point, we can determine the time intervals (if any) not allocated to any device, which are listed in the free time set $\mathbb{F}_m$. Furthermore, the users are separated into two sets: $\mathbb{J}_m$, containing the joined or scheduled devices, and $\mathbb{D}_m$, with the discarded or unscheduled devices in that lap.

Considering the devices $n \in \mathbb{J}_m$, the L2L-P algorithm calculates $\Omega = \max S_{m,n} - \max E_{m,n}$, i.e., it determines the amount of time Ω not used by FCFS after the transmission of the last scheduled uplink ($\max E_{m,n}$) and that is visible by at least one device ($\max S_{m,n}$). Note that at most $p = \lfloor \frac{\Omega}{2\delta+\tau} \rfloor$ devices from $\mathbb{J}_m$ could be reallocated to this unused time, opening transmit opportunities for devices within $\mathbb{D}_m$. Next, if $p \geq 1$, the devices in $\mathbb{J}_m$ with $S_{m,n} > \max E_{m,n}$ are included in set $\mathbb{P}_m$ and they are ordered in decreasing $S_{m,n}$. The first device in $\mathbb{P}_m$ is reallocated to the end of the visibility window so that its new $E'_{m,n}$ becomes $S_{m,n}$. The previously allocated time interval for this device moves from $\mathbb{T}_m$ to $\mathbb{F}_m$. Next, p is decremented, and if it is still larger or equal to 1, the algorithm checks if the next device in $\mathbb{P}_m$ can be reallocated, so that its set time is as close as possible to the beginning transmission time of the previously reallocated device, and so on.

Next, for each device in $\mathbb{D}_m$, the algorithm checks if its visibility time interval $V_{m,n}$ has an intersection greater than or equal to $(2\delta + \tau)$ with any element in $\mathbb{F}_m$. If so, the transmission of that n^{th} IoT device is scheduled within the idle interval found in the most efficient way (i.e., by matching $B_{m,n}$ with the left edge of the free time interval or $E_{m,n}$ with the right edge of the free time interval). Then, the scheduled transmission $T_{m,n}$ is removed from $\mathbb{F}_m$ and is included in $\mathbb{T}_m$. At the end of this procedure, up to p IoT devices from $\mathbb{D}_m$ may be moved to $\mathbb{J}_m$, increasing the uplink efficiency.

Example 2 *Consider the case discussed in Example 1 and Figure 12a, where the 4th IoT device was not scheduled. However, if we move the 2nd IoT device's uplink to the idle time interval after the 3rd device's uplink, then the 4th device's uplink can be*

Algorithm 2 L2L-P

    Input: $R_{m,n}, S_{m,n}, B_{m,n}, E_{m,n}, \tau, \delta, m$;

    Construct: $\mathbb{V}_m, \mathbb{T}_m, \mathbb{F}_m, \mathbb{J}_m, \mathbb{D}_m$;

    Initialize: $i = 1, B'_m = \emptyset$;

    Calculate: $\Omega = \max S_{m,n} - \max E_{m,n}, p = \lfloor \frac{\Omega}{2\delta+\tau} \rfloor$;

    if $p \geq 1$ **then**

        Construct $\mathbb{P}_m$ and order devices in decreasing $S_{m,n}$;

        while $p \geq 1$ **do**

            Find: $n \in \mathbb{P}_m(i)$;

            $E'_{m,n} = \min(B'_m, S_{m,n})$;

            $B'_{m,n} = E'_{m,n} - (2\delta + \tau)$;

            Include $T_{m,n}$ in $\mathbb{F}_m$ and remove it from $\mathbb{T}_m$;

            $T_{m,n} = [B'_{m,n}, E'_{m,n}]$;

            Include $B'_{m,n}$ in B'_m;

            Include $T_{m,n}$ in $\mathbb{T}_m$;

            $i = i + 1$;

            $p = p - 1$;

        end while

        for each $n \in \mathbb{D}_m$ **do**

            $I_{m,n} = V_{m,n} \cap \mathbb{F}_m$

            if $I_{m,n} \geq 2\delta+\tau$ **then**

                $T_{m,n} = I_{m,n}$ (left aligned);

                Include $T_{m,n}$ in $\mathbb{T}_m$;

            end if

        end for

    end if

    Output: Allocated time windows $\mathbb{T}_m$.

---

scheduled at the time interval that was previously reserved for the 2nd device. Thanks to this rescheduling, the uplinks of the four devices can be scheduled, as illustrated in Figure 12b.

Example 3 *As an additional illustration of the L2L-P operation, Figure 13 shows the visibility time windows $V_{m,n}$ for 250 devices under the coverage of a satellite. First, the SALSA-FCFS allocation was applied, resulting in the sequential schedule illustrated with different marker colors in Figure 13. Note that the uplinks are ordered by rise times, while several IoT devices (whose visibility windows were represented by red dots) are not initially scheduled due to their set times. However, after running the L2L-P algorithm, some of the allocated devices have their transmit times shifted to the end of the overall visibility window (the new uplinks of these devices are marked in green in Figure 13, making room for other devices that could not transmit before (these uplinks are identified with big red dots in Figure 13). Thus, the uplink efficiency can be improved concerning the FCFS strategy.*

    The above discussion and examples consider a single channel. Next, we present

Figure 13 – Visibility time window and scheduling for 250 devices using the L2L-P algorithm in a single channel scenario.

Source: The Author.
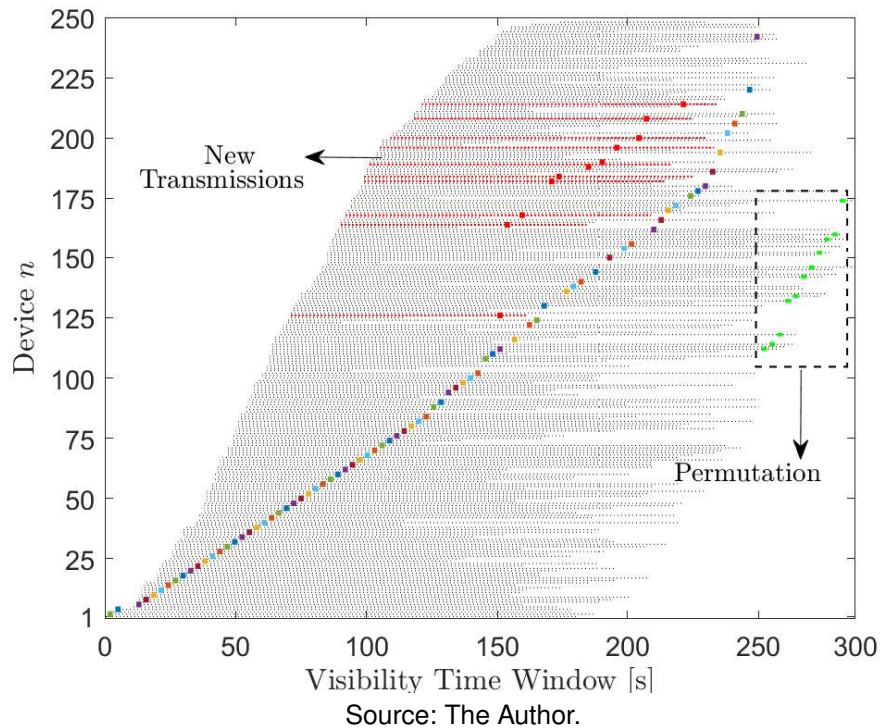
a strategy that can efficiently allocate the devices when multiple channels are available, which further leverages the potential of the L2L-P algorithm.

3.3.2 Exploiting Multiple Channels: L2L-A and L2L-AP

We design a scheduling strategy that considers the availability of H orthogonal frequency channels. First, the visible devices in the mth lap are divided into H uplink groups. For that sake, we first order the devices according to their rise times $R_{m,n}$. We then assign the devices to the groups alternately, such that the device with the first (second) rise time is assigned to the first (second) group, and so on. This first group will include all those devices located in positions multiple of H plus 1 (which will be serviced from the first channel). Devices in positions that are multiple of H plus h will belong to the hth group and will be served from the hth channel. After the devices are separated into the H groups, the FCFS policy is applied in each group, yielding the transmitting time slots allocated for each group. The above strategy is the LoRa-to-LEO with Alternating Channels (L2L-A) algorithm, which guarantees an efficient distribution of all IoT devices according to their respective rise times.

The permutation strategy described in the previous section can be applied to each group, thus increasing the number of scheduled uplinks on each channel. We refer to the application of the L2L-A method followed by the L2L-P strategy in each channel as the novel scheduling policy named L2L-AP, which is illustrated next.

Figure 14 – Uplink schedules in the mth lap, including rise-time $R_{m,n}$, set-time $S_{m,n}$, beginning time $B_{m,n}$, end time $E_{m,n}$, and guard times (in blue). Devices 1 and 3 transmit in channel $h = 1$, while devices 2 and 4 transmit in channel $h = 2$. The red arrows indicate the permutation operation.
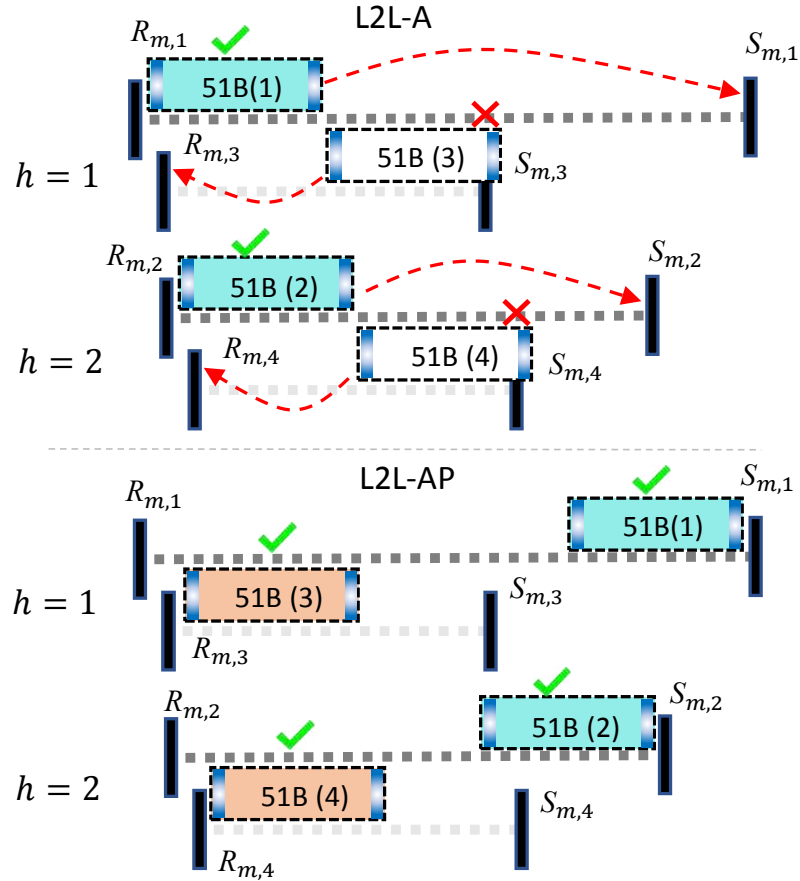
Source: The Author.

Example 4 *Consider the case illustrated in Figure 14, with N = 4 devices. If the devices were to be allocated in a single channel, using either SALSA-FCFS or L2L-P, it would not be possible for all to transmit in the same satellite lap. However, assuming there are two available channels, a more favorable allocation can be defined. Following the L2L-A logic, since there are H = 2 channels, devices 1 and 3 would be in the first group (they transmit in the first channel) and devices 2 and 4 would be in the second group (they transmit in the second channel). But even with channel allocation devices 3 and 4 would not be able to transmit. However, if after L2L-A we apply the L2L-P approach in each of the two channels, which leads to the L2L-AP algorithm, then the final allocation is as illustrated in Figure 14, in which device 3 is the first one to transmit in channel 1, followed by device 1. In channel 2, device 4 is the first to transmit, followed by device 2.*

Algorithm 3 summarize the steps of the L2L-A and L2L-AP strategies, respectively. The multi-channel approaches not only increase the number of uplink transmissions by exploiting the multiple available channels, but also increases the benefits as-

---

Algorithm 3 Multi-Channel LoRa-to-LEO Scheduling

    Input: $R_{m,n}, S_{m,n}, \tau, \delta, H$;
    Split the visible devices into H sub-groups;
    Choose: L2L-A (a) or L2L-AP (b);
    for each $h \in H$ **do**
        if (a) **then**
            Allocate time windows $T_{m,n}$ using SALSA-FCFS;
        else if (b) **then**
            Allocate time windows $T_{m,n}$ using SALSA-FCFS;
            Apply the L2L-P algorithm;
        end if
    end for
    Output: Allocated time windows $\mathbb{T}_m$ per channel.

---

sociated with permutation since ordered and unsaturated use of each channel is more efficient. This makes the L2L-AP approach very efficient in terms of uplink resources.

    Remark 1: Note that the input of L2L-AP is the output of L2L-A. Then, L2L-AP looks for potential uplink permutations to open up opportunities for unscheduled devices. Therefore, L2L-AP never performs worse than L2L-A.

    Remark 2: Given the orbit dynamics and the position of the devices, it may happen that the visibility times set $\mathbb{V}_m$ can be decomposed into two or more disjoint subsets. In such cases, the algorithms proposed in this section must be executed on each of these subsets separately.

    Remark 3: Note that the allocation of time slots could be carried out using an optimization problem similar to that in (ÁLVAREZ et al., 2022). However, such a solution is not scalable as it becomes prohibitive given the increase in its complexity with the increase in the number of IoT devices. In this work, we focus on low-complexity and highly efficient scheduling methods, which could be even executed on-board the LEO satellite if necessary and if the network server is also implemented onboard.

3.3.3 Practical Considerations

    For a practical implementation of the proposed method, the network server or system coordinator must know the trajectory of the LEO satellite and the location of the IoT devices. First, we note that satellite visibility can be predicted with great accuracy using techniques from the perspective of either the LEO satellite (WANG, H. et al., 2019; HAN et al., 2021; BAI et al., 2022) or the ground nodes (HAN et al., 2017, 2018; GU et al., 2019). Furthermore, the location of the devices can be informed to the network server during the installation and registration of each IoT device. For example, the latitude and longitude information is an input of the popular The Things Network server (THE THINGS NETWORK, 2023b). Therefore, the assumption of known ground devices' location and satellite trajectory on the network server is reasonable

for scenarios with static IoT devices, thus constituting a constraint in the proposed system model. Moreover, the computation of the scheduling times can be executed at the Earth station and transmitted to the satellite, which then could inform the devices in the downlink phase, using acknowledgment messages for class A or a synchronization beacon for class B devices. Directly related to the above considerations, it is relevant to mention that a hybrid emulation-based testbed with real LoRa devices using the baseline FCFS SALSA strategy has been successfully tested (AFHAMISIS et al., 2022), confirming its practical feasibility.

The network performance in DtS-IoT is vulnerable to potential wireless interference, including mutual interference between users (ÁLVAREZ et al., 2022; TONDO et al., 2021). Additionally, uplink transmission may be impacted by other sources. However, Semtech studies (SEMTECH, 2020) have announced the feasibility of LPWANs co-existing harmoniously with other high-power systems that generate frequency-selective interference. In our focus, the efforts are directed toward enhancing uplink efficiency. Finally, another potential issue of concern for practical deployments is that DtS-IoT communications are susceptible to the Doppler effect (KODHELI et al., 2022) due to satellite movement. However, recent experiments based on LoRa technology revealed a minimum performance impact from the Doppler effect considering LEO satellites (DOROSHKIN et al., 2019; ZADOROZHNY et al., 2022). Therefore, in line with the related literature (AFHAMISIS; PALATTELLA, 2022; ÁLVAREZ et al., 2022; ORTIGUEIRA et al., 2021), we do not consider this effect in this work as its practical implication should be minimal.

3.4 SIMULATION METHOD AND PARAMETERS

A computer simulation is deployed to evaluate the proposed scheduling methods in a realistic DtS-IoT scenario, following the approach in SALSA (AFHAMISIS, MOHAMMAD AND PALATTELLA, MARIA RITA, 2022), where the location of the N devices is randomly generated within a region. Then, we extract the location of each device on the ground, in terms of latitude and longitude, using geocoders from the Python GeoPy library (GEOPY CONTRIBUTORS, 2018). Satellite visibility times of IoT devices are estimated using the Python Skyfield astronomy library (RHODES, 2023). This library uses public data information in the Two-Line Element (TLE) set format, available from the CelesTrack platform (CELESTRACK DATABASE, 2023), for determining the locations of the satellite according to the orbit and pointing time. Thus, the IoT devices are deployed in the target area, their visibility times are determined in each satellite lap, and the different scheduling strategies are evaluated. Such evaluation, analysis, and visualization of the results are carried out in MatLab®.

In this work, we consider the region delimited by the borders of France for deploying the devices. France is well distributed in all directions, ranging around 1000 km north

Figure 15 – Deployment of 250 IoT devices (blue circles) in France, covered by LacunaSat-3.
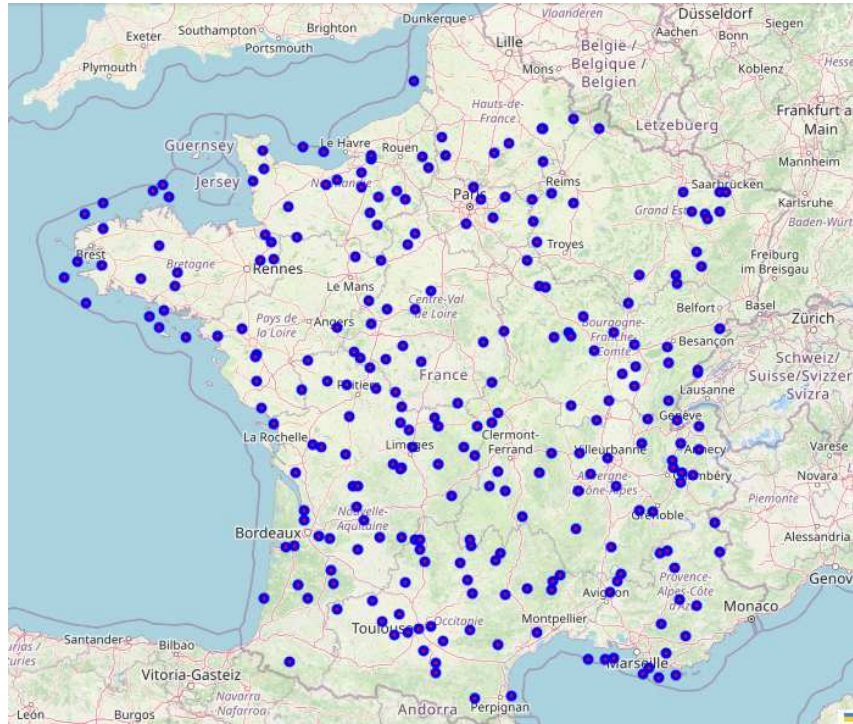
Source: The Author.

to south and east to west, so the visibility times of the IoT devices may be considerably different depending on the orbit dynamics. We consider different numbers of devices spread over the target area, from N = 100 to N = 1000. Using the OpenStreetMap library, Figure 15 illustrates one deployment of 250 devices in France. Moreover, we consider the real orbit of the LacunaSat-3 LEO satellite, with a height of 500 km to 600 km from the Earth and a minimum elevation angle of $30°$, as in (LEYVA-MAYORGA et al., 2020; AFHAMISIS; PALATTELLA, 2022), to determine the satellite footprint. In addition, we assume different numbers of channels, $H \in \{1, 2, 4, 6, 8\}$. Finally, the results consider a period of 31 days in March 2023.

3.5 NUMERICAL RESULTS

In this section, we evaluate the performance of the proposed scheduling methods. Figure 16 shows the number of uplinks per lap for N = 1000 devices in the target area. The red line indicates the number of visible devices per lap, which is also the upper bound of the number of uplinks per lap. As expected, increasing the number of channels allows more devices to transmit, while the margin by which L2L-AP outperforms L2L-A increases with H too. Moreover, in laps with few visible devices but sufficient visibility time, L2L-AP with H = 4 achieves almost the same performance as L2L-A with H = 6 channels. To understand this phenomenon, let us focus on lap m = 8. Although not

Figure 16 – Number of uplinks per lap for $N = 1000$ devices and $H \in \{1, 2, 4, 6, 8\}$ channels.

Source: The Author.
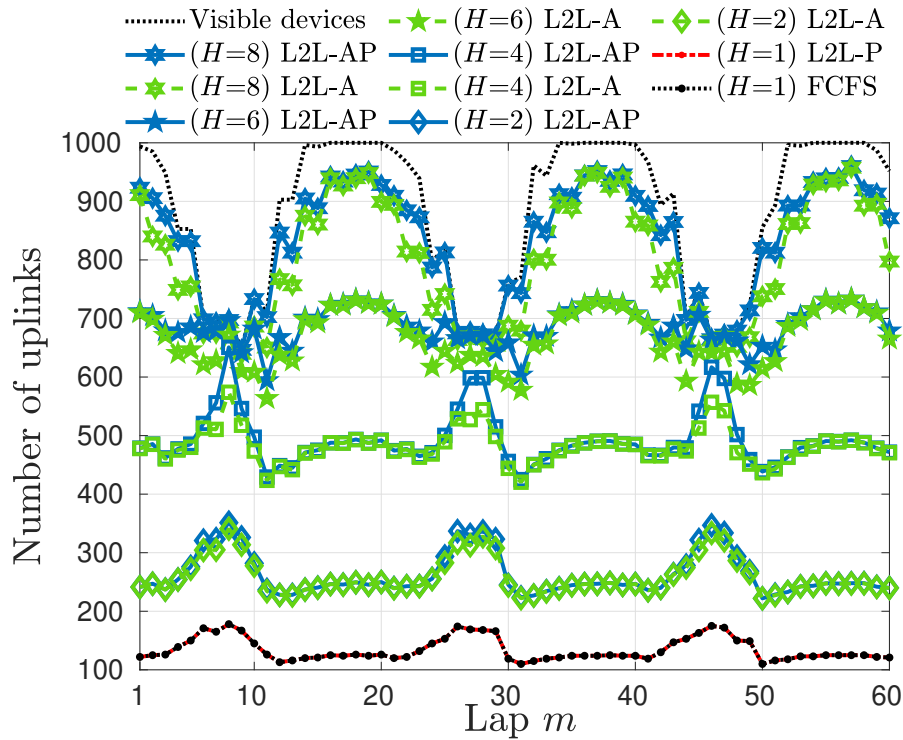
shown here, in this lap the set of visible IoT devices can be divided into two subsets of disjoint visibility windows (see Remark 2), with similar numbers of devices per subset. Moreover, the sum of the visibility times of both subsets in lap $m = 8$ (505 seconds) is greater than the overall visibility time window of lap $m = 1$ (344 seconds), while the individual visibility windows of the devices in lap $m = 1$ have a very large intersection. Such scenarios with a large number of visible devices but somewhat limited visibility time for their allocation, as in lap $m = 1$, can only be efficiently served when many channels are available. That is why L2L-AP with $H = 8$ channels is very efficient, allowing almost all visible devices to transmit in any lap. Additionally, the performances of the L2L-P and FCFS scheduling strategies are illustrated in the red and black lines.

Figure 17 shows the average number of uplinks per lap, considering 10 different deployments in the target area and $N \in \{500, 600, 700, 800, 900, 1000\}$ devices. Note that for $N = 500$, both L2L-A and L2L-AP have similar performance, between 300 and 400 uplinks. However, as the number of devices increases, the relative difference between the strategies and the number of channels becomes more visible. In particular, with $N = 1000$ devices and $H = 8$ channels, L2L-AP shows the best performance. Also note that the number of uplinks does not match the total number of devices, because the number of visible devices per lap is often less than the total number of devices in the target area.

Figure 17 – The average number of uplinks per lap as a function of the total number of IoT devices.
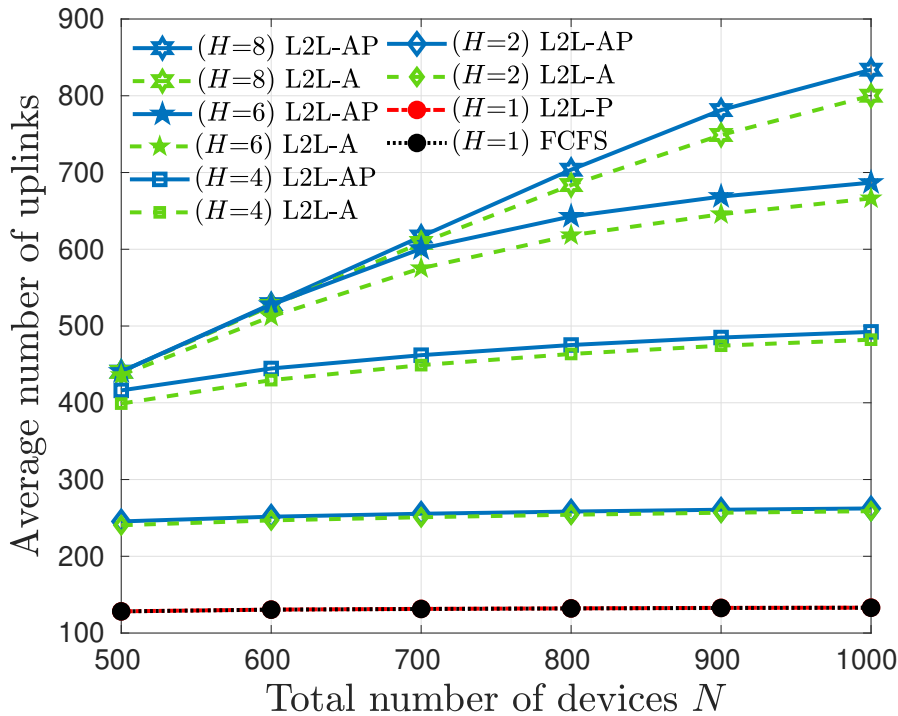
Source: The Author.

Note that FCFS in Figure 17 almost does not change its performance since for this particular payload size, guard times, orbit parameters, and target region, the maximum number of uplinks that SALSA-FCFS can schedule is less than 150. Considering only one channel, although the L2L-P method outperforms SALSA-FCFS in each lap, the average number of uplinks does not modify significantly. Long transmission queues are generated in single-channel systems when multiple IoT devices enter the satellite footprint simultaneously, which causes the maximum uplink capacity to be reached quickly. Note that the upper bound of the number of uplinks of a channel in the mth lap can be estimated by considering the minimum rise time and the maximum set time of all the IoT devices, as well as the payload size and guard times, according to $(\max_n (S_{m,n}) - \min_n (R_{m,n}))/(2\delta + \tau)$. Therefore, increasing the number of IoT devices will not lead to more transmission opportunities if the maximum capacity has already been reached for the lap in question. In addition, we also analyzed the performance of the proposed methods in terms of the system uplink efficiency, defined as the average number of uplinks per visible device, as illustrated in Figure 18. The results complement those in Figure 17, confirming that the proposed approaches exploiting multiple channels can considerably increase the uplink efficiency by approximately five times, representing an improvement of about 80% in a dense scenario with 10^3 IoT devices. Furthermore, Figure 18 also guarantees an uplink efficiency greater than 50%, applying
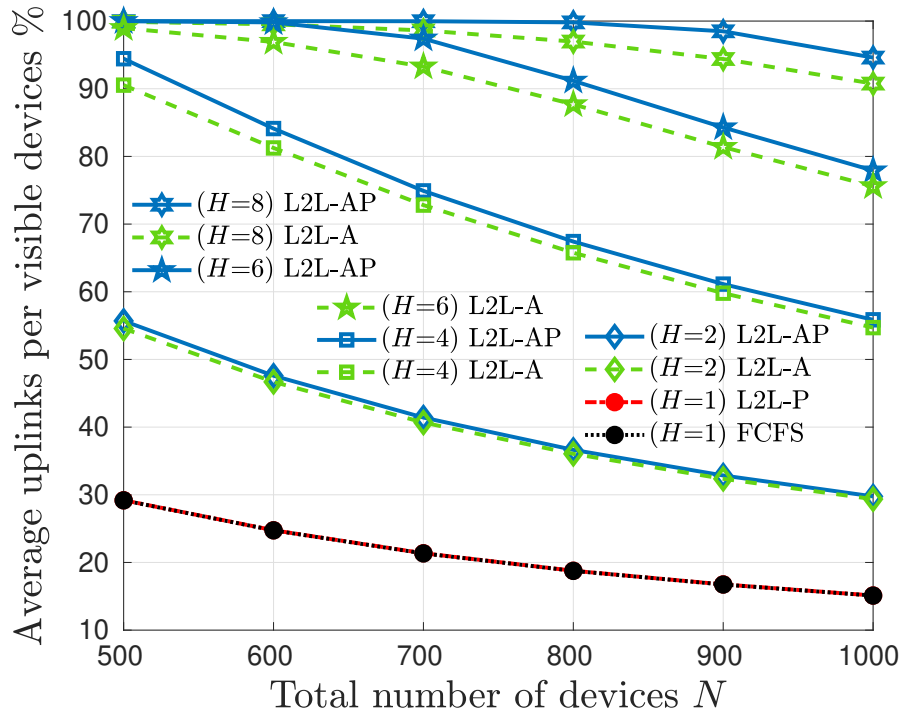
Figure 18 – The average number of uplinks per visible device as a function of the total number of IoT devices.

Source: The Author.

the scheduling algorithms with four, six, and eight multiple channels.

Finally, we investigate the impact of the payload size on the performance of the proposed methods. In Figure 19, we show the average number of uplinks per lap for different numbers of channels, devices, and payload sizes. As expected, a smaller payload size leads to a lower τ, so more uplinks can be scheduled within the visibility time window. This effect is best appreciated in the case of $H = 2$ channels. We can see that the advantage of the L2L-AP over L2L-A increases with the number of available channels H, especially for larger payload sizes. Note that the average number of uplinks per lap does not match the number of devices because not all devices are visible at all laps due to the orbit dynamics and the position of the devices. In Figure 20, we show the average number of uplinks per visible device that are scheduled when running L2L-A and L2L-AP with two or six channels for different numbers of devices and payload sizes. We can see that the proposed methods can achieve maximum efficiency in several setups. The highest uplink efficiencies are achieved with small payload sizes and the largest number of channels available. Finally, L2L-AP outperforms L2L-A in all configurations.

Figure 19 – The average number of uplinks per lap for L2L-A (left) and L2L-AP (right) with two (top) and four (bottom) channels, considering different payload sizes (2B, 32B, and 51B) and $N \in \{500,700,1000\}$ IoT devices.
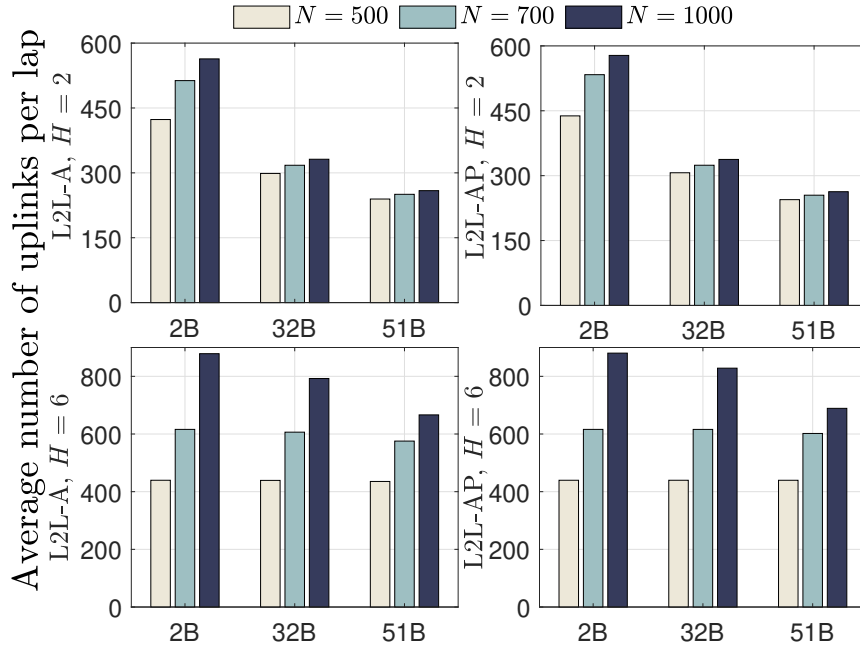
Source: The Author.

Figure 20 – The average number of uplinks per visible device for L2L-A (left) and L2L-AP (right) with two (top) and four (bottom) channels, considering different payload sizes (2B, 32B, and 51B) and $N \in \{500,700,1000\}$ IoT devices.
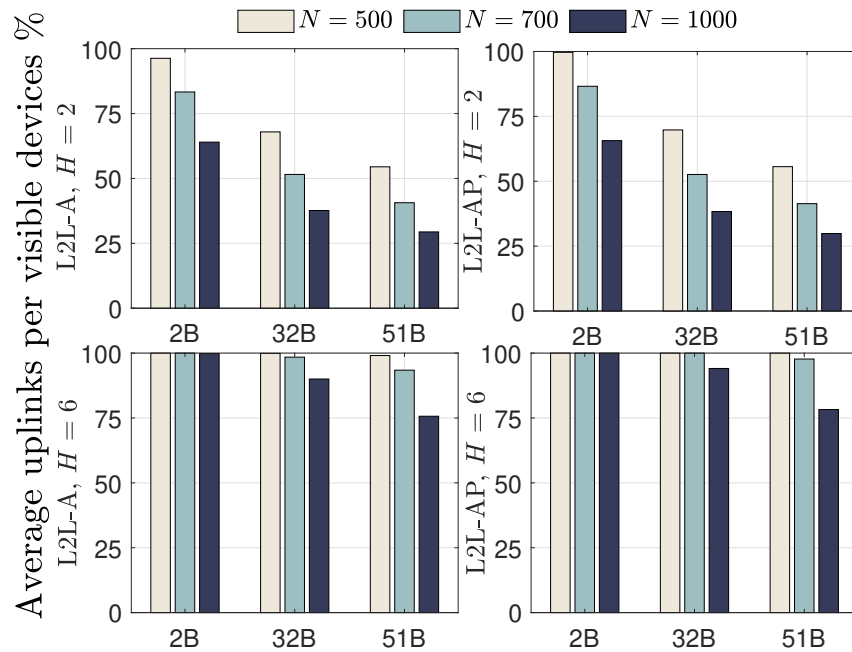
Source: The Author.

3.6   FINAL CONSIDERATIONS

We presented two novel scheduling approaches to be used in a DtS-IoT network. The L2L-A algorithm is particularly tailored to exploit multiple frequency channels efficiently. Meanwhile, the L2L-AP algorithm incorporates the possibility of swapping the time slots of already allocated devices, making room for new transmission opportunities. The numerical results demonstrate that the proposed methods can considerably improve the uplink efficiency of DtS-IoT networks, even in dense scenarios.

4 NON-ORTHOGONAL MULTIPLE-ACCESS STRATEGIES FOR DIRECT-TO-SATELLITE IOT NETWORKS

This chapter introduces two novel uplink strategies for LoRaWAN-based DtS-IoT networks, considering a detailed non-terrestrial fading model and assuming power-domain NOMA for ground devices. The main goal is to improve the uplink scalability without compromising the energy consumption and assuming no strict synchronization among devices.

More specifically, the chapter starts with related work in Section 4.1. It then describes the system model in Section 4.2 and introduces the proposed uplink strategies in Section 4.3. Following this, Section 4.4 outlines the simulation parameters and discusses the numerical results. Section 4.5 concludes with final considerations. Furthermore, Table 8 provides a list of symbols used in this chapter. Finally, the content of this chapter was published in (TONDO et al., 2024b).

4.1 RELATED WORK

In (ÁLVAREZ et al., 2022), the authors present and analyze several LoRaWAN data rate optimization strategies for a DtS-IoT scenario. The devices know the satellite trajectory, and based on the channel state information, can efficiently select the transmit data rate. On top of that, several different approaches are proposed, including a centralized scheduling optimization based on a formal mixed integer linear programming model. For this case, the authors assume a central network server with knowledge on the device's traffic pattern and packet size. The authors in (TONDO et al., 2023) introduce a novel ALOHA-based traffic allocation strategy that achieves non-zero throughput even under high traffic loads and also increases the system performance in terms of energy efficiency. However, the method requires precise a priori knowledge of the traffic pattern.

The work in (HERRERÍA-ALONSO et al., 2023) proposes that the transmission time of the devices is randomized within the visibility window instead of allowing them to transmit as soon as there is a visible satellite. Moreover, the authors propose adaptive schemes, where the devices choose to transmit or not based on some knowledge about the network traffic. Although it shows improved throughput and success probability, the algorithm relies on estimating the traffic load and the link success probability by using acknowledgments in the downlink. Even if the traffic does not vary due to changes in the network (devices entering and leaving), satellite laps generate different footprints with different devices in sight, considerably complicating practical deployments/implementations of this approach.

The authors in (AFHAMISIS; PALATTELLA, 2022) propose SALSA, a time-division multiple access scheduling scheme for LoRa to LEO satellites. It is assumed

Table 8 – List of Symbols - Chapter 4.

Variable	Description
r	The received signal at the satellite
P_u	Transmit power for device u
g_u	The path loss considering device u
h_u	Visible time interval for each device n during m satellite lap
s_u	The modulated signal for device u
u	Reference IoT devices covered by a LEO satellite
I	Set containing all interfered devices transmitting simultaneously
w	Additive White Gaussian Noise
B	The respective bandwidth
F	Noise figure for LoRa technology
σ	Variance of the log-normal shadowing
α	Elevation angle
μ	Mean of the log-normal shadowing
λ	Wavelength
β	Variance of the log-normal shadowing
I_o	Zero-order modified Bessel function
$\mathcal{C}_1$	The first condition for successful decoding
$\mathcal{C}_2$	The second condition for successful decoding
Ψ	SIR threshold defined by LoRa technology
γ	SNR threshold defined by LoRa technology
$\mathcal{M}$	Number of successfully received messages at the satellite during the lap
b	Payload size
c	Speed of light
$\mathcal{G}$	Goodput
L	Number of predefined received power level
G_t	The transmitter antenna gain
G_r	The receiver antenna gain
K	Rice factor
R	Radius of Earth
H	The orbital height of the LEO satellite.
d	The distance between IoT device and the LEO satellite
h	Fading envelop
$\mathcal{S}$	Log-normal shadowing
$\mathcal{E}$	Energy efficiency

Source: The Author.

that the network server can estimate the satellite visibility windows for each device, whose locations are known, and then allocate a transmission slot, through a downlink communication, to selected devices. Moreover, to achieve higher capacity, the server needs to know the traffic pattern of the devices to avoid assigning too many slots to a device without much data to transmit. On a similar perspective, the work in (ORTIGUEIRA et al., 2021) proposes a LoRa DtS-IoT access scheme where the satellite schedules transmissions for the devices. The whole procedure of satellite discovery

Figure 21 – The DtS-IoT architecture consists of a gateway onboard a LEO satellite, IoT devices spread over the target area, and the terrestrial backhaul.
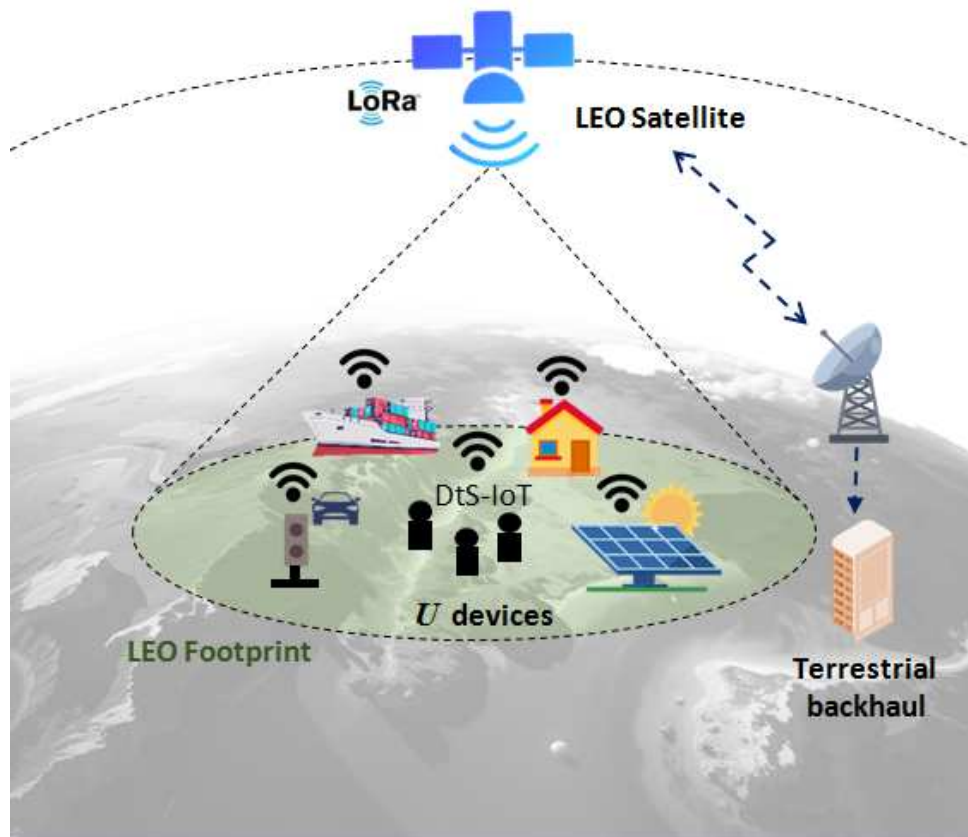
Source: The Author.

and exchange of information is detailed. However, the request-to-transmit procedure may lead to overhead signaling, especially in cases with several devices requesting simultaneously. In the same line, the work in (TONDO et al., 2024a) proposes two novel scheduling approaches for DtS-IoT with LoRa technology. The authors take advantage of multiple frequency channels to significantly increase uplink efficiency. However, a practical implementation requires the network server to know the device locations and traffic patterns.

Meanwhile, the NOMA approach is advocated as a potential direction for supporting 6G ubiquitous IoT (FANG; AL., 2021). An inherent issue in DtS-IoT is the high number of potential collided messages when many IoT devices transmit randomly in the uplink, compromising performance parameters such as scalability and energy efficiency (ORTIGUEIRA et al., 2021). Despite the efforts to address these problems in satellite-based IoT networks, the current literature does not explore non-orthogonal approaches using LoRaWAN protocols in DtS-IoT scenarios.

4.1.1 Novelty and Contribution

This chapter introduces two RA strategies for LoRa DtS-IoT, Fixed Transmission Power (FTP) and Controlled Transmission Power (CTP) methods. The strategies are designed such that transmissions from devices are received at the gateway with pre-defined average power levels. Such power levels are set with a separation such that two concurrent transmissions with different levels can be successfully decoded by SIC with high probability. In FTP, the devices choose when to transmit, within the visibility time window, to achieve one of the average power levels at the gateway. While in CTP, devices adapt their transmit power to transmit in different positions within the satellite visibility window, yielding one of the pre-determined average power levels at the satellite. Unlike (ÁLVAREZ et al., 2022; HERRERÍA-ALONSO et al., 2023; AFHAMISIS; PALATTELLA, 2022; TONDO et al., 2024a), the proposed schemes, FTP and CTP, are not dependent on network traffic estimation or immediate feedback links. Moreover, our methods are agnostic to the positioning of the devices, while solutions in (AFHAMISIS; PALATTELLA, 2022; TONDO et al., 2024a; ÁLVAREZ et al., 2022) require such knowledge. Different from (ORTIGUEIRA et al., 2021), we do not require any scheduling handshake procedure before transmission. Numerical results show the trade-off between goodput and energy efficiency for both proposed NOMA-based schemes. Comparing with the regular ALOHA protocol for 100 (600) IoT devices over France, we find goodput improvements of 65% (29%) and 52% (101%). Moreover, the CTP strategy is shown to be more energy efficient than FTP and regular ALOHA.

4.2 SYSTEM MODEL

We consider an IoT network composed of $\mathcal{N}$ devices distributed within the target area and under the coverage of a single LEO satellite. We assume that the IoT devices use LoRa technology[1] to transmit data packets to the satellite in orbit, which is equipped with a SIC-enabled LoRa gateway, as seen in Figure. 21. Meanwhile, the terrestrial backhaul consists of a ground station responsible for receiving the packets from the satellite and forwarding them to a NS. For scope reasons, only the multiple access segment is of interest in this work.

During the satellite visibility window, *i.e.*, a visible orbit over the target area, also termed lap, each IoT device transmits a single message with a payload of *b* bytes. We assume that the LEO satellite often and periodically broadcasts beacons to notify devices when they are under coverage. Suppose the reference IoT device

---

[1] The LoRa technology (SEMTECH, 2015) is based on CSS modulation. Recently, LR-FHSS modulation was added as an alternative in the LoRaWAN specification(LORA ALLIANCE TECHNICAL COMMITTEE REGIONAL PARAMETERS WORKGROUP..., 2022). There are interesting trade-offs in terms of performance, time-on-air and energy consumption related to CSS and LR-FHSS modulations (AN1200..., 2022). Due to its widespread use and rich literature, in this work we focus on CSS LoRa modulation, but the extension of the proposed methods to LR-FHSS is relatively straightforward.

Figure 22 – The ground-space geometry is described for the IoT device u as a function of altitude H, distance d, elevation angle α, and radius of Earth R.
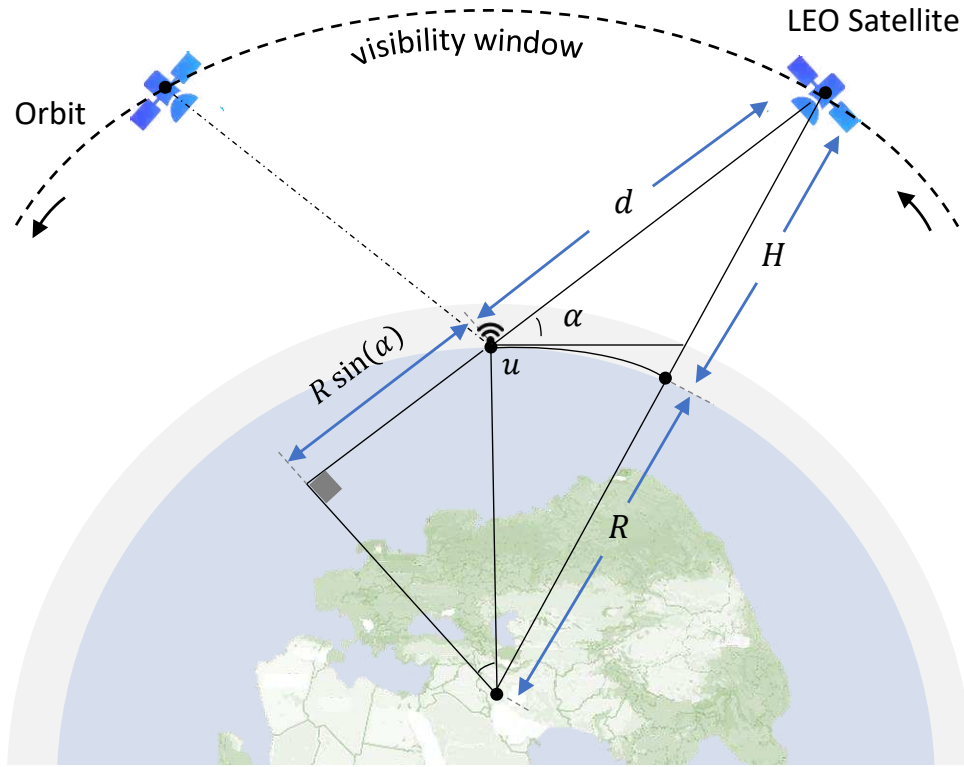
Source: The Author.

$u \in \{1, 2, ..., U\}$ transmits a message, then the received signal at the satellite can be expressed as the sum of the attenuated transmitted signal, interference from the set I containing all other devices transmitting simultaneously with u, and noise, as

$$r = \sqrt{P_u g_u}\, h_u s_u + \sum_{i \in I} \sqrt{P_i g_i}\, h_i s_i + w, \qquad (16)$$

where, for device u, P_u is the transmit power, g_u is the path loss, h_u is the channel fading and s_u is the modulated signal. Moreover, P_i, g_i, h_i and s_i have the same meaning but for the i-th interfering device, while w is Additive White Gaussian Noise (AWGN) with zero mean and power $\sigma_w^2 = -174 + F + 10 \log_{10} B$ dBm, considering receive noise figure F dB and bandwidth B Hz (SEMTECH, 2015). For the sake of clarity, in the following, the superscripts u and i are dropped whenever there is no ambiguity.

      The visibility window of each device occurs while the elevation angle between the satellite and that device is above a threshold $\alpha_{\min}$. The visibility window consists of two phases: first, the ascendant phase, where the elevation angle goes from minimum to maximum ($\alpha_{\min} \rightarrow \alpha_{\max}$), while in the descendant phase, it goes from maximum to minimum ($\alpha_{\max} \rightarrow \alpha_{\min}$). Moreover, as devices experience different maximum elevation angles, they also experience distinct visibility windows given a satellite lap. The duration of a visibility window for a given device is determined by the interval limited by the rise

Table 9 – Non-terrestrial channel fading parameters K, μ, and σ as a function of elevation angle α (CORAZZA; VATALARO, 1994).

$K(\alpha)$	μ(α)	σ(α)
$K_0 + K_1\alpha + K_2\alpha^2$	$\mu_0 + \mu_1\alpha + \mu_2\alpha^2 + \mu_3\alpha^3$	$\sigma_0 + \sigma_1\alpha$
Coefficients for empirical formulas		
$K_0 = 2.731$ $K_1 = -1.0474 \ 10^{-1}$ $K_2 - 2.7740 \ 10^{-3}$	$\mu_0 = -2.331$ $\mu_1 = 1.142 \ 10^{-1}$ $\mu_2 = -1.939 \ 10^{-3}$ $\mu_3 = -1.094 \ 10^{-5}$	$\sigma_0 = 4.5$ $\sigma_1 = -0.05$

Source: The Author.

time and set time. The rise time happens when $\alpha = \alpha_{\mathrm{min}}$ during the ascendant phase, while the set time occurs again when $\alpha = \alpha_{\mathrm{min}}$, but during the descendant phase.

In Figure. 22, we illustrate a DtS-IoT link, showing the elevation angle and the parameters required to calculate the distance between a device u and the satellite. The distance is a function of the elevation angle α (ASAD ULLAH et al., 2024; MALEKI et al., 2024)

$$d(\alpha) = \left[\sqrt{(R+H)^2 - (R\cos(\alpha))^2} - R\sin(\alpha) \right],\qquad(17)$$

where α is given in degrees, $R = 6.378 \times 10^6$ m is the Earth radius and H is the orbital height of the LEO satellite.

We model the path loss using the free-space formula (RAPPAPORT, 2024)

$$g = G_t G_r \left(\frac{\lambda}{4\pi d} \right)^2,\qquad(18)$$

where $\lambda = c/f$ is the wavelength, c is the speed of light, f is the carrier frequency, and G_t and G_r are the antenna gains at the transmitter and receiver, respectively.

4.2.1 Non-Terrestrial Fading Model

Due to the non-geostationary orbit, the elevation angle α changes with time, modifying the relative channel conditions between a device and the satellite. There are many available models in the literature (LOO, 1985; FONTAN et al., 2001; ABDI et al., 2003; AKTURAN; VOGEL, 1995), such as Loo and Nakagami - m distributions that can be used to characterize the fading in such setups, while works as (CHOI et al., 2022; CORAZZA; VATALARO, 1994; LOPEZ-SALAMANCA et al., 2020) advocate that Rice fading is an attractive approach for ground-to-space links. Inspired by (CORAZZA; VATALARO, 1994), we model the fading envelope h as a combination of two processes

$f_h(h|\mathcal{S})$ and $f_\mathcal{S}(\mathcal{S})$:

$$f_h(h) = \int_0^\infty f_h(h|\mathcal{S}) f_\mathcal{S}(\mathcal{S}). \tag{19}$$

First, $f_h(h|\mathcal{S})$ is the Rice probability distribution function (PDF) parameterized according to the shadowing $\mathcal{S}$, as (CORAZZA; VATALARO, 1994):

$$f_h(h|\mathcal{S}) = 2(K + 1)\frac{h}{\mathcal{S}^2}\exp\left[-(K + 1)\frac{h^2}{\mathcal{S}^2} - K\right]$$

$$\times \quad I_o\left(2\frac{h}{\mathcal{S}}\sqrt{K(K + 1)}\right), \tag{20}$$

where I_o is the zero-order modified Bessel function (BELL, 2013) while K is the Rice factor, the ratio between the power in the line-of-sight (LOS) component over the non-line-of-sight components (NLOS). Moreover, we model the log-normal shadowing S as (CORAZZA; VATALARO, 1994):

$$f_\mathcal{S}(\mathcal{S}) = \frac{1}{\sqrt{2\pi}\beta\sigma\mathcal{S}}\exp\left[-\frac{1}{2}\left(\frac{\ln \mathcal{S} - \mu}{\beta\sigma}\right)^2\right], \tag{21}$$

where $\beta = (\ln10)/20$, μ and $(\beta\sigma)^2$ are the mean and variance of the associated normal variate. In Table 9, we list parameters K, σ, and μ as a function of the elevation angle for a rural tree-shadowed environment (CORAZZA; VATALARO, 1994). Herein, a larger α results in smaller σ and larger Rice factor K, *i.e.*, increased channel LOS and better link conditions. Note that the model in (CORAZZA; VATALARO, 1994) is based on actual measurements.

4.2.2 Conditions for Successful Decoding

Following the literature on LoRa networks (MAHMOOD, A. et al., 2019; ÁLVAREZ et al., 2022; HERRERÍA-ALONSO et al., 2023), we assume two conditions must be met to guarantee successful decoding at the gateway. The first condition is that the Signal-to-Noise Ratio (SNR) at the gateway must be above a threshold γ defined by the LoRa technology (SEMTECH, 2015), which is a function of the spreading factor (SF). Therefore, the received power must be high enough for the gateway to detect and decode the message over the noise level. The SNR at the gateway given a transmission of device u can be written as

$$\text{SNR}_u = \frac{P_u g_u h_u^2}{\sigma_w^2}, \tag{22}$$

so that the first condition for successful decoding is

$$\mathcal{C}1 = \text{SNR}_u \geq \gamma. \tag{23}$$

The second condition states that the Signal to Interference Ratio (SIR) at the receiver must be above the capture threshold ψ, which is fixed for a given technology and it is well studied in the LoRa case (CROCE et al., 2018). The received power of a given transmission must be sufficiently higher than the sum of the interference (*i.e.*, other transmissions happening at the same time). We express the SIR of a given transmission as

$$\text{SIR}_u = \frac{P_u g_u h_u^2}{\sum\limits_{i \in I} P_i g_i h_i^2}.$$
(24)

Therefore, the second condition for successful decoding is

$$\mathcal{C}2 = \text{SIR}_u \geq \psi.$$
(25)

In this work, we assume that once a collision between transmitted messages happens, the gateway may be able to apply SIC and potentially recover them. For that sake, besides meeting conditions $\mathcal{C}1$ and $\mathcal{C}2$, the messages must have been transmitted using orthogonal pilots (or syncwords). This additional condition is to guarantee that the gateway can, after decoding the stronger message, estimate the channel concerning the stronger user, correctly reproduce what would be the received signal corresponding to that transmitted message, remove its contribution from the overall received signal (containing the collision of all messages), and then decode the message of the second strongest user from the remaining signal. This process iterates until the weakest user is decoded.

4.3   PROPOSED SCHEMES

In this section, we introduce two novel uplink strategies for DtS-IoT. Moreover, we assume the IoT devices are empowered with a predictor of the satellite orbit. Given this knowledge, a straightforward strategy would be to use plain ALOHA and let devices transmit freely in their visibility windows. This is very simple to implement but may lead to a large number of potential colliding devices, as several of them may have non-zero intersection in their visibility windows. Another possibility would be to let devices transmit in a given particular position, such as at the time instant corresponding to their maximum elevation angle. This sounds reasonable, as this position corresponds to the minimum distance concerning the satellite, leading to a large received power. However, this strategy has the side effect of reducing the overall effective visibility window of the satellite, increasing the collision probability.

A promising alternative may be one that lays between plain ALOHA and a strategy with a single transmit opportunity per device. An option is to let devices transmit in some positions spread within their visibility windows, so that due to their different geographical location it would be unlike to have a collision. Moreover, another interesting

possibility is to consider power domain NOMA, while employing SIC at the gateway. In such a case, more than one device may successfully transmit at the same time instant, alleviating the issue with the plain ALOHA strategy. Next, we present two novel uplink strategies that exploit the above ideas.

4.3.1 Fixed Transmit Power (FTP)

In the FTP strategy, the devices employ a fixed transmit power, while they choose the transmit position[2] within their visibility windows so that the average received power at the gateway is $\mathcal{L}_l$, for $l \in \{1, 2, \ldots, L\}$, where L is the number of predefined received power levels. This is accomplished by inverting (18), considering a fixed transmit power P, obtaining

$$d^{\text{FTP}} = \frac{\lambda \sqrt{PG_t G_r}}{4\pi \sqrt{\mathcal{L}_l}}. \tag{26}$$

Thus, with a fixed transmit power P, devices choose the appropriate time to transmit such that their distance to the satellite d^{FTP} results in the desired path loss, and consequently, the desired target received power level. Note that, due to the symmetric nature of the satellite orbit over a given region, there is a maximum of $2 \times L$ possible transmit positions for a device: L times during the ascending phase and L times during the descending phase. The utilized transmit position should be randomly chosen by the device within the possible positions. Furthermore, we assume that the power levels have sufficient difference among them so that applying NOMA/SIC is possible, and that each power level is associated with an orthogonal pilot, for the reasons mentioned in Section 4.2.2.

Moreover, note that there is a relation between the distance and the elevation angle, as given by (17). For orbits with low maximum elevation angle, a device may not be able to achieve certain power levels, as they would required a high elevation angle (reduced path loss) that is just not possible in that particular satellite lap for that device. Finally, note that transmissions are subject to fading and shadowing, causing the received power to deviate from the target power levels, so that SIC may fail if the actual received power levels are not sufficiently apart.

4.3.2 Controlled Transmit Power (CTP)

The FTP strategy limits the transmissions to particular slots within the visibility windows of each device, thus contributing to reduce collisions. However, it is vulnerable to a potential contender device with a very similar distance to the satellite. To address this limitation, the CTP strategy allows devices to transmit at any time during the orbit by

---

[2] We refer to the transmit position within the trajectory of the LEO satellite, such as the initial position (rise time) and the end position (set time).

Figure 23 – Visibility windows from device $u = 1$ to device $u = 10$ in peach color tone, and power levels: $\mathcal{L}_1$ (in blue) and $\mathcal{L}_2$ (in red). (a) In FTP, the devices $u \in \{1, 3, 5\}$ could generate both power levels in different opportunities while the other devices could generate only $\mathcal{L}_1$. (b) In CTP, nearly the entire visibility window can be exploited by the devices.

(a) FTP.   (b) CTP
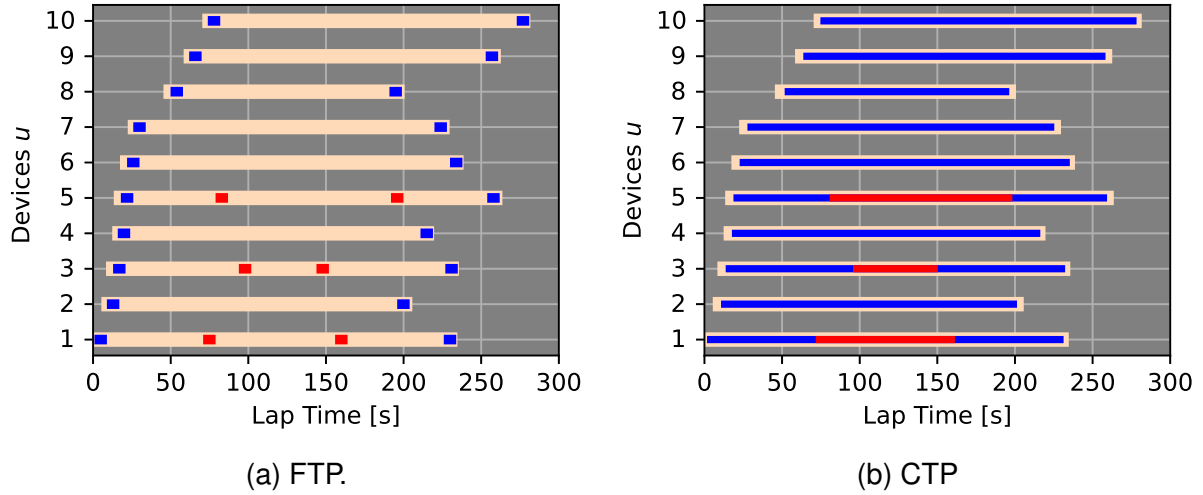
Source: The Author.

adapting their transmit power, while respecting a maximum transmit power constraint, therefore spreading more their transmissions within the visibility window while still employing NOMA. In this scenario, by rearranging (26) we find the required transmit power to yield a given average received power at the satellite considering a particular position within the visibility time window as

$$P^{\mathrm{CTP}} = \frac{16\pi^2 d^2 \mathcal{L}_l}{\lambda^2 G_t G_r}. \tag{27}$$

4.3.3 Performance Metrics

The performance of the proposed methods is evaluated in terms of two metrics, the goodput $\mathcal{G}$ and the energy efficiency $\mathcal{E}$. The goodput is defined as the average number of successfully received bytes at the satellite per lap (bytes/lap)

$$\mathcal{G} = \mathcal{M}b, \tag{28}$$

considering the number of successfully received messages $\mathcal{M} \leq U$ at the satellite during that lap and the number of bytes b per message.

The energy efficiency, in bytes/J, is the ratio between the goodput and the average transmit power $\bar{P}$ used by the end devices during that lap, so that it can be calculated as

$$\mathcal{E} = \frac{\mathcal{G}}{U\bar{P}}. \tag{29}$$

Table 10 – Simulation Parameters.

	Value	Parameter
Maximum Transmit Power	14 [dBm]	P
Transmitter Antenna Gain	0 [dBi]	G_t
Receiver Antenna Gain	13.5 [dBi]	G_r
Channel Bandwidth	125 [kHz]	B
Carrier Frequency	868 [MHz]	f
Time-on-Air	1.8104 [s]	ToA
Payload size	20 [Bytes]	b
Spreading Factor	12	SF
Sensitivity	−137 [dBm]	-
SNR Threshold	−20 [dB]	γ
SIR Threshold	1 [dB]	ψ
Noise Figure	6 [dB]	F

Source: The Author.

Finally, although the methods proposed here can be applied to any number of power levels, in this work we constrain the application of SIC to only two power levels due to practical reasons. With more SIC rounds, the complexity at the gateway increases, the potential accumulation of residual interference can decrease the performance of SIC, and the probability to meet conditions $\mathcal{C}1$ and $\mathcal{C}2$ for several SIC iterations would certainly decrease considerably.

4.4 NUMERICAL RESULTS

In this section, we present numerical results to evaluate the trade-off between the average number of successfully decoded transmissions and energy consumption considering the regular ALOHA protocol and the proposed schemes. The simulation parameters are listed in Table 10. Aiming at a realistic scenario, the device locations are uniformly distributed over France according to geographic coordinates using the Python GeoPy library (GEOPY CONTRIBUTORS, 2018). The distance between each device and the gateway is estimated with the Skyfield astronomy library (RHODES, 2023). Utilizing data from the CelesTrack platform (CELESTRACK DATABASE, 2023), this public library fits information in the two-line element (TLE) set format to determine the satellite's locations based on its orbit and pointing time. More specifically, the satellite visibility times allow us to compute the distance to the devices using (CELESTRACK DATABASE, n.d.). Furthermore, we consider the real orbit of the LacunaSat-3 LEO satellite, positioned at an altitude ranging from 500 km to 600 km above Earth (NANOSATS DATABASE, 2020). As in (ÁLVAREZ et al., 2022; HERRERÍA-ALONSO et al., 2023), we also assume a minimum elevation angle of 30°. Moreover, following (AFHAMISIS; PALATTELLA, 2022; HERRERÍA-ALONSO et al., 2023; TONDO et al., 2024a; ORTIGUEIRA et al., 2021), we consider the use of the most robust spreading factor.

Figure 24 – The average number of successfully received bytes per lap as a function of the number of IoT devices for the proposed FTP (in red) and CTP (in green) schemes, as well as for regular ALOHA (in blue).
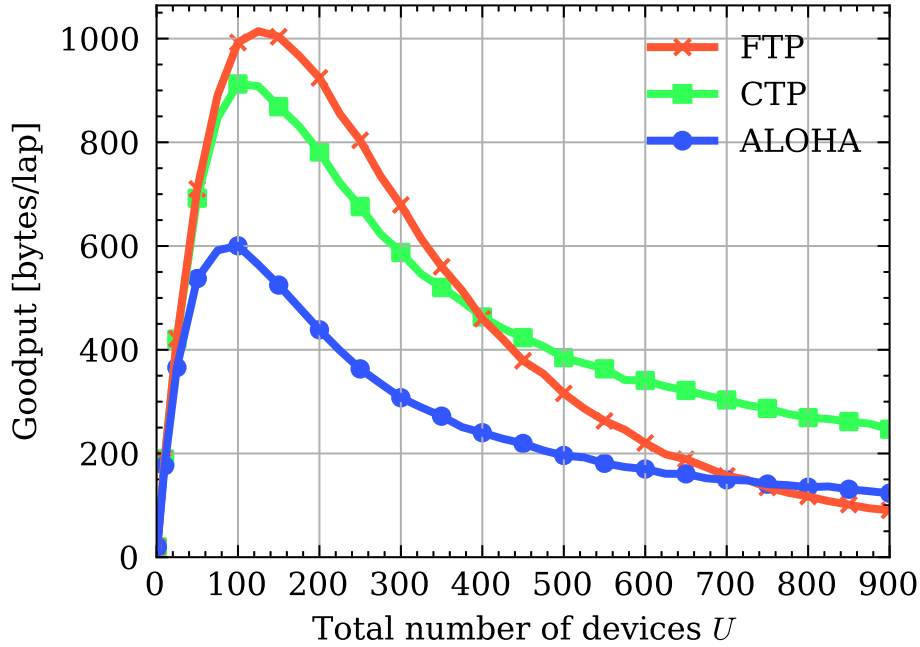
Source: The Author.

We start by illustrating the behavior of the proposed multiple-access strategies. Figure 23 shows a vulnerability analysis for $U = 10$ devices considering $L = 2$ power levels. In both cases, the peach color tone represents the visibility windows at the point of view of each device. Additionally, blue and red colors represent the time intervals during which the device is able to generate power levels $\mathcal{L}_1$ and $\mathcal{L}_2$ at the satellite, respectively. Figure 23a shows that, considering the FTP scheme, there are very specific intervals of time that $\mathcal{L}_1$ or $\mathcal{L}_2$ could be received at the LEO gateway, depending on the distance d^{FTP}. Moreover, in the case of CTP shown in Figure. 23b, the IoT devices can more effectively utilize the time window. In other words, selecting the required transmit power P^{CTP}, they can generate $\mathcal{L}_1$ or $\mathcal{L}_2$ at the satellite while transmitting at different positions within the visibility time window, spreading their transmissions. Finally, note that only devices $u \in \{1, 3, 5\}$ can generate two power levels, consequently, the FTP scheme allows for just four transmission opportunities, while CTP offers multiple opportunities for the uplink. Note that, in CTP, if the device chooses to generate power level $\mathcal{L}_1$, then it may transmit basically at anytime within the visibility window, but if it chooses $\mathcal{L}_2$, then such interval considerably decreases. This makes CTP a midday between FTP (very localized transmissions) and ALOHA (transmissions at anytime).

Next, Figure 24 shows the goodput of the proposed DtS-IoT schemes, FTP (in red) and CTP (in green), as well as that of regular ALOHA (in blue) versus the number

Figure 25 – The energy efficiency as a function of the number of IoT devices for the proposed FTP (in red) and CTP (in green) schemes, as well as for regular ALOHA (in blue).
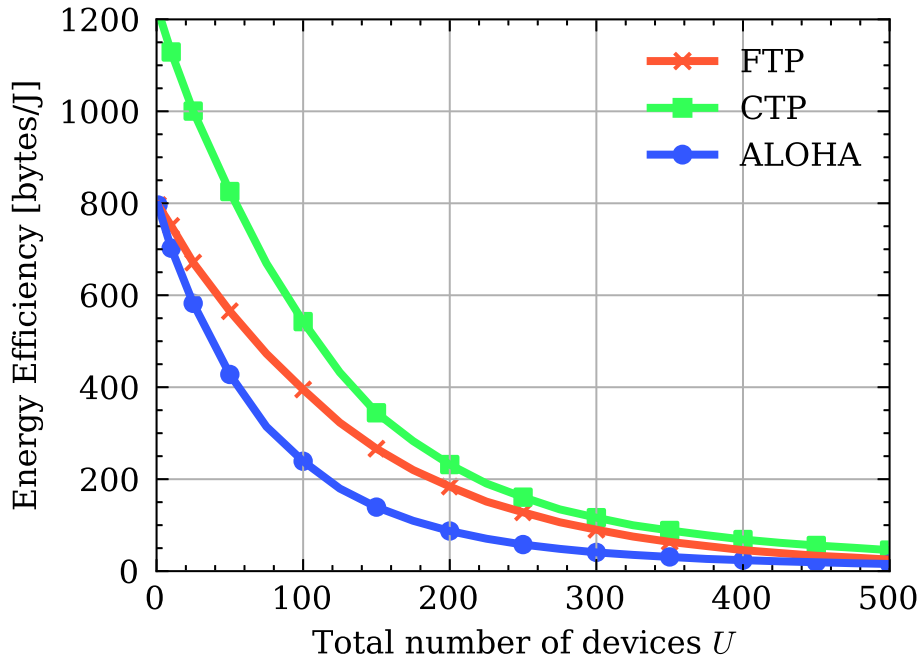

Source: The Author.

of devices and a payload of b = 20 bytes. For U = 100 devices, FTP achieves an improvement of 65% (992 bytes/lap) over regular ALOHA (601 bytes/lap), while CTP performs 52% (913 bytes/lap) better than ALOHA. Note that, as illustrated by Figure 23, with a relatively small number of devices FTP has the advantage that collisions are less frequent since the devices transmit only at particular intervals in the visibility windows. However, as more devices appear in the satellite footprint, a large number of them have similar positions, leading to similar transmit time within their visibility windows. This issue increases the probability of collisions in FTP, so that CTP performs better for a sufficient number of devices. In the case of Figure 24, this happens for $U > 400$. For instance, in the case of U = 600, CTP and FTP achieve an improvement of 101% (341 bytes/lap) and 29% (220 bytes/lap) over regular ALOHA (170 bytes/lap).

To evaluate our proposed schemes in terms of energy efficiency, Figure 25 shows this metric versus the number of IoT devices U. Note that the CTP method offers a significant advantage in terms of energy efficiency with respect to FTP and ALOHA. With U = 100 devices, CTP provides a gain of 37% in terms of energy efficiency with respect to FTP, while this gain is of 127% with respect to ALOHA. Moreover, CTP outperforms FTP and ALOHA for all numbers of IoT devices, compensating the fact that it is outperformed by FTP in terms of goodput for less dense networks. The advantage of CTP in terms of energy efficiency comes from the fact that the devices can adapt their

Figure 26 – Device count *versus* type of collision events considering $U = 100$ devices for FTP (in red), CTP (in green) and ALOHA (in blue). The collisions are classified as none, simple and multiple.
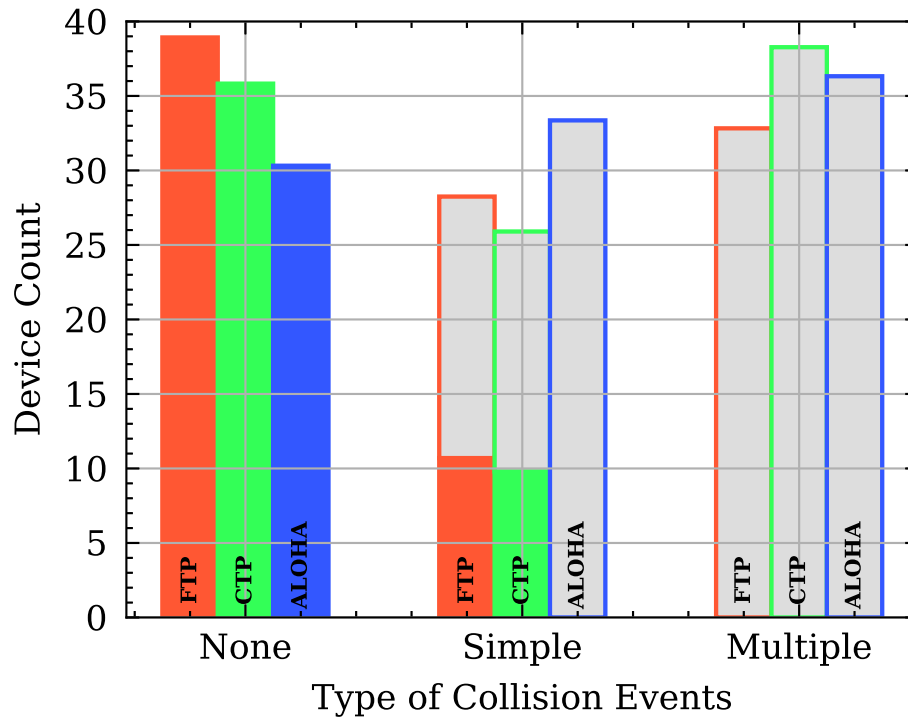
Source: The Author.

transmit power (respecting a maximum transmit power constraint), leading to energy savings, what is very desirable in IoT networks.

In order to better understand the goodput results, we classify the collision events for $U = 100$ devices in Figure 26 as: (i) None, where the message was received without collisions; (ii) Simple, where a collision was detected between two transmitted messages; and (iii) Multiple, where more than two messages were received simultaneously. The number of collision events in each of the above three classes are shown for FTP (bars in red), CTP (bars in green) and ALOHA (bars in blue). Moreover, the fraction of each bar filled in gray represents the collided messages that could not be decoded. For simple events, the satellite gateway can decode FTP and CTP messages if, and only if, they have different power levels (*i.e*, one message was received with power $\mathcal{L}_1$ and the other with $\mathcal{L}_2$). Figure 26 shows that FTP has 38.92 events of the type "none" per lap in average, more than the other methods, but also has more successfully decoded messages with simple collisions (10.68 events per lap in average). Consequently, FTP achieves the largest goodput (38.92 + 10.68 successfully decoded messages of 20 bytes each, leading to 992 bytes/lap) among all for $U = 100$ devices. Moreover, Figure 27 shows the same illustration but for $U = 600$ devices, where the number of multiple collided messages considerably increases for all methods. Moreover, CTP

Figure 27 – Device count *versus* type of collision events considering $U = 600$ devices for FTP (in red), CTP (in green) and ALOHA (in blue). The collisions are classified as none, simple and multiple.
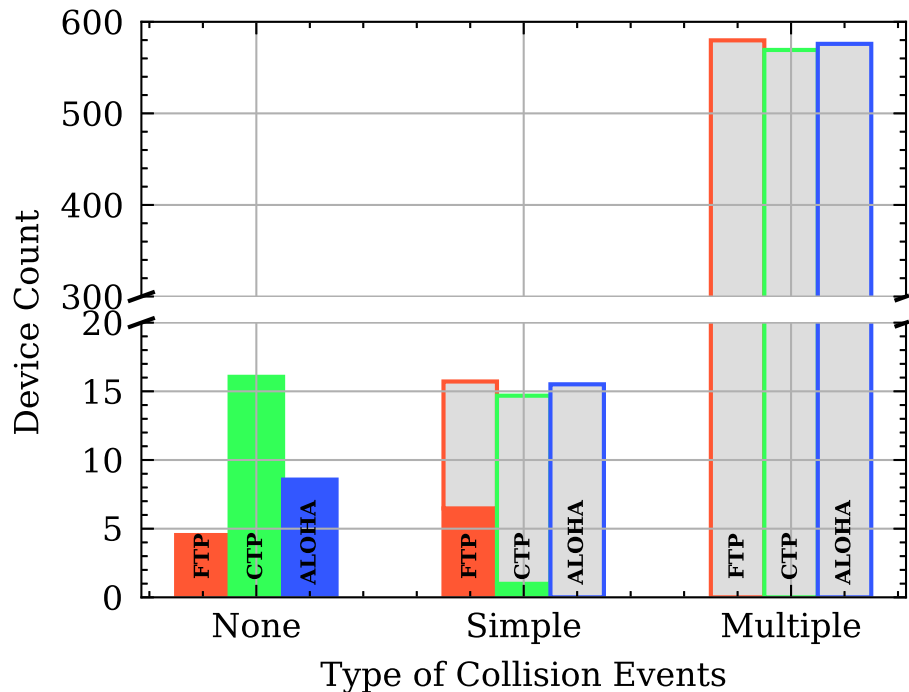

Source: The Author.

presents many more events of the type "none" than FTP and ALOHA, leading to a larger goodput. In denser networks, it is more relevant to distribute the transmissions in larger time intervals as CTP does, what can be seen as a midway between what ALOHA does (the device is free to transmit at anytime within the visibility window) and what FTP does (the devices are allowed to transmit at only very particular points in the trajectory).

4.5 FINAL CONSIDERATIONS

This work presented two novel DtS-IoT multiple access schemes using power domain NOMA. To explore particular positions of each IoT device within the visibility time window, we propose power domain NOMA strategies, FTP and CTP, using either fixed and controlled transmit power. We evaluated the goodput and energy efficiency of both strategies and compared with regular ALOHA. The proposed methods greatly outperform ALOHA in terms of goodput, with FTP performing better up to a number of devices, while CTP performs better for denser networks. Moreover, in terms of energy efficiency CTP showed to be superior for all numbers of devices.

5 CONCLUSIONS

This thesis contributes to the global connectivity trend expected for future 6G networks, which includes the efforts to enhance resource allocation for IoT-based systems covered by LEO satellites. We introduced a novel optimal traffic load allocation strategy for Aloha-based IoT LEO constellations. The link between the cluster of IoT devices and each satellite in the constellation was modelled by an erasure probability, following the On-Off fading channel model. To maximize the achievable system throughput, we proposed a low-complexity SCA-based technique.

Then, inspired by SALSA, we presented two novel low computational cost scheduling strategies for DtS-IoT networks. As a first novelty, we introduce the LoRa-to-LEO scheduling with permutation (L2L-P) of scheduled times. This strategy takes advantage of the ability to change the scheduling order of the IoT devices within the visibility time window and explores unused time by the previously proposed SALSA. Furthermore, we presented the LoRa-to-LEO with Alternating channels (L2L-A), a strategy that effortlessly re-distributes the order of IoT devices to optimize the efficient utilization of available channels. The numerical results showed that combining both strategies in L2L-AP considerably improves the average number of uplinks.

Finally, we proposed two novel DtS-IoT schemes using power domain NOMA in the uplink with either fixed (FTP) or controlled (CTP) transmit power. Using real geographic location and trajectory data, we evaluated the performance of the average number of successfully decoded transmissions, goodput, and energy efficiency as a function of the number of network devices. Numerical results showed the trade-off between goodput and energy efficiency for both proposed schemes. CTP effectively leverages transmission opportunities as the network size increases, outperforming the other strategies. Moreover, CTP shows the best performance in energy efficiency compared to FTP and ALOHA.

5.1 FUTURE WORKS

The previously discussed elements demonstrate the relevance of the study of energy efficiency in DtS-IoT scenarios and the potential impact of using this indicator as a design metric for traffic load allocation strategies and medium access protocols in satellite constellation networks. In this sense, aiming at future works, first note that Chapter 2 currently assumes that the nodes always transmit their data packets, which may not be optimal in a real scenario, where the decision not to transmit can be a way to increase the system energy efficiency and extend the lifetime. Moreover, Chapter 3 only evaluates the permutation of scheduled times using multi-channels. A new method could be proposed where the segmentation of transmitted messages is applied to increase the average number of uplinks. Using the insights provided by Chapter 4,

other multiple-access strategies that incorporate machine learning could be developed to maximize successful decoded messages or energy efficiency. Furthermore, Table 11 summarizes potential research opportunities for each chapter.

Table 11 – Future investigation/possibilities for each chapter of this thesis.

System Model	Future Investigation
Chapter 2	• Evaluate system throughput performance considering the imperfect knowledge of the IoT devices' positions and different visibility times for each IoT device; • Consider device traffic characteristics, such as retransmissions, to enhance the proposed approaches; • Modify the optimization problem including the energy efficiency as the performance metric. The instantaneous traffic load of some devices may be set to zero at certain positions to improve energy efficiency. However, fairness issues may arise and should be adequately dealt with.
Chapter 3	• Analyze the segmentation of the payload to take advantage of short unused times within a lap and the parallel transmission of a message; • A new scenario may involve multiple satellites covering the target area. In this case, L2L-P and L2L-AP mechanisms could be further explored to improve the number of uplinks or avoid message collisions at the receiver side.
Chapter 4	• Explore the flexibility of our proposed protocols in adapting to energy constraints and awareness (typical of IoT setups), including energy harvesting possibilities; • Study of the impact of different payload sizes and data rates; • Extend the proposed methods to consider the use of LR-FHSS modulation.

Source: The Author.

REFERENCES

ABDI, A.; LAU, W.C.; ALOUINI, M.-S.; KAVEH, M. A new simple model for land mobile satellite channels: first- and second-order statistics. **IEEE Transactions on Wireless Communications**, v. 2, n. 3, p. 519–528, 2003.

ABRAMSON, Norman. THE ALOHA SYSTEM: Another Alternative for Computer Communications. In: PROCEEDINGS of the November 17-19, 1970, Fall Joint Computer Conference. Houston, Texas: Association for Computing Machinery, 1970. (AFIPS '70 (Fall)), p. 281–285.

AFHAMISIS, Mohammad; BARILLARO, Sebastian; PALATTELLA, Maria Rita. A Testbed for LoRaWAN Satellite Backhaul: Design Principles and Validation. In: 2022 IEEE International Conference on Communications Workshops (ICC Workshops). Seoul, South Korea: IEEE, 2022. P. 1171–1176.

AFHAMISIS, Mohammad; PALATTELLA, Maria Rita. SALSA: A Scheduling Algorithm for LoRa to LEO Satellites. **IEEE Access**, v. 10, p. 11608–11615, 2022.

AFHAMISIS, MOHAMMAD AND PALATTELLA, MARIA RITA. **SALSA Algorithm**. Accessed: Jul. 26, 2023. 2022. Available from: `%7B%7Bhttps://github.com/list-luxembourg/salsa%7D%7D`.

AKTURAN, R; VOGEL, WJ. Elevation angle dependence of fading for satellite PCS in urban areas. **Electronics Letters**, IET, v. 31, n. 14, p. 1125–1127, 1995.

AKYILDIZ, Ian F.; KAK, Ahan. The Internet of Space Things/CubeSats. **IEEE Network**, v. 33, n. 5, p. 212–218, 2019.

AKYILDIZ, Ian F.; KAK, Ahan; NIE, Shuai. 6G and Beyond: The Future of Wireless Communications Systems. **IEEE Access**, v. 8, p. 133995–134030, 2020.

ALLIANCE, LoRa. **The LoRa Alliance Wide Area Networks for Internet of Things**. Boulder, CO: LoRa Alliance. `https://www.lora-alliance.org`. [Accessed: October 17, 2024].

ÁLVAREZ, Guido et al. Uplink Transmission Policies for LoRa-based Direct-to-Satellite IoT. **IEEE Access**, v. 10, p. 72687–72701, 2022.

ASAD ULLAH, Muhammad; PASOLINI, Gianni; MIKHAYLOV, Konstantin; ALVES, Hirley. Understanding the Limits of LoRa Direct-to-Satellite: The Doppler Perspectives. **IEEE Open Journal of the Communications Society**, v. 5, p. 51–63, 2024.

AZARI, M. Mahdi et al. Evolution of Non-Terrestrial Networks From 5G to 6G: A Survey. **IEEE Communications Surveys** & **Tutorials**, v. 24, n. 4, p. 2633–2672, 2022.

BACCO, Manlio; CASSARÀ, Pietro; COLUCCI, Marco; GOTTA, Alberto. Modeling Reliable M2M/IoT Traffic Over Random Access Satellite Links in Non-Saturated Conditions. **IEEE Journal on Selected Areas in Communications**, v. 36, n. 5, p. 1042–1051, 2018.

BAI, Shengzhou; ZHANG, Yujin; JIANG, Yiping. Minimum-observation method for rapid and accurate satellite coverage prediction. **GPS Solutions**, v. 26, n. 4, p. 110, 2022.

BECK, Amir; BEN-TAL, Aharon; TETRUASHVILI, Luba. A sequential parametric convex approximation method with applications to nonconvex truss topology design problems. **Journal of Global Optimization**, Springer, v. 47, n. 1, p. 29–51, 2010.

BELL, William Wallace. **Special Functions for Scientists and Engineers**. Revised Dover Edition. Mineola, NY: Dover Publications, 2013. Originally published in 1968 by D. Van Nostrand Company, Ltd. ISBN 9780486317564.

BERIOLI, Matteo; COCCO, Giuseppe; LIVA, Gianluigi; MUNARI, Andrea. Modern Random Access Protocols. **Foundations and Trends® in Networking**, v. 10, n. 4, p. 317–446, 2016. ISSN 1554-057X.

BOYD, Stephen; VANDENBERGHE, Lieven. **Convex Optimization**. Cambridge: Cambridge University Press, 2004.

CAPEZ, Gabriel Maiolini; HENN, Santiago; FRAIRE, Juan A.; GARELLO, Roberto. Sparse Satellite Constellation Design for Global and Regional Direct-to-Satellite IoT Services. **IEEE Transactions on Aerospace and Electronic Systems**, v. 58, n. 5, p. 3786–3801, 2022.

CASINI, Enrico; DE GAUDENZI, Riccardo; DEL RIO HERRERO, Oscar. Contention Resolution Diversity Slotted ALOHA (CRDSA): An Enhanced Random Access Schemefor Satellite Access Packet Networks. **IEEE Transactions on Wireless Communications**, v. 6, n. 4, p. 1408–1419, 2007.

CASSARÁ, Pietro; GOTTA, Alberto; COLA, Tomaso de. A statistical framework for performance analysis of diversity framed slotted ALOHA with interference cancellation. **IEEE Transactions on Aerospace and Electronic Systems**, v. 56, n. 6, p. 4327–4337, 2020.

CELESTRACK DATABASE. **CelesTrack Database**. Accessed: Jun. 26, 2024. 2023. Available from: `https://celestrak.org/`.

CELESTRACK DATABASE. **Earth Satellites**. Accessed: Jun. 26, 2024. Available from: `%7Bhttps://rhodesmill.org/skyfield/earth-satellites.html$%5C#$generating-a-satellite-position/%7D`.

CENTENARO, Marco et al. A Survey on Technologies, Standards and Open Challenges in Satellite IoT. **IEEE Communications Surveys** & **Tutorials**, v. 23, n. 3, p. 1693–1720, 2021.

CHEN, Shanzhi; SUN, Shaohui; KANG, Shaoli. System integration of terrestrial mobile communication and satellite communication —The trends, challenges and key technologies in B5G and 6G. **China Communications**, v. 17, n. 12, p. 156–171, 2020.

CHOI, Jinho et al. Grant-Free Random Access in Machine-Type Communication: Approaches and Challenges. **IEEE Wireless Communications**, v. 29, n. 1, p. 151–158, 2022.

CIONI, Stefano; DE GAUDENZI, Riccardo; DEL RIO HERRERO, Oscar; GIRAULT, Nicolas. On the Satellite Role in the Era of 5G Massive Machine Type Communications. **IEEE Network**, v. 32, n. 5, p. 54–61, 2018.

CISCO VISUAL, Networking. Global Internet adoption and devices and connection, 2018-2023. **Cisco, San Jose, CA, USA, Tech**, p. 1–1, 2020.

CLAZZER, Federico; MUNARI, Andrea; LIVA, Gianluigi; LAZARO, Francisco; STEFANOVIC, Cedomir; POPOVSKI, Petar. **From 5G to 6G: Has the Time for Modern Random Access Come?** eess.SP: arXiv, 2019. arXiv: `1903.03063` `[eess.SP]`. Available from: `https://arxiv.org/abs/1903.03063`.

CORAZZA, G.E.; VATALARO, F. A statistical model for land mobile satellite channels and its application to nongeostationary orbit systems. **IEEE Transactions on Vehicular Technology**, v. 43, n. 3, p. 738–742, 1994.

CROCE, D. et al. Impact of LoRa Imperfect Orthogonality: Analysis of Link-Level Performance. **IEEE Comm. Lett.**, v. 22, n. 4, 2018.

DAI, Haibo; BIAN, Hui; LI, Chunguo; WANG, Baoyun. UAV-aided wireless communication design with energy constraint in space-air-ground Integrated green IoT networks. **IEEE Access**, v. 8, p. 86251–86261, 2020.

DENG, Minglong; CHENG, Ziyang; HE, Zishu. Co-Design of waveform correlation matrix and antenna positions for MIMO radar transmit beampattern formation. **IEEE Sensors Journal**, v. 20, n. 13, p. 7326–7336, 2020.

DI, Boya; ZHANG, Hongliang; SONG, Lingyang; LI, Yonghui; LI, Geoffrey Ye. Ultra-Dense LEO: Integrating Terrestrial-Satellite Networks Into 5G and Beyond for Data Offloading. **IEEE Transactions on Wireless Communications**, v. 18, n. 1, p. 47–62, 2019.

DOGRA, Anutusha; JHA, Rakesh Kumar; JAIN, Shubha. A Survey on Beyond 5G Network With the Advent of 6G: Architecture and Emerging Technologies. **IEEE Access**, v. 9, p. 67512–67547, 2021.

DOROSHKIN, Alexander A. et al. Experimental Study of LoRa Modulation Immunity to Doppler Effect in CubeSat Radio Communications. **IEEE Access**, v. 7, p. 75721–75731, 2019.

DU, Pengfei; YANG, Qinghai; SHEN, Zhong; KWAK, Kyung Sup. Quality of information maximization in lifetime-constrained wireless sensor networks. **IEEE Sensors Journal**, v. 16, n. 19, p. 7278–7286, 2016.

EMPRESA BRASILEIRA DE PESQUISA AGROPECUÁRIA. **Pesquisa mostra o retrato da agricultura digital brasileira**. 2020. Available from: `www.embrapa.br/busca-de-noticias/-/noticia/54770717/pesquisa-mostra-o-retrato-da-agricultura-digital-brasileira`. Visited on: 18 Dec. 2024.

FANG, Xinran; AL., et. 5G Embraces Satellites for 6G Ubiquitous IoT: Basic Models for Integrated Satellite Terrestrial Networks. **IEEE Internet of Things Journal**, v. 8, n. 18, p. 14399–14417, 2021.

FANG, Xinran; FENG, Wei; WANG, Yanmin; CHEN, Yunfei; GE, Ning; DING, Zhiguo; ZHU, Hongbo. NOMA-Based Hybrid Satellite-UAV-Terrestrial Networks for 6G Maritime Coverage. **IEEE Transactions on Wireless Communications**, v. 22, n. 1, p. 138–152, 2023.

FENGLER, Alexander; HAGHIGHATSHOAR, Saeid; JUNG, Peter; CAIRE, Giuseppe. Grant-Free Massive Random Access With a Massive MIMO Receiver. In: 2019 53rd Asilomar Conference on Signals, Systems, and Computers. Pacific Grove, CA, USA: IEEE, 2019. P. 23–30.

FERRER, Tomás; CÉSPEDES, Sandra; BECERRA, Alex. Review and Evaluation of MAC Protocols for Satellite IoT Systems Using Nanosatellites. **Sensors**, v. 19, n. 8, 2019. ISSN 1424-8220.

FONTAN, F.P.; VAZQUEZ-CASTRO, M.; CABADO, C.E.; GARCIA, J.P.; KUBISTA, E. Statistical modeling of the LMS channel. **IEEE Transactions on Vehicular Technology**, v. 50, n. 6, p. 1549–1567, 2001.

FORMAGGIO, Francesco; MUNARI, Andrea; CLAZZER, Federico. On receiver diversity for grant-free based machine type communications. **Ad Hoc Networks**, Elsevier, v. 107, p. 102245, 2020.

FOURATI, Fares; ALOUINI, Mohamed-Slim. Artificial intelligence for satellite communication: A review. **Intelligent and Converged Networks**, v. 2, n. 3, p. 213–243, 2021.

FRAIRE, Juan; HENN, Santiago; DOVIS, Fabio; GARELLO, Roberto; TARICCO, Giorgio. Sparse Satellite Constellation Design for LoRa-based Direct-to-Satellite Internet of Things. In: ICC 2020 - 2020 IEEE International Conference on Communications (ICC). Dublin, Ireland: IEEE, 2020. P. 1–6.

FRAIRE, Juan A.; CÉSPEDES, Sandra; ACCETTURA, Nicola. Direct-To-Satellite IoT - A Survey of the State of the Art and Future Research Perspectives. In: PALATTELLA, Maria Rita; SCANZIO, Stefano; COLERI ERGEN, Sinem (Eds.). **Ad-Hoc, Mobile, and Wireless Networks**. Cham: Springer International Publishing, 2019. P. 241–258.

FRAIRE, Juan A.; IOVA, Oana; VALOIS, Fabrice. Space-Terrestrial Integrated Internet of Things: Challenges and Opportunities. **IEEE Communications Magazine**, v. 60, n. 12, p. 64–70, 2022.

GAMAGE, Amalinda; LIANDO, Jansen; GU, Chaojie; TAN, Rui; LI, Mo; SELLER, Olivier. LMAC: Efficient carrier-sense multiple access for LoRa. **ACM Transactions on Sensor Networks**, ACM New York, NY, v. 19, n. 2, p. 1–27, 2023.

GAO, Zhixiang; LIU, Aijun; LIANG, Xiaohu. The Performance Analysis of Downlink NOMA in LEO Satellite Communication System. **IEEE Access**, v. 8, p. 93723–93732, 2020.

GE, Ruixing et al. Performance Analysis of Cooperative Nonorthogonal Multiple Access Scheme in Two-Layer GEO/LEO Satellite Network. **IEEE Systems Journal**, v. 16, n. 2, p. 2300–2310, 2022.

GEOPY CONTRIBUTORS. **GeoPy: Python Geocoding Toolbox**. Accessed: Jun. 26, 2024. 2018. Available from: `https://pypi.org/project/geopy/`.

GEORGIOU, Orestis; RAZA, Usman. Low Power Wide Area Network Analysis: Can LoRa Scale? **IEEE Wireless Communications Letters**, v. 6, n. 2, p. 162–165, 2017.

GONGORA-TORRES, Juan Misael; VARGAS-ROSALES, Cesar; ARAGÓN-ZAVALA, Alejandro; VILLALPANDO-HERNANDEZ, Rafaela. Link Budget Analysis for LEO Satellites Based on the Statistics of the Elevation Angle. **IEEE Access**, v. 10, p. 14518–14528, 2022.

GRANT, Michael; BOYD, Stephen. **CVX: Matlab Software for Disciplined Convex Programming, Version 2.2**. [S.l.: s.n.], 2020. Accessed: October 17, 2024. Available from: `http://cvxr.com/cvx/`.

GU, Yi; HAN, Chao; WANG, Xinwei. A Kriging Based Framework for Rapid Satellite-to-Site Visibility Determination. In: IEEE 10th International Conference on Mechanical and Aerospace Engineering (ICMAE). Brussels, Belgium: IEEE, 2019. P. 262–267.

HAN, Chao; GAO, XiaoJie; SUN, XiuCong. Rapid satellite-to-site visibility determination based on self-adaptive interpolation technique. **Science China Technological Sciences**, v. 60, p. 264–270, 2017.

HAN, Chao; YANG, Pengbin; WANG, Xiaohui; LIU, Shenggang. A fast computation method for the satellite-to-site visibility. In: IEEE Congress on Evolutionary Computation (CEC). [S.l.: s.n.], 2018. P. 1–8.

HAN, Chao; ZHANG, Yujin; BAI, Shengzhou; SUN, Xiucong; WANG, Xinwei. Novel method to calculate satellite visibility for an arbitrary sensor field. **Aerospace Science and Technology**, v. 112, p. 106668, 2021.

HAROUNABADI, Mehdi; HEYN, Thomas. Toward Integration of 6G-NTN to Terrestrial Mobile Networks: Research and Standardization Aspects. **IEEE Wireless Communications**, v. 30, n. 6, p. 20–26, 2023.

HERRERÍA-ALONSO, Sergio; RODRÍGUEZ-PÉREZ, Miguel; RODRÍGUEZ-RUBIO, Raúl F.; PÉREZ-FONTÁN, Fernando. Improving Uplink Scalability of LoRa-Based Direct-to-Satellite IoT Networks. **IEEE Internet of Things Journal**, v. 10, n. 20, p. c4–c4, Oct. 2023. ISSN 2327-4662.

AL-HRAISHAWI, Hayder; CHOUGRANI, Houcine; KISSELEFF, Steven; LAGUNAS, Eva; CHATZINOTAS, Symeon. A Survey on Nongeostationary Satellite Systems: The Communication Perspective. **IEEE Communications Surveys & Tutorials**, v. 25, n. 1, p. 101–132, 2023.

AL-HRAISHAWI, Hayder; MATURO, Nicola; LAGUNAS, Eva; CHATZINOTAS, Symeon. Scheduling Design and Performance Analysis of Carrier Aggregation in Satellite Communication Systems. **IEEE Transactions on Vehicular Technology**, v. 70, n. 8, p. 7845–7857, 2021.

INSTITUTO BRASILEIRO DE GEOGRAFIA E ESTATÍSTICA. **Em 2023, 88% das pessoas com 10 anos ou mais utilizaram internet**. Accessed:Jan.03,2025. 2024. Available from: https://agenciadenoticias.ibge.gov.br/agencia-noticias/2012-agencia-de-noticias/noticias/41026/.

IVANOV, Andrey; BYCHKOV, Roman; TCATCORIN, Evgenii. Spatial resource management in LEO satellite. **IEEE Transactions on Vehicular Technology**, v. 69, n. 12, p. 15623–15632, 2020.

JAKOVETIĆ, Dušan; BAJOVIĆ, Dragana; VUKOBRATOVIĆ, Dejan; CRNOJEVIĆ, Vladimir. Cooperative Slotted ALOHA for Multi-Base Station Systems. **IEEE Transactions on Communications**, v. 63, n. 4, p. 1443–1456, 2015.

JIANG, Hao; WANG, Hai; HU, Yulin; WU, Jing. Dynamic User Association in Scalable Ultra-Dense LEO Satellite Networks. **IEEE Transactions on Vehicular Technology**, v. 71, n. 8, p. 8891–8905, 2022.

KASSAB, Rahif; MUNARI, Andrea; CLAZZER, Federico; SIMEONE, Osvaldo. Grant-Free Coexistence of Critical and Noncritical IoT Services in Two-Hop Satellite and Terrestrial Networks. **IEEE Internet of Things Journal**, v. 9, n. 16, p. 14829–14843, 2022.

KASSAB, Rahif; SIMEONE, Osvaldo; MUNARI, Andrea; CLAZZER, Federico. Space Diversity-Based Grant-Free Random Access for Critical and Non-Critical IoT Services. In: ICC 2020 - 2020 IEEE International Conference on Communications (ICC). Virtual Conference: IEEE, 2020. P. 1–6.

KAWAMOTO, Yuichi; NISHIYAMA, Hiroki; FADLULLAH, Zubair Md; KATO, Nei. Effective data collection via Satellite-Routed Sensor System (SRSS) to realize global-scaled Internet of things. **IEEE Sensors Journal**, v. 13, n. 10, p. 3645–3654, 2013.

KODHELI, Oltjon; MATURO, Nicola; CHATZINOTAS, Symeon; ANDRENACCI, Stefano; ZIMMER, Frank. NB-IoT via LEO Satellites: An Efficient Resource Allocation Strategy for Uplink Data Transmission. **IEEE Internet of Things Journal**, v. 9, n. 7, p. 5094–5107, 2022.

KODHELI, Oltjon et al. Satellite Communications in the New Space Era: A Survey and Future Challenges. **IEEE Communications Surveys** & **Tutorials**, v. 23, n. 1, p. 70–109, 2021.

KOZIOL, Michael. **Satellites can be a surprisingly great option for IoT**. Online: IEEE, Aug. 2021. Available from:
`https://spectrum.ieee.org/satellites-great-option-iot`.

KUA, Jonathan et al. Internet of Things in Space: A Rev. of Opportunities and Challenges from Satellite-Aided Computing to Digitally-Enhanced Space Living. **Sensors**, v. 21, n. 23, 2021.

KUMAR, Dileep; KALEVA, Jarkko; TOLLI, Antti. Blockage-Aware Reliable mmWave Access via Coordinated Multi-Point Connectivity. **IEEE Transactions on Wireless Communications**, v. 20, n. 7, p. 4238–4252, 2021.

LACUNA SPACE. **An ultra-low cost tracking and sensor detection service for small amounts of data**. Online; accessed Jul. 26, 2023. 2023. Available from:
`https://lacuna.space/`.

LAMAIRE, R.O.; ZORZI, M. Effect of correlation in diversity systems with Rayleigh fading, shadowing, and power capture. **IEEE Journal on Selected Areas in Communications**, v. 14, n. 3, p. 449–460, 1996.

LEDESMA, Oscar; LAMO, Paula; FRAIRE, Juan A. Trends in LPWAN Technologies for LEO Satellite Constellations in the NewSpace Context. **Electronics**, v. 13, n. 3, 2024. ISSN 2079-9292.

LENG, Tao; LI, Xiaoyao; HU, Dongwei; CUI, Gaofeng; WANG, Weidong. Collaborative Computing and Resource Allocation for LEO Satellite-Assisted Internet of Things. **Wireless Communications and Mobile Computing**, v. 2021, n. 1, p. 4212548, 2021. eprint: `https://onlinelibrary.wiley.com/doi/pdf/10.1155/2021/4212548`.

LEYVA-MAYORGA, Israel; SORET, Beatriz; RÖPER, Maik; WÜBBEN, Dirk; MATTHIESEN, Bho; DEKORSY, Armin; POPOVSKI, Petar. LEO Small-Satellite Constellations for 5G and Beyond-5G Communications. **IEEE Access**, v. 8, p. 184955–184964, 2020.

LI, Peng; JIAN, Xin; WANG, Fang; FU, Shu; ZHANG, Zhaotao. Theoretical Throughput Analysis for Massive Random Access With Spatial Successive Decoding. **IEEE Transactions on Vehicular Technology**, v. 69, n. 7, p. 7998–8002, 2020.

LI, Zhipeng; LI, Meng; WANG, Qian. Predator–Prey Model Based Asymmetry Resource Allocation in Satellite–Terrestrial Network. **Symmetry**, v. 13, n. 11, 2021.

LIN, Wenliang et al. A Novel Load Balancing Scheme for Satellite IoT Networks Based on Spatial-Temporal Distribution of Users and Advanced Genetic Algorithms. **Sensors**, v. 22, n. 20, 2022.

LIU, Yifei; FENG, Lang; WU, Liang; ZHANG, Zaichen; DANG, Jian; ZHU, Bingcheng; WANG, Lei. Joint optimization based satellite handover strategy for low Earth orbit satellite networks. **IET Communications**, v. 15, n. 12, p. 1576–1585, 2021.

LIVA, Gianluigi. Graph-Based Analysis and Optimization of Contention Resolution Diversity Slotted ALOHA. **IEEE Transactions on Communications**, v. 59, n. 2, p. 477–487, 2011.

LOO, Chun. A statistical model for a land mobile satellite link. **IEEE Transactions on Vehicular Technology**, v. 34, n. 3, p. 122–127, 1985.

LÓPEZ, Onel L. A.; KUMAR, Dileep; SOUZA, Richard Demo; POPOVSKI, Petar; TÖLLI, Antti; LATVA-AHO, Matti. Massive MIMO With Radio Stripes for Indoor Wireless Energy Transfer. **IEEE Transactions on Wireless Communications**, v. 21, n. 9, p. 7088–7104, 2022.

LOPEZ-SALAMANCA, Julian J.; SEMAN, Laio Oriel; BEREJUCK, Marcelo D.; BEZERRA, Eduardo A. Finite-State Markov Chains Channel Model for CubeSats Communication Uplink. **IEEE Transactions on Aerospace and Electronic Systems**, v. 56, n. 1, p. 142–154, 2020.

LOPEZ-SALAMANCA, Julian J.; SEMAN, Laio Oriel; BEZERRA, Eduardo A.; SOUZA, Richard Demo; MONTEJO-SÁNCHEZ, Samuel. Multi-sector discrete-time channel model for data link layer evaluation of CubeSat communications. **Expert Systems with Applications**, v. 203, p. 117375, 2022. ISSN 0957-4174.

LORA ALLIANCE. **LoRa Alliance Technical Committee Regional Parameters Workgroup, Version 1.0.4 and Regional Parameters RP002**. [S.l.], Sept. 2022. Available from: `https://resources.lora-alliance.org/technical-specifications/rp002-1-0-4-regional-parameters`.

LORA ALLIANCE. **Connect with purpose**. Online; accessed Jul. 26, 2023. 2023a. Available from: `https://oneweb.net/`.

LORA ALLIANCE. **LoRaWAN 1.1 Specification**. Accessed: October 17, 2024. July 2023b. Available from: `https://resources.lora-alliance.org/home/lorawan-specification-v1-1`.

LORA ALLIANCE. **RP2-1.0.2 LoRaWAN Regional Parameters**. [S.l.: s.n.], 2020. Online; accessed Jul. 26, 2023. Available from: `%7Bhttps://lora-alliance.org/resourcehub/rp2-102-lorawan-regional-parameters/%7D`.

M. ELHALAWANY, Basem et al. Outage Analysis of Coordinated NOMA Transmission for LEO Satellite Constellations. **IEEE Open Journal of the Communications Society**, v. 3, p. 2195–2202, 2022.

MA, Ting; ZHOU, Haibo; QIAN, Bo; CHENG, Nan; SHEN, Xuemin; CHEN, Xiang; BAI, Bo. UAV-LEO integrated backbone: A ubiquitous data collection approach for B5G Internet of remote things networks. **IEEE Journal on Selected Areas in Communications**, v. 39, n. 11, p. 3491–3505, 2021.

MAHMOOD, Aamir et al. Scalability Analysis of a LoRa Network Under Imperfect Orthogonality. **IEEE Transactions on Industrial Informatics**, v. 15, n. 3, p. 1425–1436, 2019.

MAHMOOD, M. Rezwanul et al. A Comprehensive Rev. on Artificial Intelligence/Machine Learning Algorithms for Empowering the Future IoT Toward 6G Era. **IEEE Access**, v. 10, p. 87535–87562, 2022.

MAHMOOD, Nurul Huda et al. White Paper on Critical and Massive Machine Type Communication Towards 6G. **CoRR**, abs/2004.14146, 2020. arXiv: `2004.14146`.

MALEKI, Alireza; NGUYEN, Ha H.; BEDEER, Ebrahim; BARTON, Robert. Outage Probability Analysis of LR-FHSS and D2D-Aided LR-FHSS Protocols in Shadowed-Rice Fading Direct-to-Satellite IoT Networks. **IEEE Internet of Things Journal**, v. 11, n. 6, p. 11101–11116, 2024.

MAO, Sun; HE, Shunfan; WU, Jinsong. Joint UAV position optimization and resource scheduling in space-air-ground integrated networks with mixed cloud-edge computing. **IEEE Systems Journal**, v. 15, n. 3, p. 3992–4002, 2020.

MORÓN-LÓPEZ, Jesús; RODRÍGUEZ-SÁNCHEZ, María Cristina; CARREÑO, Francisco; VAQUERO, Joaquín; POMPA-PERNÍA, Ángel G; MATEOS-FERNÁNDEZ, Myriam; AGUILAR, Juan Antonio Pascual. Implementation of smart buoys and satellite-based systems for the remote monitoring of harmful algae bloom in inland waters. **IEEE Sensors Journal**, v. 21, n. 5, p. 6990–6997, 2020.

MUKHERJEE, Amrit et al. On-Demand Efficient Clustering for Next Generation IoT Applications: A Hybrid NN Approach. **IEEE Sensors Journal**, v. 21, n. 22, p. 25457–25464, 2021.

MUNARI, Andrea; CLAZZER, Federico; LIVA, Gianluigi. Multi-receiver Aloha systems - a survey and new results. In: IEEE International Conference on Communication Workshop (ICCW). London, UK: IEEE, 2015. P. 2108–2114.

MUNARI, Andrea; CLAZZER, Federico; LIVA, Gianluigi; HEINDLMAIER, Michael. Multiple-Relay Slotted ALOHA: Performance Analysis and Bounds. **IEEE Transactions on Communications**, v. 69, n. 3, p. 1578–1594, 2021.

NANBA, S.; KONISHI, S.; NOMOTO, S. Optimum traffic distribution algorithm for multiple-satellite systems under power constraints. **IEEE Journal on Selected Areas in Communications**, v. 22, n. 3, p. 492–500, 2004.

NANOSATS DATABASE. **LacunaSat-1**. Accessed: Jul. 26, 2023. 2020. Available from: `https://www.nanosats.eu/sat/lacunasat/`.

NASSAR, Almuthanna; YILMAZ, Yasin. Reinforcement Learning for Adaptive Resource Allocation in Fog RAN for IoT With Heterogeneous Latency Requirements. **IEEE Access**, v. 7, p. 128014–128025, 2019.

NOKIA. **Global coverage through non-terrestrial networks**. [S.l.], Feb. 2023.

ORTIGUEIRA, Raydel et al. RESS-IoT: A Scalable Energy-Efficient MAC Protocol for Direct-to-Satellite IoT. **IEEE Access**, v. 9, p. 164440–164453, 2021.

ORTIGUEIRA, Raydel; MONTEJO-SÁNCHEZ, Samuel; HENN, Santiago; FRAIRE, Juan A.; CÉSPEDES, Sandra. Satellite Visibility Prediction for Constrained

Devices in Direct-to-Satellite IoT Systems. **IEEE Sensors Journal**, v. 24, n. 16, p. 26630–26644, 2024.

PARRA, Pablo Ilabaca et al. Network Size Estimation for Direct-to-Satellite IoT. **IEEE Internet of Things Journal**, v. 10, n. 7, p. 6111–6125, 2023.

PERRON, E.; REZAEIAN, M.; GRANT, A. The On-Off fading channel. In: IEEE International Symposium on Information Theory. Bordeaux, France: IEEE, 2003. P. 244–244.

QU, Zhicheng; ZHANG, Gengxin; CAO, Haotong; XIE, Jidong. LEO Satellite Constellation for Internet of things. **IEEE Access**, v. 5, p. 18391–18401, 2017.

RAPPAPORT, Theodore S. **Wireless Communications: Principles and Practice**. [S.l.]: Cambridge University Press, 2024.

RAQUEL KATIGBAK, IBM DISTINGUISHED INDUSTRY LEADER. Accessed: Jun. 15, 2024. 2023. Available from: `https://www.ibm.com/blog/the-economy-of-things-the-next-value-lever-for-telcos/`.

RAZA, Usman; KULKARNI, Parag; SOORIYABANDARA, Mahesh. Low Power Wide Area Networks: An Overview. **IEEE Communications Surveys Tutorials**, v. 19, n. 2, p. 855–873, 2017.

RHODES, Brandon. **Skyfield: Elegant astronomy for Python**. Accessed: Jul. 26, 2023. 2023. Available from: `https://pypi.org/project/skyfield/`.

ROSEN, Kenneth H. **Discrete mathematics and Its applications**. 5th. Available online: McGraw-Hill Higher Education, 2002. ISBN 0072424346.

SAEED, Nasir et al. CubeSat Communications: Recent Advances and Future Challenges. **IEEE Communications Surveys & Tutorials**, v. 22, n. 3, p. 1839–1862, 2020.

SCUTARI, Gesualdo; FACCHINEI, Francisco; SONG, Peiran; PALOMAR, Daniel P.; PANG, Jong-Shi. Decomposition by Partial Linearization: Parallel Optimization of Multi-Agent Systems. **IEEE Transactions on Signal Processing**, v. 62, n. 3, p. 641–656, 2014.

SEMTECH. **AN1200. 22 LoRa modulation basics**. 2015.

SEMTECH. **Coexistence of LoRaWAN and UHF RFID**. Online; accessed Dez. 20, 2023. 2020. Available from: `https://Lora-developers.semtech.com/documentation`.

SEMTECH. **LoRa and LoRaWAN: A Technical Overview**. Online; accessed Jul. 26, 2023. 2022. Available from: `https://www.semtech.com/lora`.

SEMTECH CORP. **AN1200.64: LR-FHSS System Performance,** [s.l.], 2022. Rev. 1.3. Available from:
`%7Bhttps://www.semtech.com/products/wireless-rf/lora-connect/lr1121%7D`.

SEMTECH CORPORATION. **Lacuna Space Shoots for the Stars with LoRaWAN**. Accessed: 2024-12-28. 2019. Available from:
`https://blog.semtech.com/lacuna-space-shoots-for-the-stars-with-lorawan`.

SIGFOX. **SIGFOX: The Global Communications Service Provider for the Internet of Things**. [S.l.: s.n.]. Available from: `www.sigfox.com`.

SOUTO, Victoria et al. Emerging MIMO Technologies for 6G Networks. **Sensors**, v. 23, 23(4):1921, Feb. 2023.

SPACE.COM. **How many Starlink satellites are in orbit?** Accessed: 2025-1-7. 2025. Available from: `www.space.com/spacex-starlink-satellites.html`.

STARLINK. **Starlink mission**. Online; accessed Jul. 26, 2023. 2023. Available from: `https://www.spacex.com/`.

STEFANOVIC, Cedomir; POPOVSKI, Petar. ALOHA Random Access that Operates as a Rateless Code. **IEEE Transactions on Communications**, v. 61, n. 11, p. 4653–4662, 2013.

SWARM SPACE. **Global, affordable IoT connectivity**. Online; accessed Jul. 26, 2023. 2023. Available from: `https://swarm.space/`.

TELESAT. **Affordable, Quality Internet Everywhere**. [S.l.: s.n.], 2022. Available from: `https://www.telesat.com/`.

THE MATHWORKS, Inc. **fmincon:Find minimum of constrained nonlinear multivariable function**. [S.l.: s.n.], 2022. Available from:
`https://www.mathworks.com/help/optim/ug/fmincon.html`.

THE THINGS NETWORK. **LoRaWAN airtime calculator**. Online: accessed Jul. 26, 2023. 2023a. Available from:
`%7B%7Bhttps://www.thethingsnetwork.org/airtime-calculator%7D%7D`.

THE THINGS NETWORK. **Modulation** & **Data Rate**. Accessed: Jun. 26, 2024. Available from: `%7B%7Bhttps://www.thethingsnetwork.org/docs/lorawan/modulation-data-rate/%7D%7D`.

THE THINGS NETWORK. **The Things Network Console**. Accessed: Nov. 24, 2023. 2023b. Available from: `https://console.cloud.thethings.network/`.

TONDO, Felipe Augusto et al. Multiple Channel LoRa-to-LEO Scheduling for Direct-to-Satellite IoT. **IEEE Access**, v. 12, p. 30627–30637, 2024a.

TONDO, Felipe Augusto et al. Optimal Traffic Load Allocation for Aloha-Based IoT LEO Constellations. **IEEE Sensors Journal**, v. 23, n. 3, p. 3270–3282, 2023.

TONDO, Felipe Augusto; MONTEJO-SÁNCHEZ, Samuel; PELLENZ, Marcelo Eduardo; CÉSPEDES, Sandra; SOUZA, Richard Demo. Direct-to-satellite IoT slotted Aloha systems with multiple satellites and unequal erasure probabilities. **Sensors**, v. 21, n. 21, 2021.

TONDO, Felipe Augusto; SOUZA SANT'ANA, Jean Michel de; MONTEJO-SÁNCHEZ, Samuel; LÓPEZ, Onel Luis Alcaraz; CÉSPEDES, Sandra; SOUZA, Richard Demo. **Non-Orthogonal Multiple-Access Strategies for Direct-to-Satellite IoT Networks**. [S.l.: s.n.], 2024b. arXiv: `2409.02748 [eess.SP]`. Available from: `https://arxiv.org/abs/2409.02748`.

TSIROPOULOU, Eirini Eleni; PARUCHURI, Surya Teja; BARAS, John S. Interest, energy and physical-aware coalition formation and resource allocation in smart IoT applications. In: 51ST Annual Conference on Information Sciences and Systems (CISS). [S.l.: s.n.], 2017. P. 1–6.

TUBIANA, Douglas Alisson; FARHAT, Jamil; BRANTE, Glauber; SOUZA, Richard Demo. Q-Learning NOMA Random Access for IoT-Satellite Terrestrial Relay Networks. **IEEE Wireless Communications Letters**, v. 11, n. 8, p. 1619–1623, 2022.

VARGAS, L.S.; QUINTANA, V.H.; VANNELLI, A. A tutorial description of an interior point method and its applications to security-constrained economic dispatch. **IEEE Transactions on Power Systems**, v. 8, n. 3, p. 1315–1324, 1993.

VISWANATHAN, Harish; MOGENSEN, Preben E. Communications in the 6G Era. **IEEE Access**, v. 8, p. 57063–57074, 2020.

WANG, Anyue; LEI, Lei; HU, Xin; LAGUNAS, Eva; PÉREZ-NEIRA, Ana I.; CHATZINOTAS, Symeon. Adaptive Beam Pattern Selection and Resource Allocation for NOMA-Based LEO Satellite Systems. In: GLOBECOM 2022 - 2022 IEEE Global Communications Conference. [S.l.: s.n.], 2022. P. 674–679.

WANG, Huijiang; HAN, Chao; SUN, Xiucong. Analytical field-of-regard representation for rapid and accurate prediction of agile satellite imaging opportunities. **Journal of Astronomical Telescopes, Instruments, and Systems**, v. 5, n. 3, p. 037001–037001, 2019.

WANG, Qiwei; REN, Guangliang; GAO, Steven; WU, Kun. A framework of non-orthogonal slotted Aloha (NOSA) protocol for TDMA-based random multiple access in IoT-oriented satellite networks. **IEEE Access**, v. 6, p. 77542–77553, 2018.

WU, Tingwei; QU, Dexin; ZHANG, Gengxin. Research on LoRa Adaptability in the LEO Satellites Internet of Things. In: 15TH International Wireless Communicat. & Mobile Comput. Conf. (IWCMC). [S.l.: s.n.], 2019. P. 131–135.

YAN, Xiaojuan; AN, Kang; LIANG, Tao; ZHENG, Gan; DING, Zhiguo; CHATZINOTAS, Symeon; LIU, Yan. The Application of Power-Domain Non-Orthogonal Multiple Access in Satellite Communication Networks. **IEEE Access**, v. 7, p. 63531–63539, 2019.

YE, Yinyu. **Interior Point Algorithms: Theory and Analysis**. Hoboken, NJ: John Wiley & Sons, 2011. P. 480. ISBN 978-0471174202.

ZADOROZHNY, Alexander M.; DOROSHKIN, Alexander A.; GOREV, Vasily N.; MELKOV, Alexander V.; MITROKHIN, Anton A.; PROKOPYEV, Vitaliy Yu.; PROKOPYEV, Yuri M. First Flight-Testing of LoRa Modulation in Satellite Radio Communications in Low-Earth Orbit. **IEEE Access**, v. 10, p. 100006–100023, 2022.

ZHANG, Xuewei; REN, Yuan; WANG, Junxuan; LV, Tiejun. Joint Design of Multicast Transmission and In-Network Caching for Green Internet of Things. **IEEE Sensors Journal**, v. 22, n. 12, p. 12404–12414, 2022.

ZHANG, Zeqi; JIANG, Chunxiao; GUO, Song; QIAN, Yi; REN, Yong. Temporal Centrality-Balanced Traffic Management for Space Satellite Networks. **IEEE Transactions on Vehicular Technology**, v. 67, n. 5, p. 4427–4439, 2018.

ZHAO, Bo; REN, Guangliang; DONG, Xiaodai; ZHANG, Huining. Optimal Irregular Repetition Slotted ALOHA Under Total Transmit Power Constraint in IoT-Oriented Satellite Networks. **IEEE Internet of Things Journal**, v. 7, n. 10, p. 10465–10474, 2020.

ZHEN, Li; BASHIR, Ali Kashif; YU, Keping; AL-OTAIBI, Yasser D; FOH, Chuan Heng; XIAO, Pei. Energy-efficient random access for LEO satellite-assisted 6G internet of remote things. **IEEE Internet of Things Journal**, v. 8, n. 7, p. 5114–5128, 2020.

ZORZI, M. Mobile radio slotted ALOHA with capture, diversity and retransmission control in the presence of shadowing. **Wireless Networks**, v. 4, p. 379–388, 1997.

Appendix

APPENDIX A – THROUGHPUT WITH DIFFERENT ERASURE PROBABILITIES

In this appendix, using the inclusion-exclusion principle (ROSEN, 2002) we can determine the cardinality of the union of the sets of packets successfully received by each satellite constellation position, therefore discounting the received multiplicities. So, assuming $D_{m,k}$ as a set that would contain the data packets successfully received by the kth different satellite at the mth constellation position, we can generalize for K sets as

$$\left| \bigcup_{k=1}^{K} D_{m,k} \right| = \sum_{\substack{\forall \mathbb{J} \subseteq \{1,\cdots,K\} \\ \mathbb{J} \neq \emptyset}} (-1)^{|\mathbb{J}|+1} \left| \bigcap_{j \in \mathbb{J}} D_{m,j} \right|, \tag{30}$$

where $\mathbb{J}$ is a set with indexes of the subsets whose intersection must be evaluated. Note that the above expression does not admit a simplification step applied in (MUNARI et al., 2021), which requires the setup to be symmetrical. In our particular case, as the erasure probabilities are different, the ordering (or numbering) of the satellites and constellation topology are relevant [1]. In addition, it is fundamental to know $\left| \bigcap_{j \in \mathbb{J}} D_{m,j} \right|$, the cardinality of the intersection of the sets of packets successfully received by a subset $\mathbb{J} \subseteq \{1,\ldots,K\}$ of satellites with cardinality $|\mathbb{J}|$ in m constellation position.

After the realization of many time-slots N, the average number of packets jointly received by $|\mathbb{J}|$ satellites is $\left| \bigcap_{j \in \mathbb{J}} D_{m,j} \right| = N \sum_{u=0}^{\infty} q_{m,k}(u) \, \mathbb{P}[U = u]$. Thus, the average number of data packets successfully received at the kth satellite in a given time slot in the mth constellation position is

$$\begin{aligned}
\mathcal{T}_m &= \lim_{N \to \infty} \frac{1}{N} \sum_{\substack{\forall \mathbb{J} \subseteq \{1,\cdots,K\} \\ \mathbb{J} \neq \emptyset}} (-1)^{|\mathbb{J}|+1} \left| \bigcap_{j \in \mathbb{J}} D_{m,j} \right| \\
&= \sum_{\substack{\forall \mathbb{J} \subseteq \{1,\cdots,K\} \\ \mathbb{J} \neq \emptyset}} (-1)^{|\mathbb{J}|+1} \sum_{u=0}^{\infty} \left[\frac{(G_m)^u e^{-G_m}}{u!} u \prod_{k \in \mathbb{J}} (1 - \varepsilon_{m,k})(\varepsilon_{m,k})^{u-1} \right] \\
&= \sum_{\substack{\forall \mathbb{J} \subseteq \{1,\cdots,K\} \\ \mathbb{J} \neq \emptyset}} (-1)^{|\mathbb{J}|+1} e^{-G_m} \prod_{k \in \mathbb{J}} (1 - \varepsilon_{m,k}) \sum_{u=0}^{\infty} \left[\frac{u(G_m)^u}{u!} \left(\prod_{k \in \mathbb{J}} \varepsilon_{m,k} \right)^{u-1} \right] \\
&= \sum_{\substack{\forall \mathbb{J} \subseteq \{1,\cdots,K\} \\ \mathbb{J} \neq \emptyset}} (-1)^{|\mathbb{J}|+1} G_m \prod_{k \in \mathbb{J}} (1 - \varepsilon_{m,k}) \, e^{-G_m \left(1 - \prod_{k \in \mathbb{J}} \varepsilon_{m,k} \right)}. \tag{31}
\end{aligned}$$

---

[1] For instance, for the case of three sets $D_{m,1}$, $D_{m,2}$, and $D_{m,3}$ at m^{th} constellation position, we can determinate the number of different received packets as: $|D_{m,1} \cup D_{m,2} \cup D_{m,3}| = |D_{m,1}| + |D_{m,2}| + |D_{m,3}| - |D_{m,1} \cap D_{m,2}| - |D_{m,1} \cap D_{m,3}| - |D_{m,2} \cap D_{m,3}| + |D_{m,1} \cap D_{m,2} \cap D_{m,3}|$

APPENDIX B – INTELLIGENT TRAFFIC LOAD DISTRIBUTION - (ITLD)

In this appendix, we explain the ITLD strategy summarized in Algorithm 4 below. Assuming a uniform load distribution, the total traffic load, G_T, to be offered during a complete lap of the satellite constellation, can be written as

$$G_m^{(u)} = \frac{G_T}{M},\tag{32}$$

where $G_m^{(u)}$, $m \in \{1, ..., M\}$, is the traffic load uniformly distributed per position.

The load factor Q_m is the proportion each constellation position contribute to the overall throughput. So, when the traffic load is uniformly distributed we can write the load factor as:

$$Q_m = \frac{\mathcal{T}_m(G_m^{(u)})}{\sum_{m=1}^{M} \mathcal{T}_m(G_m^{(u)})}.\tag{33}$$

Following the hypothesis that higher performing positions can successfully take on higher traffic load, we propose to use this load factor as the appropriate weight to conveniently distribute the traffic load in a simple and effective manner. Then, the non-uniform traffic load, per position, is defined as follows:

$$G_m^{(nu)} = Q_m \, G_T.\tag{34}$$

The overall system throughput considering either the uniform or the non-uniform distribution is computed as

$$\mathcal{T}^{(x)} = \sum_{m=1}^{M} \mathcal{T}_m(G_m^{(x)}),\tag{35}$$

where $x = \{u, nu\}$ in the case of uniform or non-uniform distribution strategy, respectively.

By its turn, ITLD selects the traffic load distribution as

$$G_m^{(ITLD)} = \begin{cases} G_m^{(nu)} & \text{if} \quad \mathcal{T}_m^{(nu)} > \mathcal{T}_m^{(u)} \\ G_m^{(u)} & \text{if} \quad \mathcal{T}_m^{(nu)} < \mathcal{T}_m^{(u)} \end{cases},\tag{36}$$

so that the ITLD throughput is

$$\mathcal{T}_T^{(ITLD)} = \max(\mathcal{T}_T^{(u)}, \mathcal{T}_T^{(nu)}).\tag{37}$$

Finally, Algorithm 4 describes the implementation of the ITLD algorithm.

Algorithm 4 ITLD - Intelligent Traffic Load Distribution

1: According to the satellite spacing s, obtain the number of positions M;

2: Evaluating (32), compute the uniform traffic load distribution per position $G_m^{(u)}$;

3: For $G_m^{(u)}$, calculate the throughput per position $\mathcal{T}_m$ with (4);

4: Determine the overall throughput with uniform load distribution, $\mathcal{T}_T^{(u)} = \sum_{m=1}^{M} \mathcal{T}_m(G_m^{(u)})$;

5: Find the load factor Q_m in each position using (33);

6: Following (34), compute the non-uniform traffic load distribution per position $G_m^{(nu)}$;

7: Repeat step *4* now to find $\mathcal{T}_m$ with $G_m^{(nu)}$ for the proposed strategy;

8: Determine the overall throughput with non-uniform load distribution $\mathcal{T}_T^{(nu)} = \sum_{m=1}^{M} \mathcal{T}_m(G_m^{(nu)})$;

9: If $\mathcal{T}_m^{(nu)} > \mathcal{T}_m^{(u)}$, then $G_m = G_m^{(nu)}$. Else, $G_m = G_m^{(u)}$. Thus, $\mathcal{T}_T = \max(\mathcal{T}_T^{(nu)}, \mathcal{T}_T^{(u)})$.